ASD-TDR-62-719
Part III

THERMAL RADIATION CHARACTERISTICS OF TRANSPARENT SEMI-TRANSPARENT AND TRANSLUCENT MATERIALS UNDER NON-ISOTHERMAL CONDITIONS

Henry A. Hobbs
Robert C. Folweiler

Lexington Laboratories, Inc.

TECHNICAL DOCUMENTARY REPORT ASD-TDR-65-719, Part III

March, 1966

Air Force Materials Laboratory
Research and Technology Division
Air Force Systems Command
Wright-Patterson Air Force Base, Ohio

NOTICES

When Government drawings, specifications, or other data are used for any purpose other than in connection with a definitely related Government procurement operation, the United States Government thereby incurs no responsibility nor any obligation whatsoever; and the fact that the Government may have formulated, furnished, or in any way supplied the said drawings, specifications, or other data, is not to be regarded by implication or otherwise as in any manner licensing the holder or any other person or corporation, or conveying any rights or permission to manufacture, use, or sell any patented invention that may in any way be related thereto.

Copies of this report should not be returned to the Research and Technology Division unless return is required by security considerations, contractual obligations, or notice on a specific document.

THERMAL RADIATION CHARACTERISTICS OF TRANSPARENT SEMI-TRANSPARENT AND TRANSLUCENT MATERIALS UNDER NON-ISOTHERMAL CONDITIONS

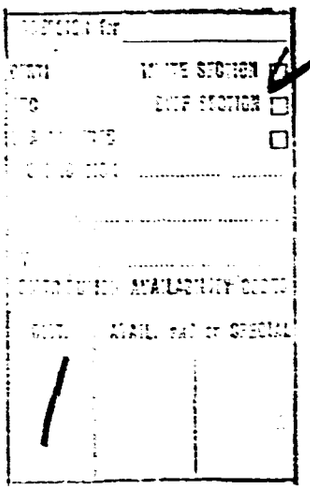

Henry A. Hobbs
Robert C. Folweiler

FOREWORD

This report was prepared by Lexington Laboratories, Inc., Cambridge, Massachusetts under USAF Contract AF33(657)-11280. This contract was initiated under Project No. 7360, "The Chemistry and Physics of Materials", Task No. 736001, "Thermodynamics and Heat Transfer". The work was administered under the direction of the Air Force Materials Laboratory, Research and Technology Division, Wright-Patterson Air Force Base, Ohio, with Mr. R. J. Prezecki and Mr. E. J. Rolinski acting as project engineers.

Robert C. Folweiler is Project Engineer on the contract for Lexington Laboratories, Inc. Contributors to the project include W. B. Fraser, H. A. Hobbs, W. D. Kingery, and D. W. Moore.

Manuscript released by authors March 1966 for publication as an RTD Technical Report.

This technical report has been reviewed and is approved.

Jules I. Wittebort, Chief
Thermal and Solid State Branch
Materials Physics Division
Air Force Materials Laboratory

ABSTRACT

Over the range of wavelengths from one to six microns where oxide ceramics are partially transparent, radiant energy emission must be treated as a volume rather than a surface phenomena. As a result the absorption coefficient (mainly determined by composition) and the scattering coefficient (mainly determined by microstructure) are important variables. In addition, temperature gradients affect radiant energy emission so that the effective "emissivity" under non-isothermal conditions is neither a material constant nor a sample constant.

Analytical relationships have been derived for spectral radiant energy emission as a function of absorption coefficient, scattering coefficient, surface temperature and temperature gradient. Experimental measurements of non-isothermal radiant energy emission of Al_2O_3 and $SrTiO_3$ samples are in agreement with these calculations. Analytical relations and experimental measurements for diffuse and parallel light transmission are reported. Comparison of the Hamaker approximation with an exact solution show that the approximation is suitable for these materials and conditions.

TABLE OF CONTENTS

TABLE OF CONTENTS (CONTINUED)

LIST OF TABLES

LIST OF ILLUSTRATIONS

LIST OF ILLUSTRATIONS (CONTINUED)

LIST OF ILLUSTRATIONS (CONTINUED)

SYMBOLS

a	Absorption coefficient for diffuse radiation in a material containing scattering centers
A	Hamaker constant see Eq. 6.18
b	Radiation constant see Eq. 6.10
B	Hamaker constant see Eq. 6.19
C	Hamaker constant see Eq. 6.20
C_1	Constant in Wien's equation
C_2	Constant in Wien's equation
d	Thickness of sample
D	Hamaker constant see Eq. 6.21
E	Blackbody Radiant Energy Flux
f	Forward scattering coefficient for diffuse radiation
f'	Forward scattering coefficient for parallel radiation
g'	Extinction coefficient used by Ryde
H	Net heat flux
h	Planck's Constant
I	Radiant energy flux in the direction of the positive x-axis
I_o	Radiant energy flux in the direction of the positive x-axis at x = 0
I'	Specific intensity of radiation
I'^{+}_{o}	Specific intensity of forward radiation at x = 0
I'^{-}_{o}	Specific intensity of backward radiation at x = 0
I_p	Parallel forward flux
I_{p_i}	Parallel flux incident on surface of slab
$\bar{I}'$	Average specific energy
j(x)	Emission coefficient for radiation in the material
J	Radiant energy flux in the direction of the negative x-axis

J_o	Radiant energy flux in the direction of the negative x-axis at x = 0
k	Lattice thermal conductivity
K	Scattering factor (non-dimensional)
ℓ	Path length in direction θ
m	Reciprocal index of refraction; m = 1/n
n	Index of refraction
N	Number of pores per unit volume
p	Dimensionless parameter $p = 4\pi r \left\| m-1 \right\| / \lambda m$
P	Volume fraction porosity
r	Pore radius
s	Backward scattering coefficient for diffuse radiation (scattering factor in Hamaker equations)
s'	Backward scattering coefficient for parallel radiation
S	Scattering coefficient for parallel radiation
T	Absolute temperature
U	Material constant defined by Eq. 4.9
V	Material constant defined by Eq. 4.10
x	Distance along x-axis
α	Absorption coefficient
β	Material constant; $\beta = \sigma/(a + 2s)$
β_o	Material constant; $\beta_o = \sigma_o/(a + 2s)$
Δ	Constant denominator defined in Eq. 4.23
ε	Emissivity
ε_n	Non-isothermal emissivity
ε_i	Isothermal emissivity
θ	Angle measured from x-axis within the sample
θ'	Angle measured from x-axis outside the sample

κ Material constant defined by Hamaker (Philips Res. Rpts. Vol. 2 (1947).

$$\kappa = \frac{2b\beta}{k\sigma}$$

λ Wavelength of radiation in free space

ν Frequency of radiation

ρ Reflectivity

ρ_i Reflection coefficient for diffuse energy emerging from the sample

ρ_o Reflection coefficient for diffuse energy incident on the sample

ρ_n Reflection coefficient for normal incidence

σ Material constant for non-isothermal case

$$\sigma = \sigma_o \sqrt{1 + \kappa}$$

σ_o Material constant $\sigma_o = \sqrt{a(a + 2s)}$

σ' Stefan-Boltzmann constant

ϕ Azimuthal angle

ψ Spectral radiant energy

ω Solid angle

1.0 INTRODUCTION

In Part I of the present study,[1] general equations describing emission, transmission and reflectance of scattering and absorbing systems were derived in a form that allows determination of the necessary material constants and calculation of emissivity under isothermal and non-isothermal conditions. Methods of evaluating conditions under which these equations are applicable were derived, and a simple expression for radiant energy transfer when conduction in the solid is negligible relative to the radiant energy transfer in the solid was developed.

Experimental apparatus was developed and measurements made of isothermal emissivity of several refractory oxides and single crystal transmission over the wavelength range 1-15 microns at temperatures up to 1350°C. Emissivity was found to depend strongly on composition, microstructure and wavelength. Different grades of "alumina" ceramics range from about 0.2 to above 0.9 in the near infra-red.

Diffuse transmission measurements permitted calculations of the pertinent material constants as well as the separate scattering and absorption coefficients. For these systems scattering was large for diffuse radiation, in the range 1000-5000 cm^{-1}; as a result of these large values calculations of emissivity were of low precision, but agreed with experimental measurements. Results showed that the normal emissivity in these systems was substantially larger than the hemispherical emissivity, in contrast to opaque solids where they are nearly the same.

In Part II of the study[2], emissivity values were calculated for specially prepared Al_2O_3, MgO, SiO_2 and $SrTiO_3$ samples from appropriate reflectivities, absorption coefficients and scattering coefficients derived from material characteristics (index of refraction, single crystal transmissivity, pore size and concentration).

Experimental measurements of emissivity for these samples were made at temperatures up to 1200°C and at wavelengths from one to fifteen microns. Calculated and measured values were in good agreement for Al_2O_3 and SiO_2. Absorption coefficients of the MgO and $SrTiO_3$ samples were greater than the single crystal values, leading to higher measured (than calculated) emissivities. Samples of commercial alumina had higher

emissivities than the specially prepared high purity samples.

The Hamaker equations for non-isothermal emissivity, which linearize the temperature gradient, were compared with the exact solution by numerical integration. Results were in good agreement for all cases of practical interest for application to ceramic oxides. Solutions to the Hamaker equations were derived for new boundary conditions.

Evaluation of the rotating blackbody slot system used for isothermal emissivity measurements indicated that it gave results in good agreement with an external blackbody. An apparatus for measuring the effective emissivity of a non-isothermal sample was constructed and tested.

In the present final phase of the study our major effort has been devoted to further evaluation of the factors affecting both total and spectral emissivity from ceramic oxides and carrying out experimental measurements of non-isothermal emissivity on well characterized samples. We have also extended our comparison of the Hamaker approximations and an exact solution to actual values of material constants. Anticipating our results we can say that we have experimentally observed the influence of non-isothermal conditions on radiant energy emission from ceramic oxides and found our results to be in reasonable agreement with calculated values.

At the same time we have evaluated analytically the transmission of radiant energy by ceramic oxides containing scattering centers, and made experimental measurements. The low radiant energy transmission has seriously limited our experimental precision, but results are in general accord with calculations.

Overall, we now have a sound basis for estimating the thermal emissivity, both isothermal and non-isothermal, from proper material characterization and for evaluating the effect of changing material characteristics on thermal emissivity behavior.

2.0 NON-ISOTHERMAL EMISSION OF RADIANT ENERGY

2.1 Total Emission of Radiant Energy

We shall assume that a sample of radiating material has a specified temperature distribution given by

$$T(x) = T_o + \left(\frac{dT}{dx}\right)_o x$$

where x measures the distance into the sample from the surface. The sample has an absorption coefficient α, scattering coefficient S, and index of refraction n. Let $I'(x, \theta)$ be the specific intensity of radiation in the material, where θ is the polar angle with respect to the + x axis (Fig. 2.1). Assume axial symmetry.

Vacuum n = 1 Material n = n

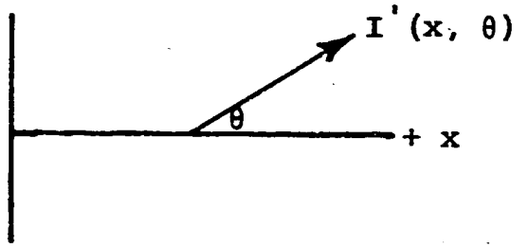

Figure 2.1 Diagram of Geometry of Radiation in Absorbing and Scattering Material

The equation of transfer for the radiation in the material is

$$\cos\theta \frac{d\, I'(x, \theta)}{dx} = -(\alpha + S)\, I'(x, \theta) + j(x). \qquad (2.1)$$

j (x) is the emission coefficient for radiation in the material. It has two terms, one due to thermal emission and one due to scattering. j (x) is given by

$$j(x) = \alpha n^2 \sigma' T(x)^4 + S \bar{I}'(x), \qquad (2.2)$$

where σ' is the Stefan-Boltzmann constant, and

$$\bar{I}'(x) = 2\pi \int_{\theta=0}^{\pi} I'(x, \theta) \sin\theta\, d\theta \qquad (2.3)$$

Now assume the intensity is isotropic over each hemisphere. Take

$$I'(x, \theta) = I'^{+}(x) \quad 0 \leq \theta \leq \pi/2, \tag{2.4}$$

and

$$I'(x, \theta) = I'^{-}(x) \quad \pi/2 \leq \theta \leq \pi. \tag{2.5}$$

Then we easily find $\bar{I}'(x) = 1/2\,(I'^{+}(x) + I'^{-}(x))$. The flux is given by

$$\pi F(x) = 2\pi \int_{\theta=0}^{\pi} I(x,\theta) \cos\theta \sin\theta d\theta = \pi\left[I'^{+}(x) - I'^{-}(x)\right]. \tag{2.6}$$

In fact, in terms of the fluxes I and J we have

$$I(x) = \pi I'^{+}(x) \text{ and } J(x) = \pi I'^{-}(x).$$

Now multiply the equation of transfer by $\sin\theta d\theta$ and integrate with respect to θ from 0 to π. Using the expressions (2) and (3) for $I'(x, \theta)$ we obtain, after some simplification,

$$\frac{dF(x)}{dx} = -4\alpha \bar{I}'(x) + 4\alpha n^2 \sigma' T(x)^4 \tag{2.7}$$

Similarly, multiplying the equation of transfer by $\cos\theta \sin\theta d\theta$ and integrating as before, we obtain the result

$$\frac{4}{3}\frac{d\bar{I}'(x)}{(x)} = -(\alpha + S)F(x). \tag{2.8}$$

Combining (4) and (5) we have as our final equation

$$\frac{d^2F(x)}{dx^2} - 3\alpha(\alpha + S)F(x) = \frac{d}{dx}(4\alpha n^2 \sigma' T(x)^4) \tag{2.9}$$

We wish to solve this equation subject to the boundary condition

$$I'^{+}(o) = \bar{\rho}\, I'^{-}(o) \tag{2.10}$$

where $\bar{\rho}$ is the mean reflectance for diffuse radiation going from the material into the vacuum.

Now the equation is second order in x but we have only one boundary condition. However, if

$$3\alpha(\alpha + S) >> 1, \tag{2.11}$$

we expect F(x) does not change rapidly over the interior of the material and the equation is of boundary layer type. In any region where

$$\left|\frac{d^2F}{dx^2}\right| \quad << \quad \left|3\alpha(\alpha + S)F(x)\right|, \tag{2.12}$$

then we have

$$F(x) \simeq -\frac{4n^2\sigma'}{3(\alpha + S)} \frac{dT^4(x)}{dx} \equiv F_{int}(x). \tag{2.13}$$

Near x = 0 this interior solution is modified by the presence of the boundary. Write

$$F(x) \equiv F_{int}(x) + G(x). \tag{2.14}$$

Then G(x) satisfies

$$\frac{d^2G(x)}{dx^2} - 3\alpha(\alpha + S)G(x) = -\frac{d^2F_{int}(x)}{dx^2} \tag{2.15}$$

But

$$\frac{d^2F_{int}}{dx^2}$$

will be small so we simply take

$$\frac{d^2G(x)}{dx^2} - 3\alpha(\alpha + S)G(x) = 0. \tag{2.16}$$

Now we demand that $G(x) \longrightarrow 0$ rapidly as

$$x \longrightarrow 0 \left[\sqrt{\frac{1}{3\alpha(\alpha + S)}}\right] \tag{2.17}$$

So G(x) is proportional to

$$\exp. \left[-\sqrt{3\alpha(\alpha + S)}\, x\right].$$

We discard the solution

$$\exp. \left[+\sqrt{3\alpha(\alpha + S)}\, x\right]$$

since it increases without limit as x increases. Finally, write F(x) as

$$F(x) = n^2\sigma'\left\{-\frac{4}{3(\alpha + S)}\frac{dT^4(x)}{dx} + G\exp.\left[-\sqrt{3\alpha(\alpha + S)}\,x\right]\right\} \quad (2.18)$$

where G is a constant. The boundary condition

$$\bar{\rho}\, I'^{-}(o) = I'^{+}(o) \text{ at } x = 0 \quad (2.19)$$

determines G. From

$$\bar{I}'(x) = n^2\sigma' T^4(x) - \frac{1}{4\alpha}\frac{dF(x)}{dx}, \quad (2.20)$$

$$I'^{+}(x) = \bar{I}'(x) + \frac{F(x)}{2}, \quad (2.21)$$

and

$$I'^{-}(x) = \bar{I}'(x) - \frac{F(x)}{2} \quad (2.22)$$

we find that G is given by

$$\left[\frac{1}{4\alpha}\sqrt{3\alpha(\alpha + S)} + \frac{1}{2}\left(\frac{1 + \bar{\rho}}{1 - \bar{\rho}}\right)\right] G = -T^4(o) +$$

$$\frac{2}{3(\alpha + S)}\left(\frac{1 + \bar{\rho}}{1 - \bar{\rho}}\right)\frac{dT^4(o)}{dx} - \frac{1}{3\alpha(\alpha + S)}\frac{d^2T^4(o)}{dx^2} \quad (2.23)$$

The emitted radiation is

$$(1 - \bar{\rho})\, I'^{-}(o).$$

After some manipulation we find

$$I'^{-}(o) = \frac{n^2\sigma'}{\left(\frac{1 - \bar{\rho}}{4\alpha}\right)\sqrt{3\alpha(\alpha + S)} + \frac{1}{2}(1 + \bar{\rho})}$$

$$\left[T^4(o) + \frac{1}{\sqrt{3\alpha(\alpha + S)}}\frac{dT^4(o)}{dx} + \frac{1}{3\alpha(\alpha + S)}\frac{d^2T^4(o)}{dx^2}\right]. \quad (2.24)$$

2.2 Spectral Emission of Radiant Energy

In the preceding section, the intensity of emitted radiation $I'^{-}(o)$ was derived as a function of the total intensity of forward radiation (i.e., the Stefan-Boltzmann Law was used to derive the energy). This derivation assumed that the absorption coefficient α, the scattering coefficient S, and the index of refraction, n, were constants. This is not true, however, because all three (α, S, and n) are dependent upon wavelength (λ). Appendix I characterizes the materials used during the past year; the data tabulated there clearly indicates that the three properties do change with wavelength. In addition, the absorption coefficient, α, is a function of temperature as well as wavelength.

Because of this wavelength dependence of the material properties, either Planck's Law or Wien's Law must be used for the calculation of the intensity of spectral emission. Experimentally, we measure the energy emitted as a function of wavelength rather than the integrated energy over all wavelengths. Thus, we want to know the non-isothermal radiation intensity as a function of wavelength as well as temperature and temperature gradient.

The exact solution,when the temperature gradient is known and the surface temperature must be determined,has been derived in Appendix II. This involves the solution of a quartic polynomial equation for each discrete value of α and S. To avoid this complication, Wien's Law for spectral radiation,

$$\Psi_{\lambda,T} = \Psi = c_1 \lambda^{-5} \exp(-c_2/\lambda T) \tag{2.25}$$

can be substituted for the Stefan-Boltzmann Law,

$$I_T = n^2 \sigma' T^4 \tag{2.26}$$

Wien's Law, rather than Planck's Law,

$$\Psi_{\lambda,T} = \frac{c_1 \lambda^{-5}}{\exp(+c_2/\lambda T) - 1} \tag{2.27}$$

has been used solely for the reason that computations are more easily carried out. The error introduced by using Wien's Law is large at high wavelengths (25% at $\lambda = 10\mu$ and 1000° K) but at the wavelengths less than $\lambda = 6\mu$ where scattering is important the error decreases. For example, at $\lambda = 1\mu$ and

1000°K it is only 0.0001%, and at $\lambda = 5\mu$, the error is 0.1%.

The substitution of Wien's Law directly into the derived expression of the previous section is not strictly justified, in the sense that the integration of Wien's Law over all wavelengths does not yield the Stefan-Boltzmann energy function. It was deemed satisfactory however, because the region of interest for non-isothermal and isothermal emissivity as a volume process in ceramic oxides is below six microns, and in this region the errors introduced are not large. If we remain within the region 1-5μ, the error is less than one percent.

Substituting Wien's Law, the equation (2.24)

$$I'^{-}(o) = \frac{n^2\sigma'}{\left(\frac{1-\bar{\rho}}{4\alpha}\right)\sqrt{3\alpha(\alpha+S)} + 1/2\ (1+\bar{\rho})}$$

$$\left[T^4(o) + \frac{1}{\sqrt{3\alpha(\alpha+S)}}\ \frac{dT^4(o)}{dx} + \frac{1}{3\alpha(\alpha+S)}\ \frac{d^2T^4(o)}{dx^2}\right] \quad (2.24)$$

becomes $\Psi(o)_{(\lambda,T)} = \dfrac{n^2C_1\lambda^{-5}}{\left(\frac{1-\bar{\rho}}{4\alpha}\right)\sqrt{3\alpha(\alpha+S)} + 1/2\ (1+\bar{\rho})}$

$$\left[\exp\left(-\frac{C_2}{\lambda T}\right) + \frac{1}{\sqrt{3\alpha(\alpha+S)}}\ \frac{d\ \exp\left(-\frac{C_2}{\lambda T}\right)}{dx} + \right.$$

$$\left. \frac{1}{3\alpha(\alpha+S)}\ \frac{d^2\exp\left(-\frac{C_2}{\lambda T}\right)}{dx^2}\right] \quad (2.28)$$

$$\text{or } \Psi(o)_{(\lambda,T)} = \frac{n^2 C_1 \lambda^{-5}}{\left(\frac{1-\bar{\rho}}{4\alpha}\right)\sqrt{3\alpha(\alpha+S)} + 1/2(1+\bar{\rho})}$$

$$\left[\exp\left(-\frac{C_2}{\lambda T}\right) + \frac{1}{\sqrt{3\alpha(\alpha+S)}}\left\{\frac{C_2}{\lambda T^2}\exp\left(-\frac{C_2}{\lambda T}\right)\frac{dT}{dx}\right\} + \right.$$

$$\left.\frac{1}{3\alpha(\alpha+S)}\left\{\frac{C_2}{\lambda T^2}\exp\left(-\frac{C_2}{\lambda T}\right)\left(\frac{C_2}{\lambda T^2}-\frac{2}{T}\right)\left(\frac{dT}{dx}\right)^2\right\}\right] \quad (2.28b)$$

This expression includes the temperature gradient $(\frac{dT}{dx})$, and variations of the absorption coefficient (α), scattering coefficient (S), and reflectance $(\bar{\rho})$ with wavelength. C_1 and C_2 are the first and second radiation constants, λ the wavelength, and T the absolute temperature.

Results for one material showing the ratio of non-isothermal to isothermal energy emitted at different wavelengths are plotted in Fig. 2.2. This ratio is a measure of the expression

$$\exp\left(-\frac{C_2}{\lambda T}\right) + \frac{1}{\sqrt{3\alpha(\alpha+S)}}\left\{\frac{C_2}{\lambda T^2}\exp\left(-\frac{C_2}{\lambda T}\right)\frac{dT}{dx}\right\} \quad (2.29)$$

compared to $\exp(-\frac{C_2}{\lambda T})$. Table I is a tabulation of the specific values used in computing the theoretical curve.

The effect of increasing the magnitude of the temperature gradient is to increase the amplitude of the curve. The temperature gradient does not affect the wavelength dependency of the energy ratio.

A brief description of the three black-body radiation laws is given in Appendix IV.

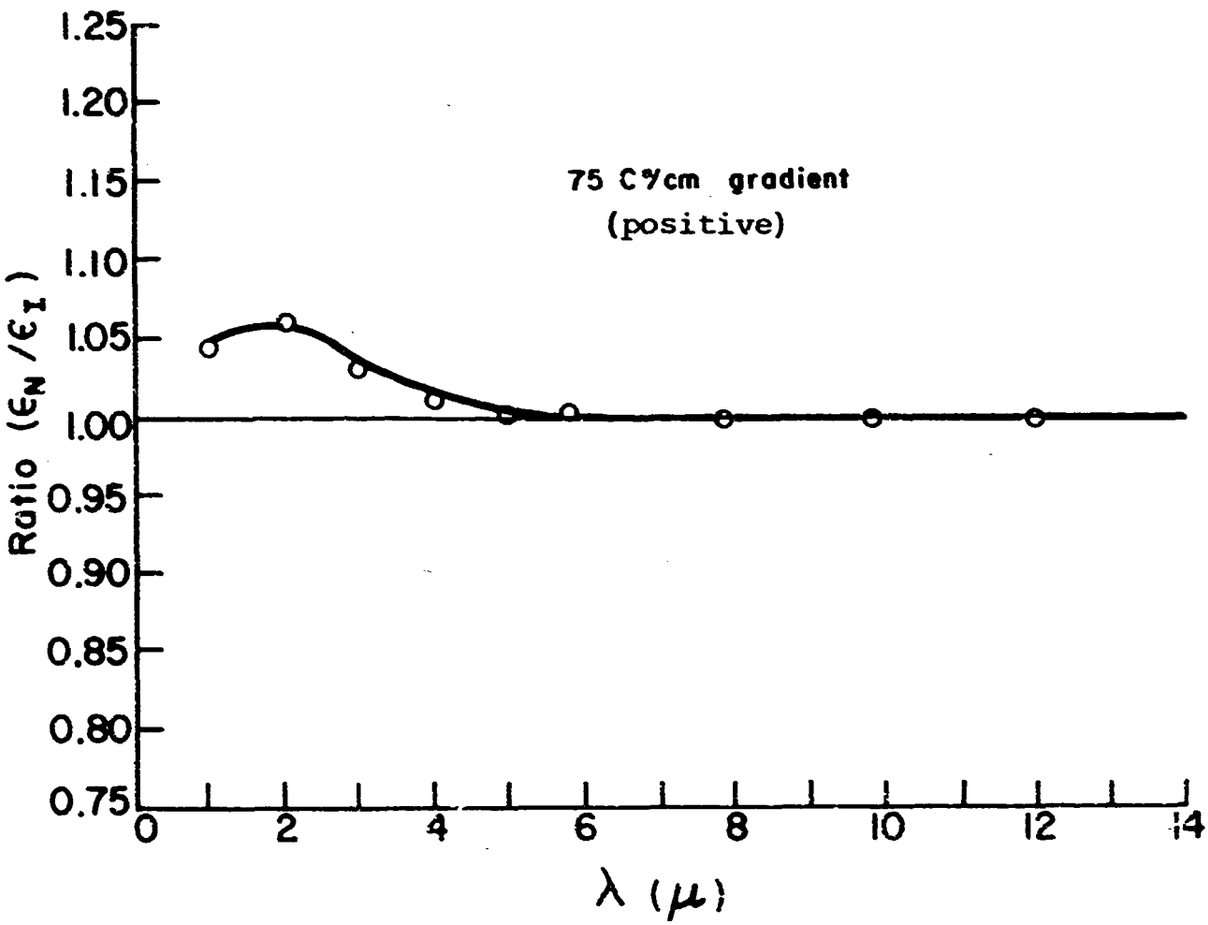

Figure 2.2 Ratio of Non-Isothermal to Isothermal Emissivity for AD-85 Calculated from Equation (2.28b).

TABLE 2-I

Values Used to Calculate Non-Isothermal Energy Ratio for AD-85 Al_2O_3 at 1100°C Surface Temperature

$\lambda(\mu)$	n_λ	$\bar{\rho}$	$\alpha(cm^{-1})$	$S(cm^{-1})$	$\frac{1}{\sqrt{3\alpha(\alpha + S)}}$	$\frac{C_2}{\lambda T^2}$
1	1.75	0.07	0.513	260	0.051	7.63×10^{-3}
2	1.74	0.07	0.117	260	0.105	3.62×10^{-3}
3	1.72	0.07	0.256	265	0.070	2.54×10^{-3}
4	1.65	0.07	0.610	263	0.046	1.91×10^{-3}
5	1.60	0.07	5.420	256	0.015	1.53×10^{-3}

2.3 Calculation of Non-isothermal Spectral Emissivities

For the samples of alumina and strontium titanate used for experimental measurements, non-isothermal spectral emissivities were calculated from Equation 2.28b. For this calculation values of the absorption coefficient, scattering coefficient and reflectance were determined as described in Reference 2. Values of surface temperature and temperature gradient were taken to correspond with the experimental conditions actually used. Results of these calculations are shown directly compared with experimental measurements in Figures 3.5-3.24.

These results for the calculated values of the ratio of non-isothermal to isothermal emissivity indicate that above 6 microns, the non-isothermal effect is nil. At lower wavelengths, the effect of a temperature gradient is to increase the emissivity whenever there is a positive gradient, and to decrease the emissivity whenever there is a negative temperature gradient. The temperature of the surface itself has less effect on the non-isothermal emissivity than the gradient. That is, the term containing the gradient in equation (2.29) is of greatest significance.

3.0 NON-ISOTHERMAL EMISSIVITY MEASUREMENTS

3.1 Apparatus for Measuring Non-Isothermal Emissivity

The purpose of the apparatus is to produce a controlled temperature gradient across a disc-shaped ceramic sample whose emissive properties are to be measured. The gradient is produced only in the radial direction, thereby reducing the analysis to that of a one dimensional heat transfer problem. A rotating sample arrangement is used to maintain symmetric temperature conditions.

The apparatus operates inside the same furnace which has been used for isothermal emissivity measurement; the latter has been described previously[1]. The furnace heating elements are used to adjust the surface temperature. An internal resistance element is used to produce a positive temperature gradient across the sample; forced air cooling through a hollow shaft is used to produce a negative temperature gradient across the sample. The complete apparatus is shown in Figure 3.1.

The samples and the internal heating element are supported on a one-half inch alumina shaft. The alumina shaft is supported and rotated by stainless steel shafts with conical points which mate with conical holes at each end of the alumina shaft. The two stainless steel shafts are rotated by an electric motor and synchronized by a pair of selsyns. This arrangement assures minimum stress and vibration on the shaft and sample assembly while giving a uniform rate of rotation.

In order to minimize the effects of thermal variations, the apparatus was designed to produce a radial temperature gradient in the sample. The gradient is obtained in a sample which has a width of one-half inch and which is placed between ceramic discs of the same dimensions and made of a material with similar thermal properties. The discs are held together by an axial spring load; the resulting thin air gap between adjacent discs reduces axial heat transfer and resultant temperature gradients along the samples and support plates.

The interior heating element is wound for a length of nine inches under the sample and support plates, with the samples located at the center of the winding. This arrangement gives a uniform axial heat zone in the region of the sample and support plate assembly; no axial gradient is possible since there is no variation in thermal properties in the axial direction.

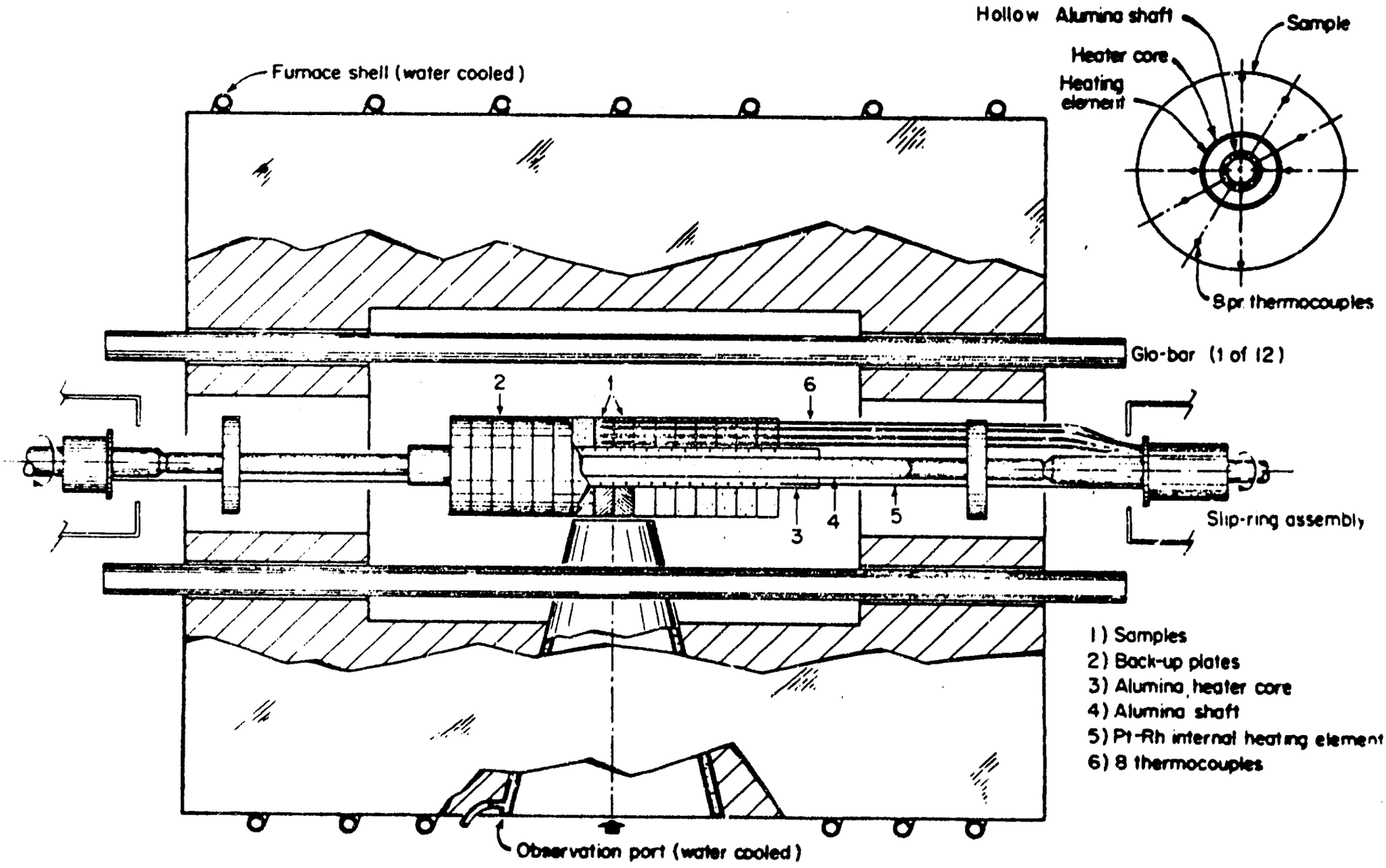

Figure 3.1 Non-Isothermal Emissivity Apparatus.

3.1.1 Internal Heating Element

The internal heating element, producing the non-isothermal condition consists of a Pt-40% Rh alloy resistance element rotating with the samples. This wire element is spirally wound around a one-inch O.D. alumina core. The core is grooved for a ten turns per inch winding and flame sprayed with alumina to cover the resistance wire. The outer surface is ground true to facilitate assembly of the sample and support plates on the heating element. The power for this heater is supplied to the rotating element through two slip-ring assemblies located on the drive shafts at either end of the furnace.

3.1.2 Internal Cooling Apparatus

The internal cooling of the emissivity samples is accomplished by forcing compressed air through the hollow alumina support shaft and stainless steel shafts. The alumina shaft is sealed to the stainless steel shafts by means of o-rings and set screws (Fig. 3.2). The compressed air supply can be regulated to flow air through the shaft at from 0-15 psi, which in turn controls the amount of heat transferred away from the specimen. Gradients which have been established under steady state conditions for alumina samples are shown in Fig. 3.3.

Cracking of the back-up plates when subjected to an increase in cooling air flow while at temperature was a major problem. In order to avoid cracking, it was necessary to flow the cooling air at the chosen rate at all times. This eliminated the complete fracture of both sample and back-up plates, but did not totally eliminate cracking.

3.1.3 Measurement of Temperature Gradient

The sample temperature and temperature distribution were measured by a series of thermocouples, four in each sample. The thermocouple junctions were arranged in a radial spiral covering an arc of 90° to avoid possible thermal interaction which might have resulted if a single radial line were used. Two samples were normally run simultaneously, requiring one set of thermocouples to pass completely through the sample nearest the slip ring assembly.

Thermocouple elements of chromel-alumel sheathed in inconel tubing or platinum-rhodium sheathed in platinum tubing were used. For temperatures above 1000°C, platinum-rhodium elements

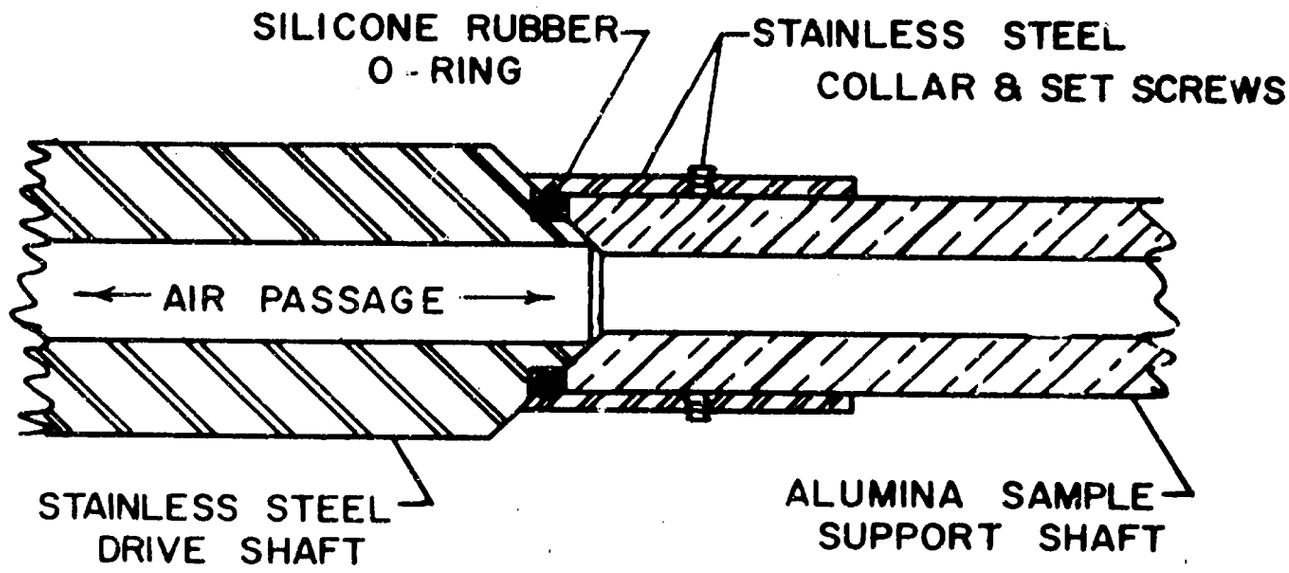

Figure 3.2 Seal Design Between Stainless Steel Shaft and Alumina Shaft.

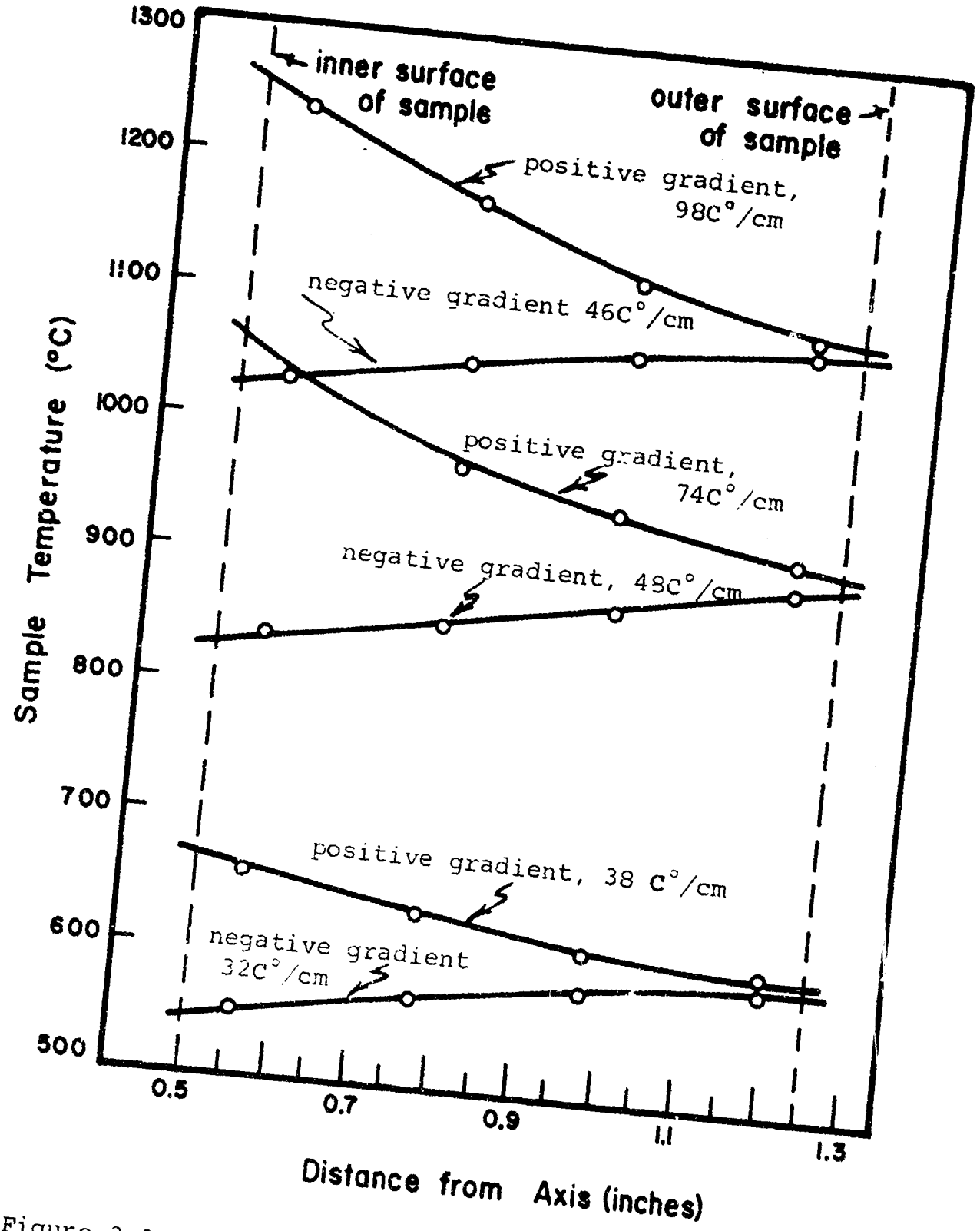

Figure 3.3 Temperature of Sample versus Distance From Axis During Non-Isothermal Furnace Operation. Sample Aℓ-4.

were used exclusively. A Leeds and Northrup K-3 potentiometer was used to measure the thermocouple EMF. A low-noise slip-ring assembly transferred the thermocouple signal from the rotating shaft to the potentiometer.

The maximum outer surface temperature achieved under non-isothermal conditions was approximately 1100°C (1373°K) for both negative and positive temperature gradients. At this outer surface temperature, the gradient achieved with the inner surface at a higher temperature than the outer surface (positive gradient) was 98 C°/cm. The negative gradient achieved at this surface temperature was 46C°/cm. At a surface temperature around 905°C (1178°K), the maximum positive gradient was 74 C°/cm and the maximum negative gradient was 46 C°/cm. The maximum positive gradient was 38 C°/cm and the maximum negative gradient was 32 C°/cm at 605°C (878°K).

3.2 Emissivity Measurement

The optical system used for non-isothermal emissivity measurement is shown in Fig. 3.4. Input to the spectrometer chopper comes (a) from the sample and (b) from a blackbody furnace (described in reference 2) maintained at a temperature close to the surface temperature of the sample.

Because the blackbody used during the non-isothermal measurements is not an integral part of the emissivity sample, temperature control and corrections for temperature differences become critical. A difference in temperature of 5° between two blackbodies at 1000°K causes difference in emitted energy of 5% at a wavelength of one micron. This means that temperature must be accurately controlled as discussed in reference (2). Otherwise, emitted energy differences due to inaccurate temperature control will be a significant contribution to the total non-isothermal radiant energy measured.

In the measurements reported here, temperature differences between the blackbody and sample surface were maintained at less than 2°C (2% error at $\lambda = 1\ \mu$; < 0.5% error at $\lambda > 4\ \mu$).

In order to obtain a direct measure of the influence of temperature gradients in the sample, each sample was measured under (a) isothermal, (b) positive temperature gradient, and (c) negative temperature gradient at the same surface temperature. Results were then analyzed directly as the ratio between isothermal and non-isothermal emissivity.

In addition to problems of temperature measurement there are fluctuations in data resulting from the spectrometer

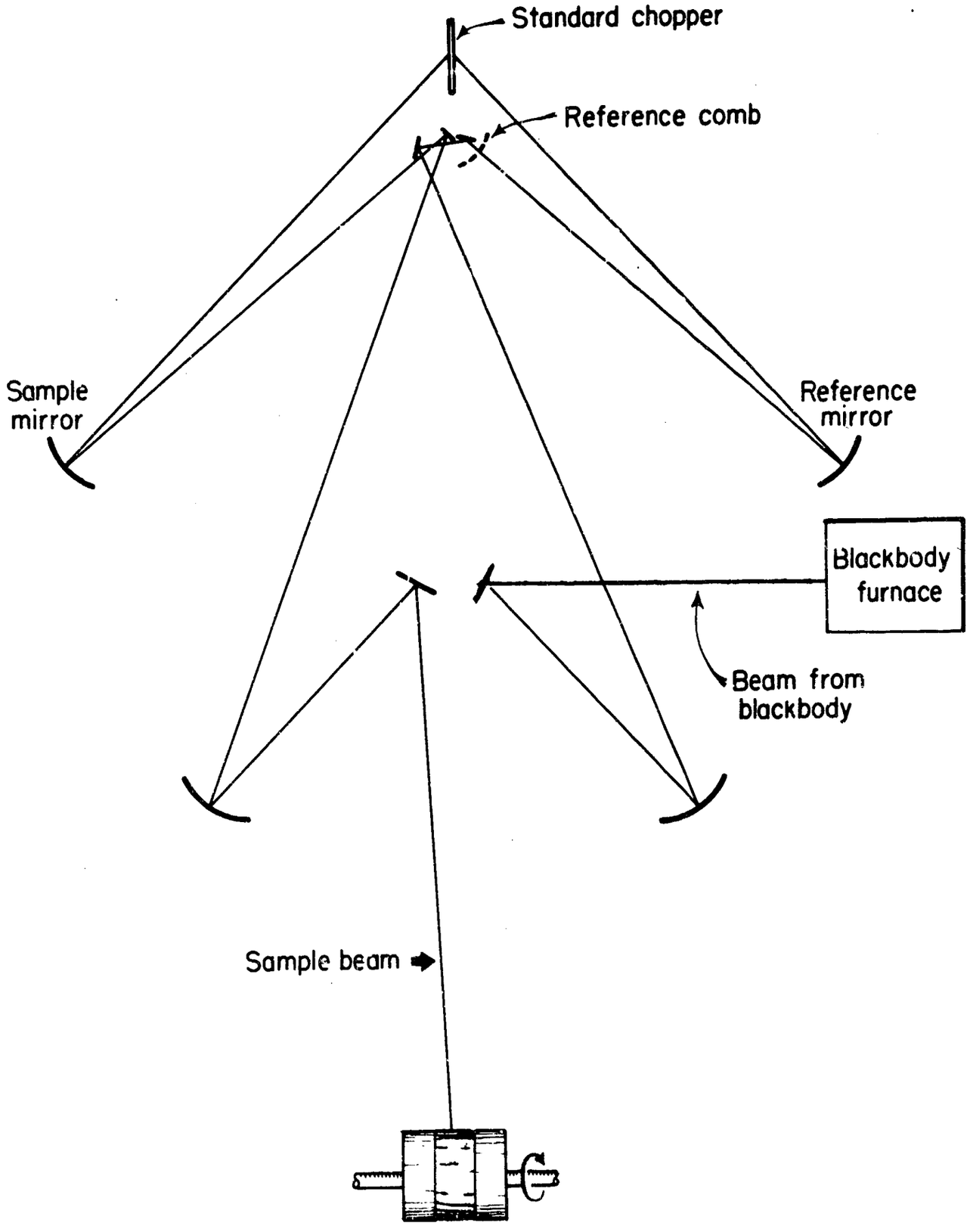

Figure 3.4 Non-Isothermal Optical System.

precision of 0.5% of full scale reading. Thus as discussed previously[2] individual measurements are estimated as having an overall precision of ± 0.01 emissivity units.

3.3 Results

Results of the non-isothermal emissivity measurements are plotted in Figs. 3.5 - 3.24 as the ratio of non-isothermal emissivity (ε_n) to isothermal emissivity (ε_i) versus wavelength (λ). On these figures, calculated values (section 2.3) are also shown. Measurements were run at surface temperatures of approximately 600, 900, and 1100°C for the alumina samples, and at 600 and 900°C for the strontium titanate and Pyroceram specimens. The maximum gradient achieved was 98C°/cm, and the usual gradient 30 to 50 C°/cm.

3.3.1 Aluminum Oxide

Measured and calculated values of the emissivity ratio for the four alumina specimens are shown in Fig. 3.5-3.16.

The measured curves show some deviation from the calculated values over the region 1-5 microns, but the measured ratio is within the estimated accuracy of the measurements.

3.3.2 Strontium Titanate

Measured and calculated results for strontium titanate are shown in Figs. 3.17 - 3.20. The experimental data agrees with the calculated values within the estimated accuracy of the measurements.

3.3.3 Pyroceram 9606 and 9608

The measured values for Pyroceram 9606 and 9608 are shown in Figs. 3.21 - 3.24. These curves have the same general shape as do the alumina and strontium titanate curves.

3.4 Discussion

The spectral region of most interest is over the wavelength range of 1 to 5 microns. For the materials studied, the high scattering coefficients lead to measured isothermal emissivities in the range 0.05 ± 0.01 to 0.25 ± 0.01. At these low values even though the absolute precision is good, the relative error is large (20% - to 4% of the measured value). Similar results are found for the non-isothermal measurements.

Thus when we compare the two as the ratios plotted in Figs. 3.5-3.24 the relative error is the sum of the two, and may be as large as $\pm$ 40% depending on the absolute level of the emissivities involved. The most common absolute values are in the emissivity range 0.15 - 0.20, corresponding to a precision of $\pm$ 15-10% for the ratio.

The assumption that scattering is isotropic in the forward and backward directions was made in the derivation for the intensity of emitted radiation. This assumption is valid only when the size of the scattering centers is small compared to the wavelength of the incoming light, or for large scattering centers compared to the wavelength of the incoming light when the relative index of refraction (m) of the scattering centers is zero (Fig. 3.25). For large pores in alumina, the forward scattering is approximately three times the backward scattering. Therefore the measured non-isothermal to isothermal emissivity ratio is expected to be somewhat greater than the calculated value for a positive temperature gradient, and less than the calculated value for a negative gradient. For strontium titanate, the forward scattering for large pores is about one and one-half times the backward scattering.

In the wavelength region 1-5 microns where emissivity is a volume process, there is agreement between the measured and calculated values within the limits of experimental precision. In all cases with a positive temperature gradient the non-isothermal emissivity is greater than the isothermal value; in all cases with a negative temperature gradient non-isothermal emissivity is smaller than the isothermal value. The differences between the non-isothermal and isothermal values are clearly significant, having ratios as large as 1.35 for the relatively modest temperature gradients imposed.

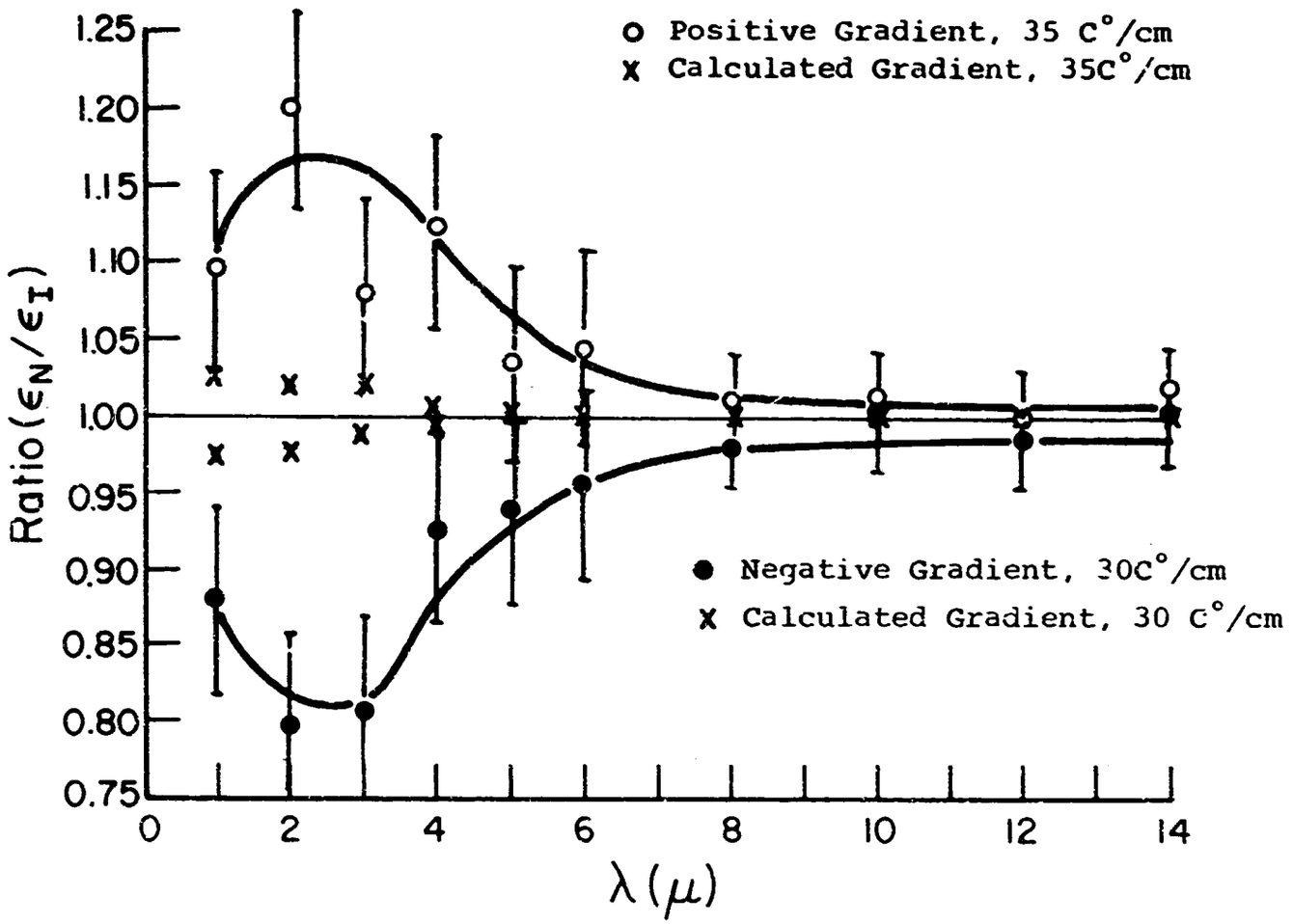

Figure 3.5 Emissivity Ratio vs. Wavelength for AD-995 at approximately 600°C.

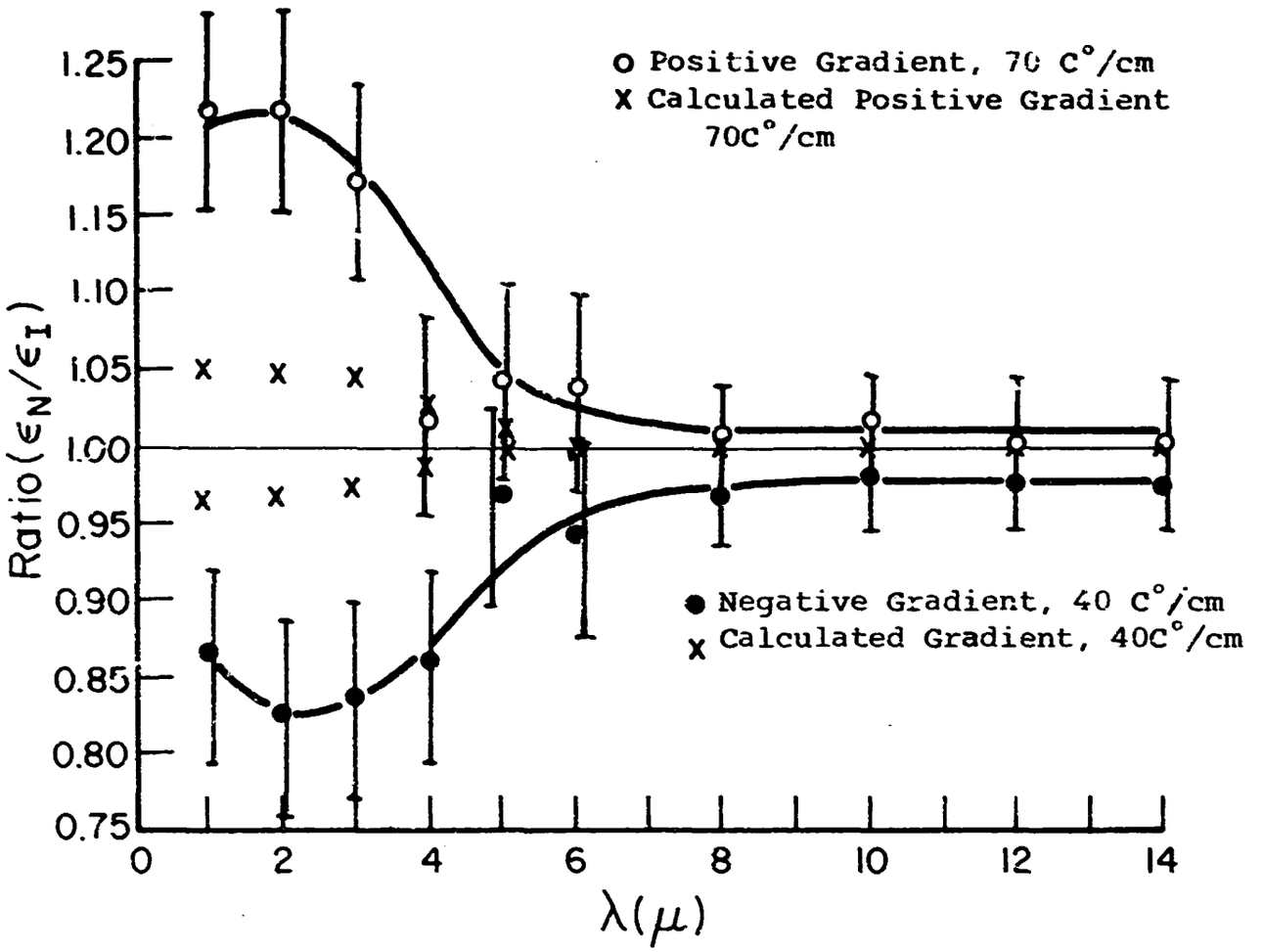

Figure 3.6 Emissivity Ratio vs. Wavelength for AD-995 at approximately 900°C.

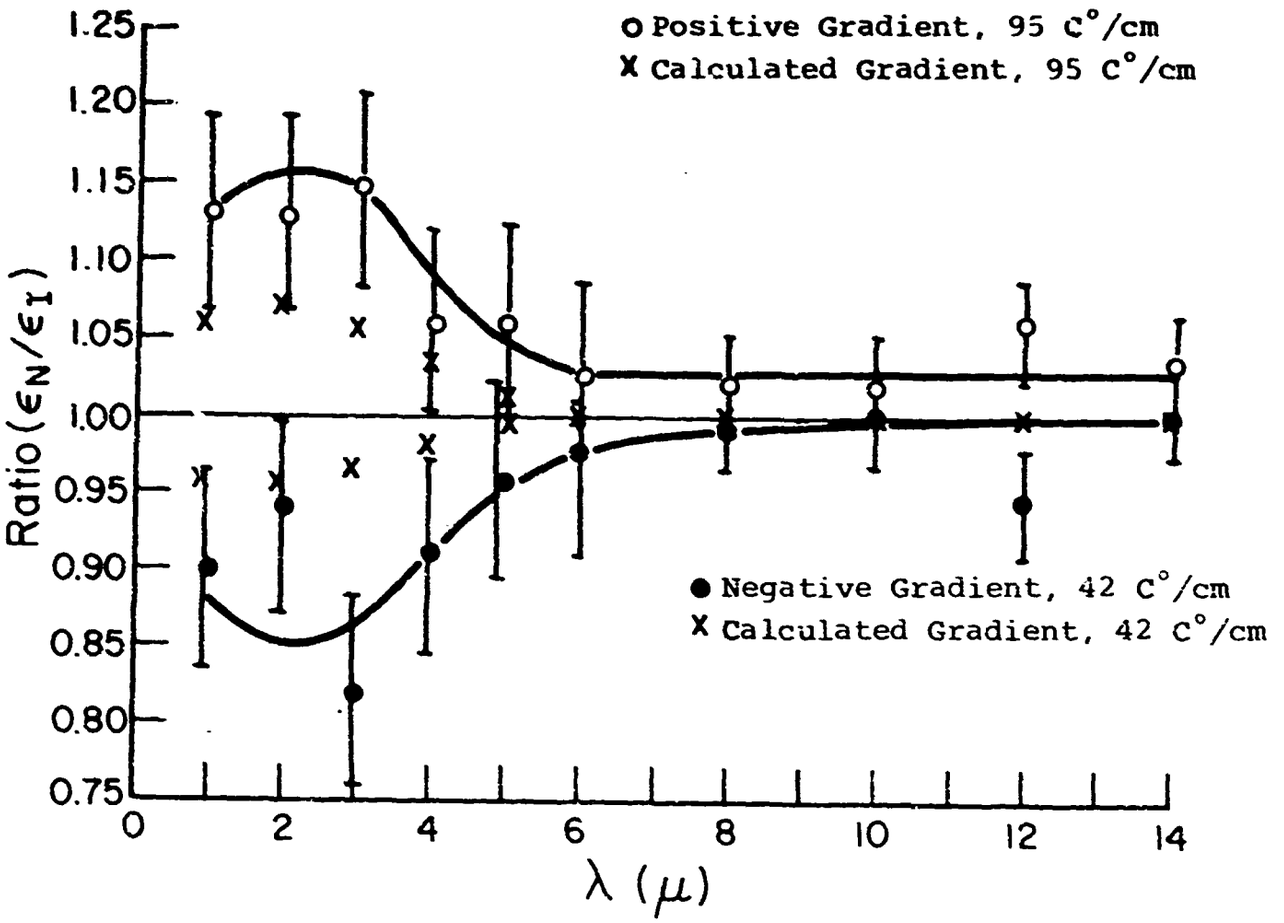

Figure 3.7 Emissivity Ratio vs. Wavelength for AD-995 at approximately 1100°C.

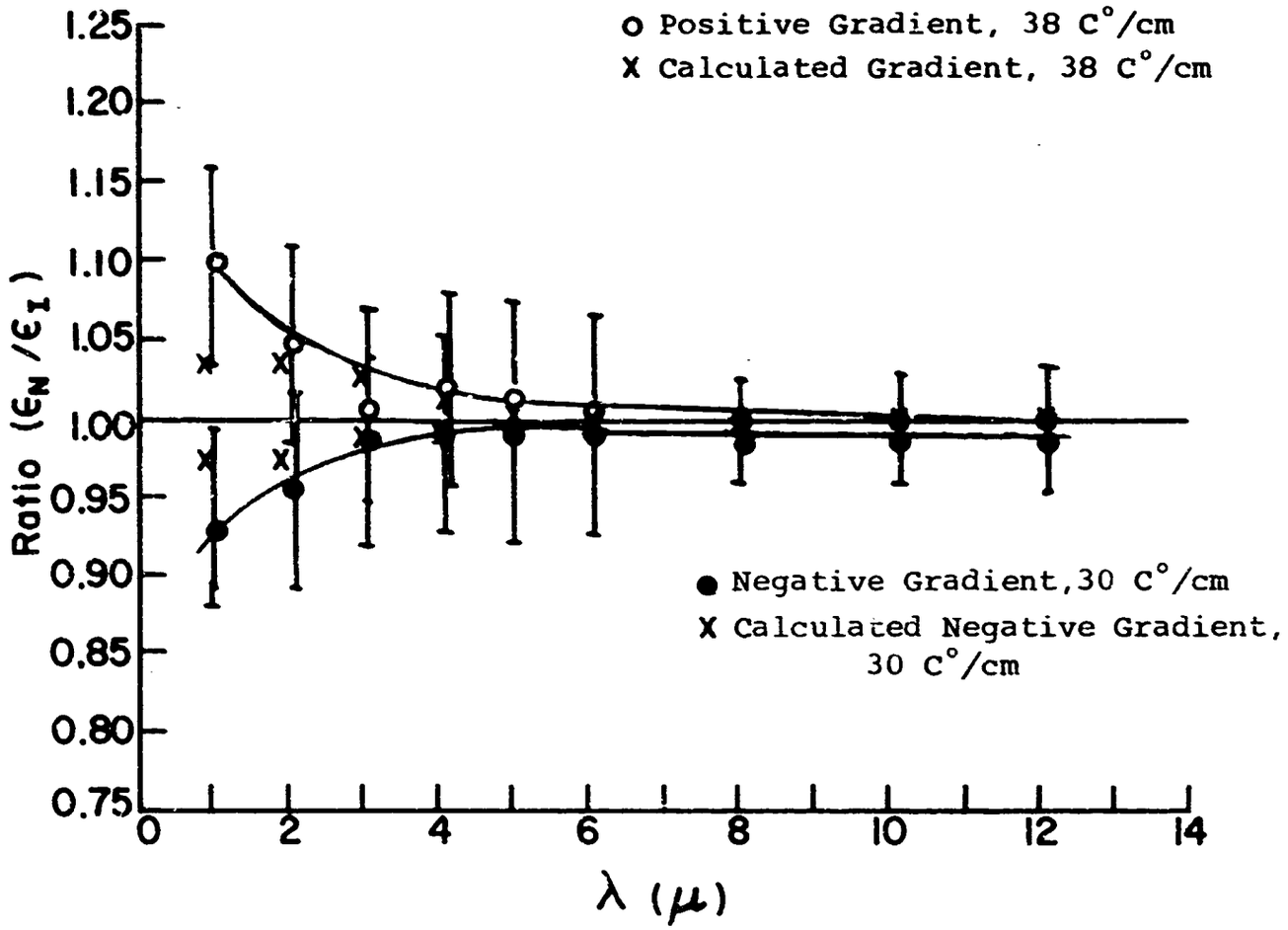

Figure 3.8 Emissivity Ratio vs. Wavelength for AD-85 at approximately 600°C.

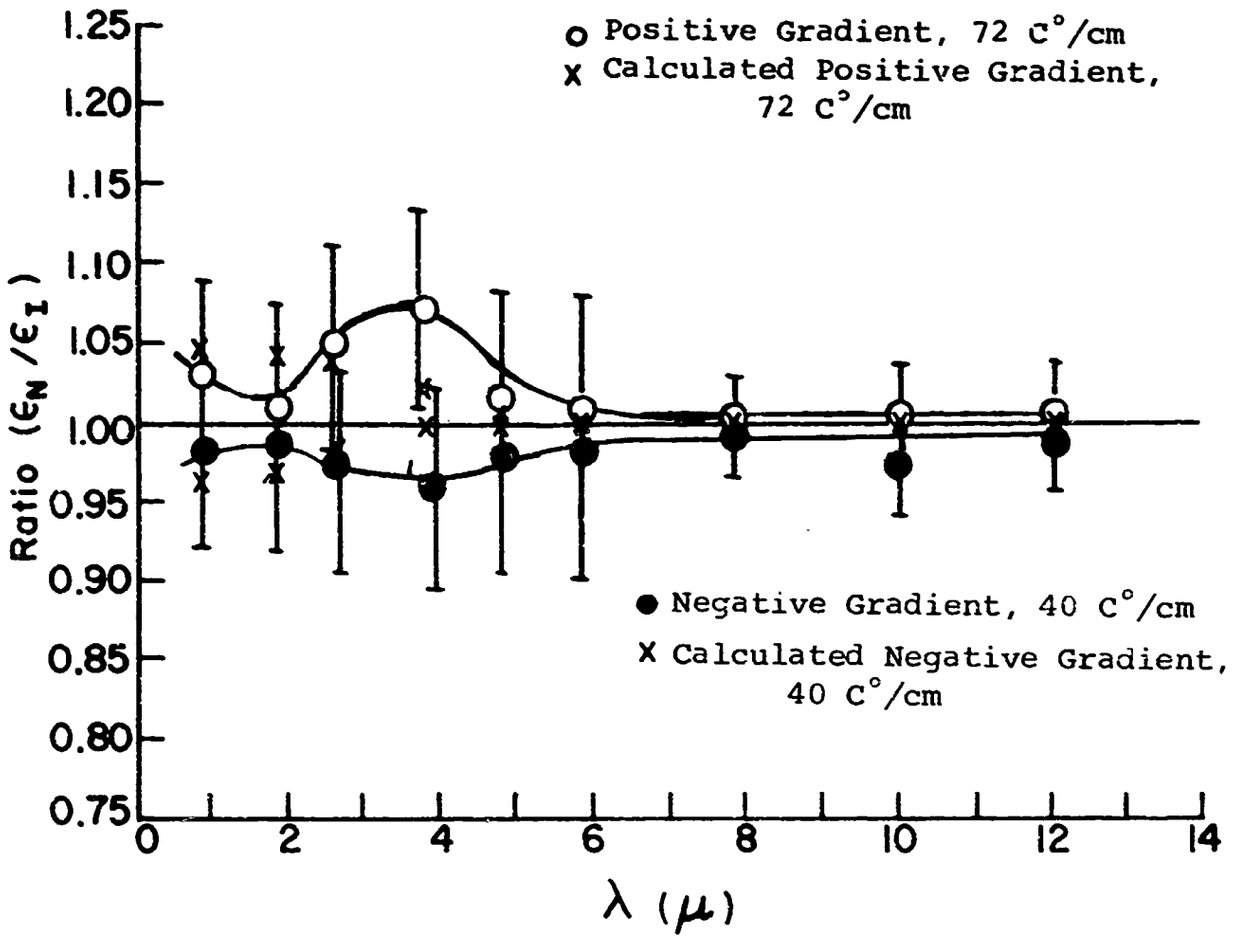

Figure 3.9 Emissivity Ratio vs. Wavelength for AD-85 at approximately 900°C.

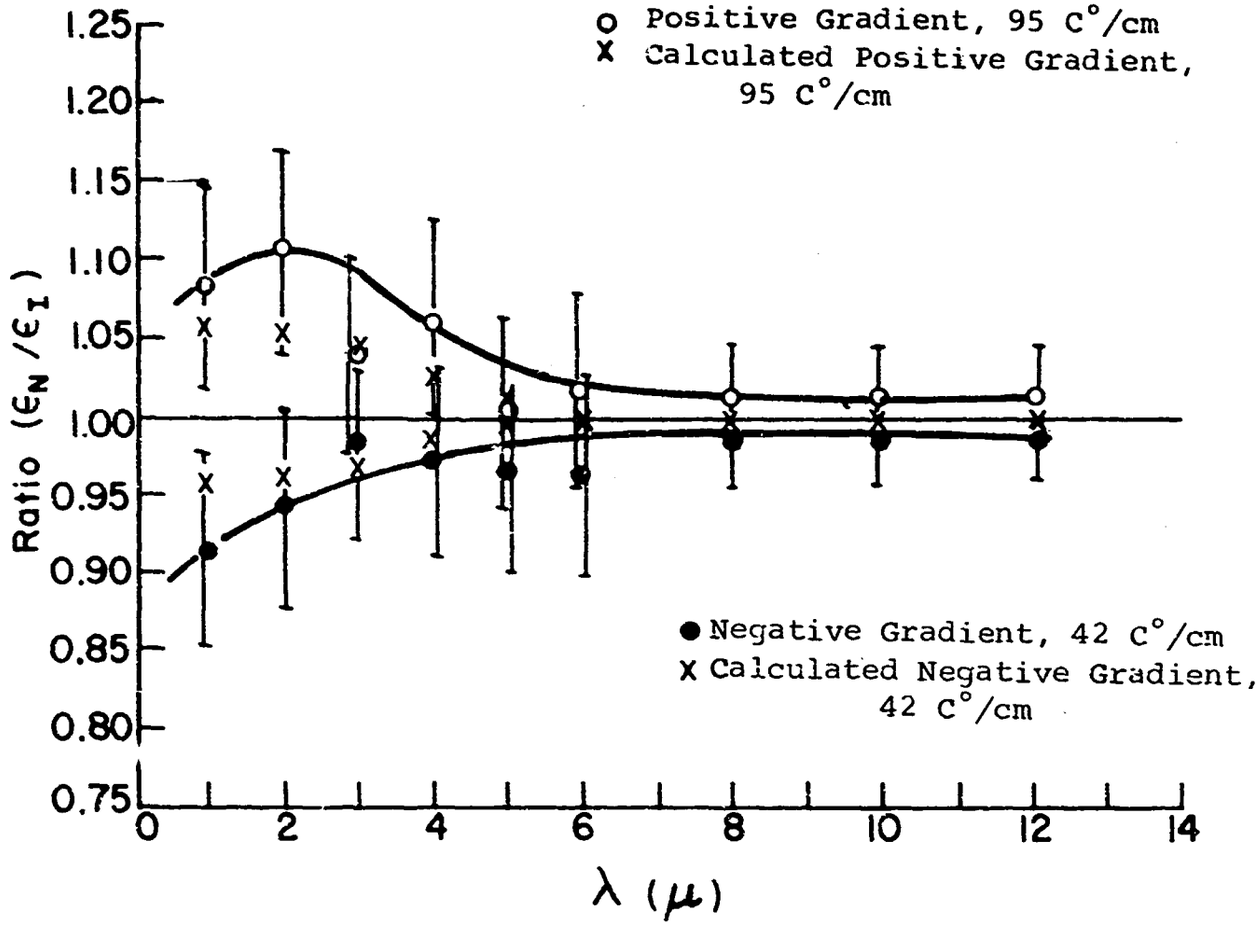

Figure 3.10 Emissivity Ratio vs. Wavelength for AD-85 at approximately 1100°C.

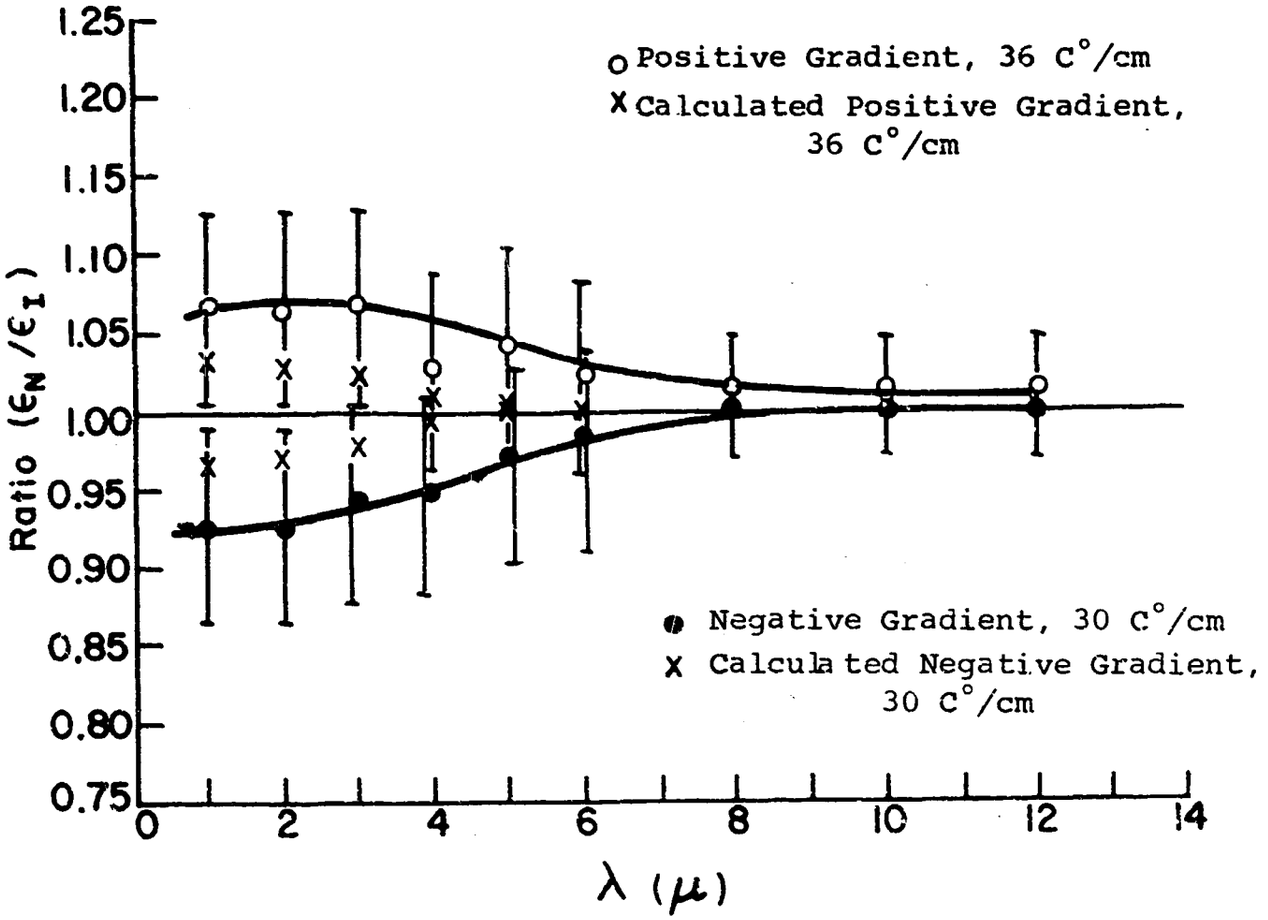

Figure 3.11 Emissivity Ratio vs. Wavelength for Aℓ-1 at approximately 600°C.

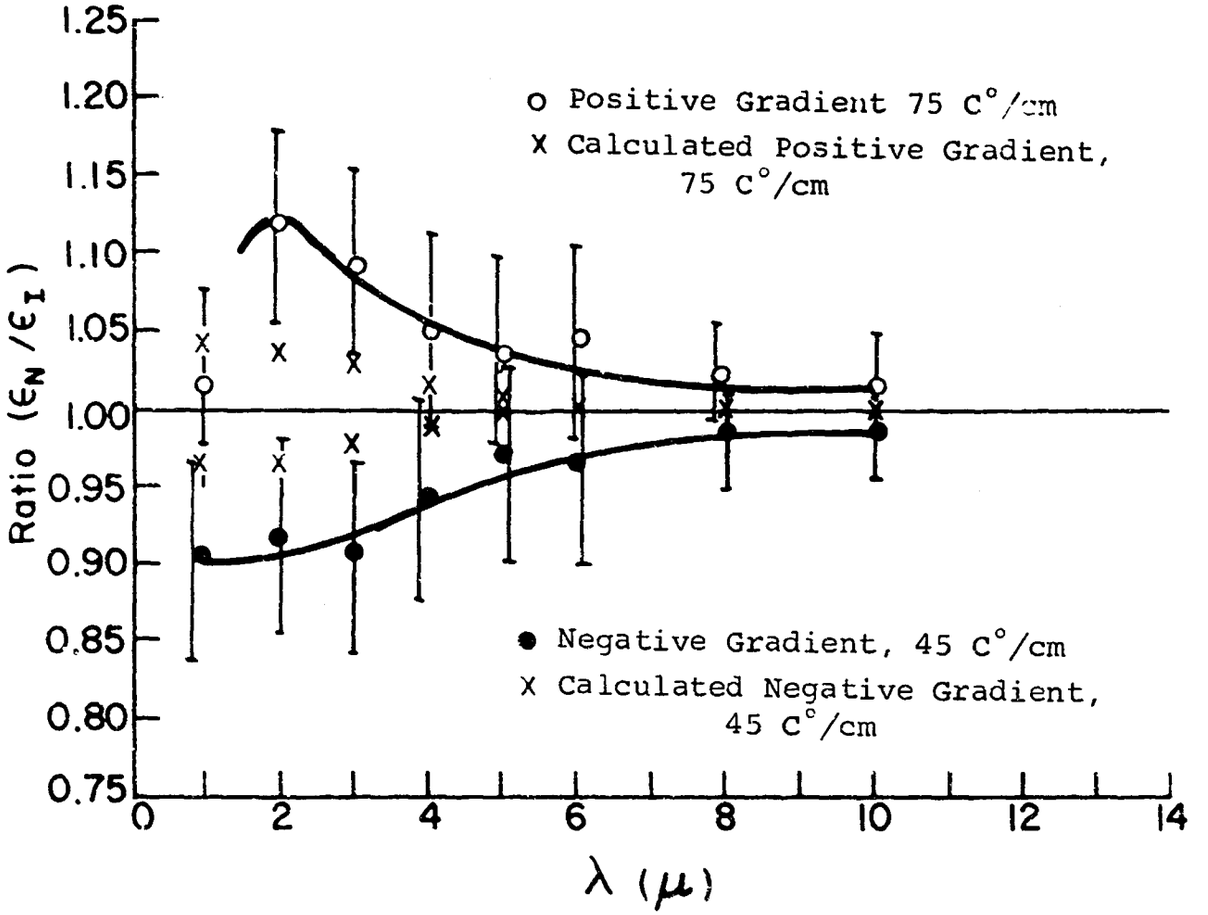

Figure 3.12 Emissivity Ratio vs. Wavelength for Aℓ-1 at approximately 900°C.

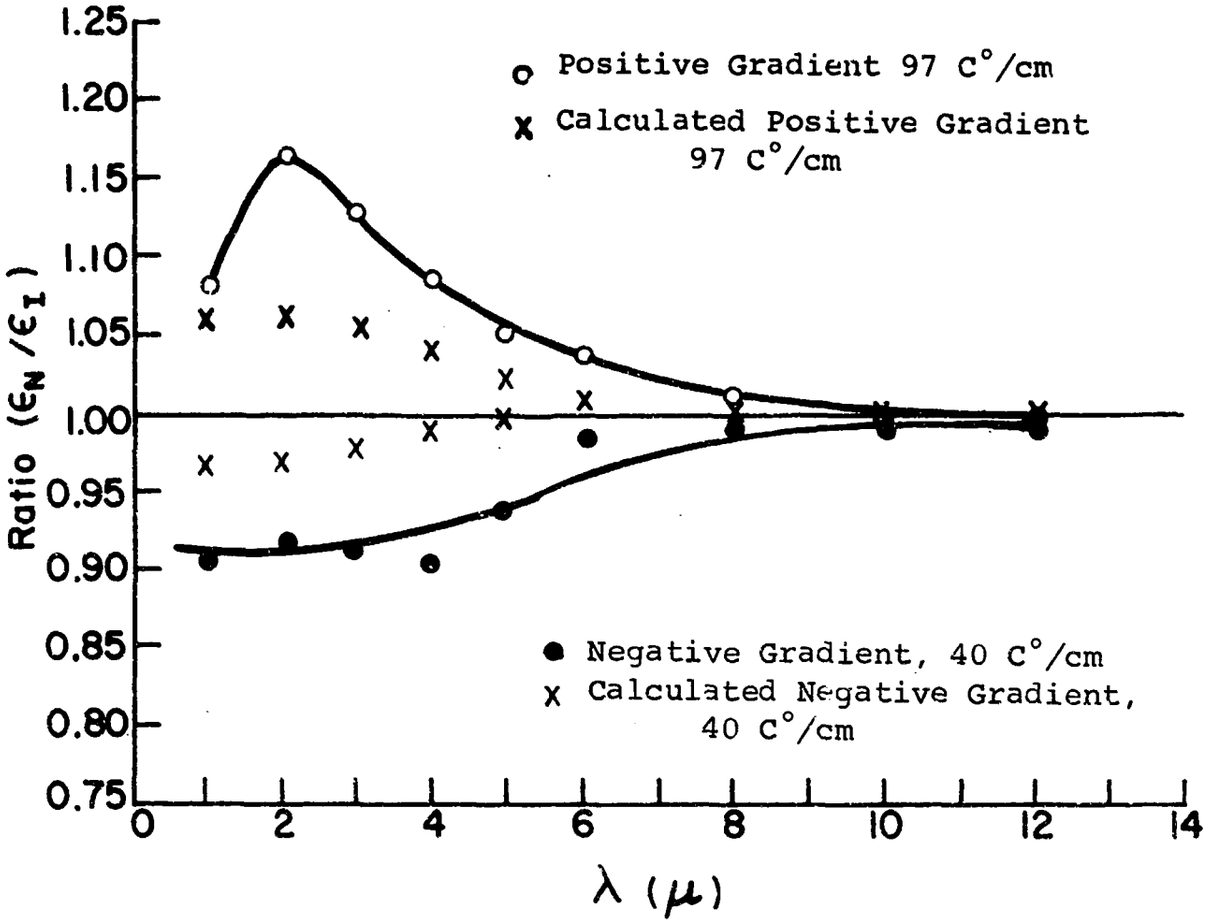

Figure 3.13 Emissivity Ratio vs. Wavelength for Aℓ-1 at approximately 1100°C.

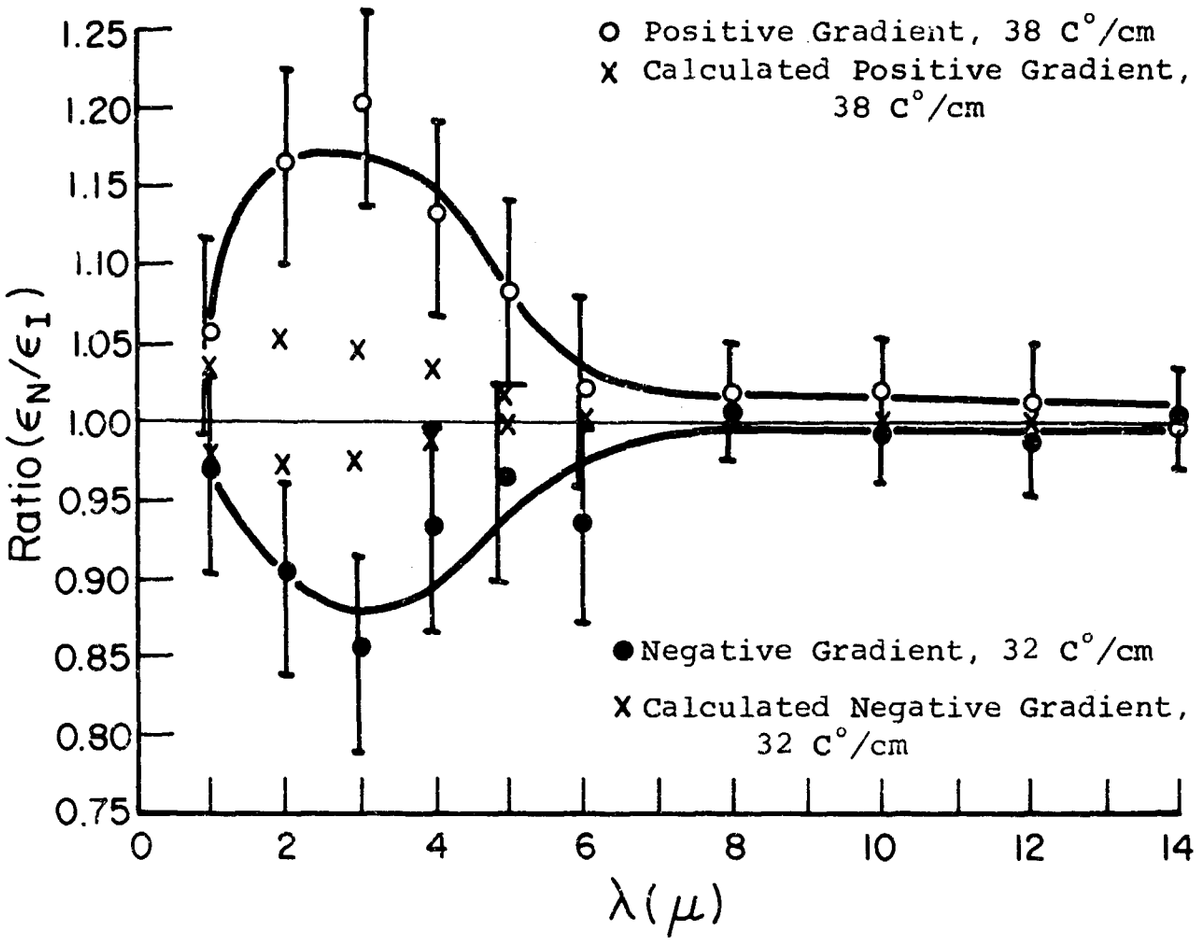

Figure 3.14 Emissivity Ratio vs. Wavelength for Aℓ-4 at approximatelv 600°C.

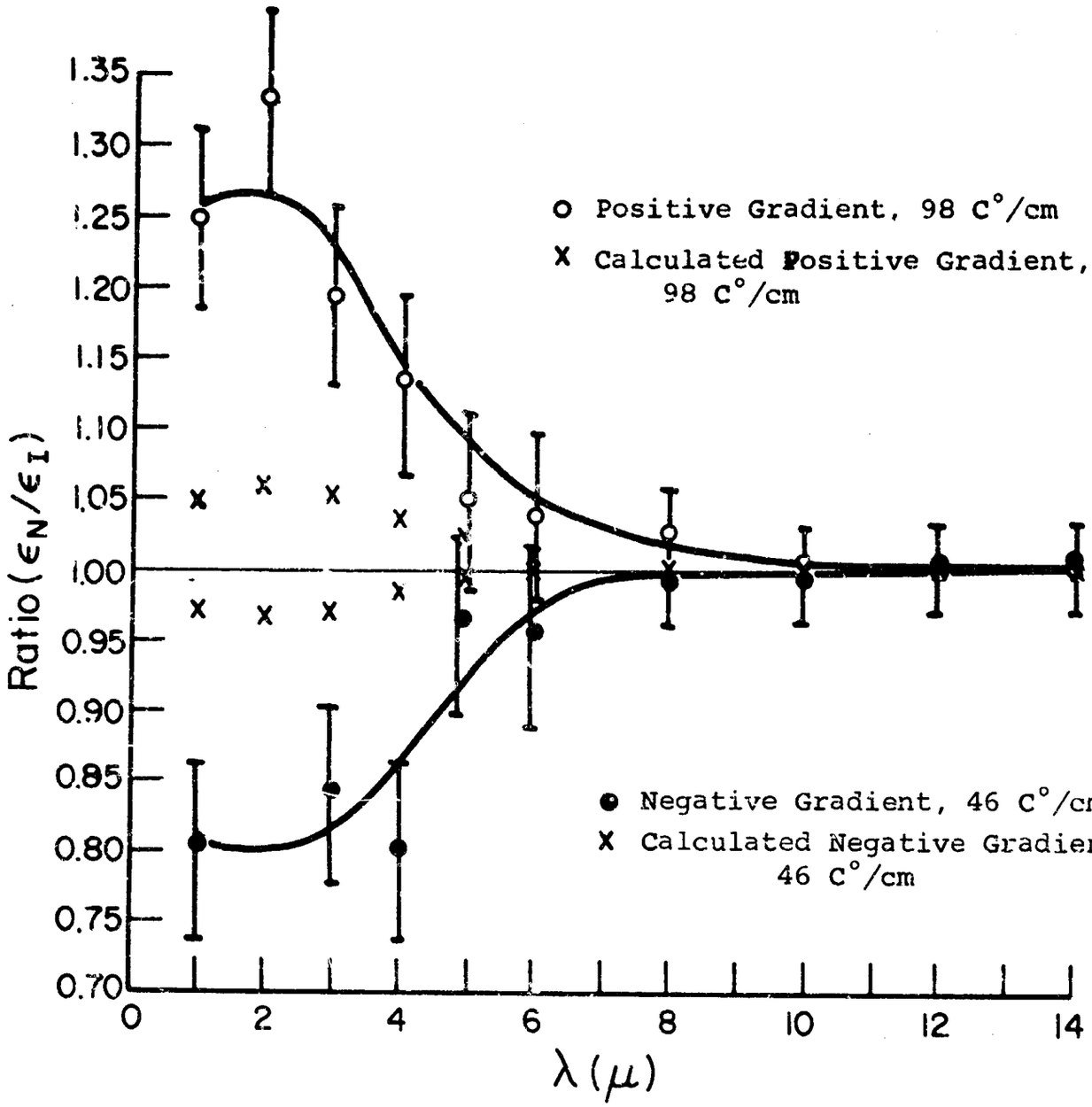

Figure 3.15 Emissivity Ratio vs. Wavelength for Al-4 at approximately 900°C.

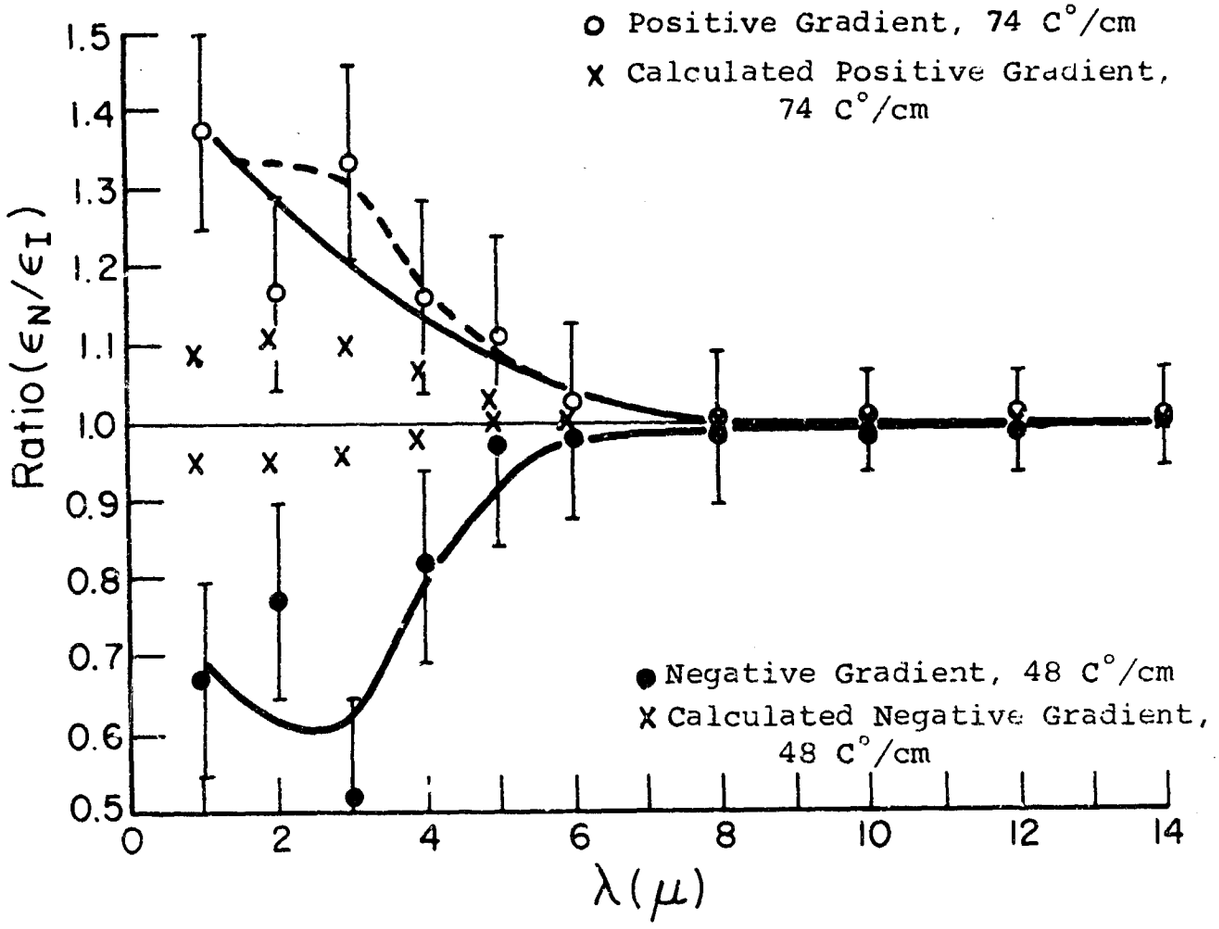

Figure 3.16 Emissivity Ratio vs. Wavelength for Aℓ-4 at approximately 1100°C.

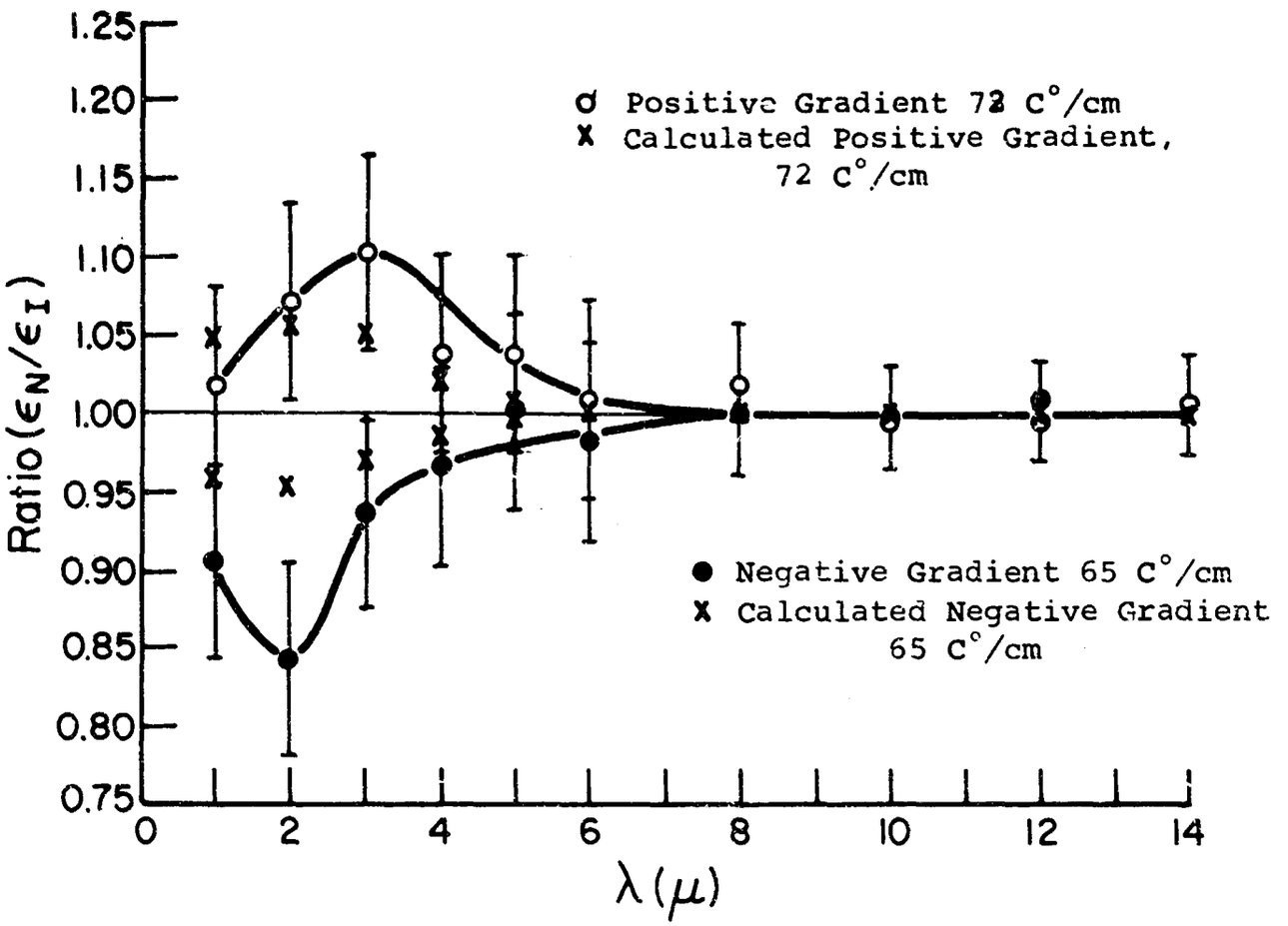

Figure 3.17 Emissivity Ratio vs. Wavelength for $SrTiO_3A$ at approximately 600°C.

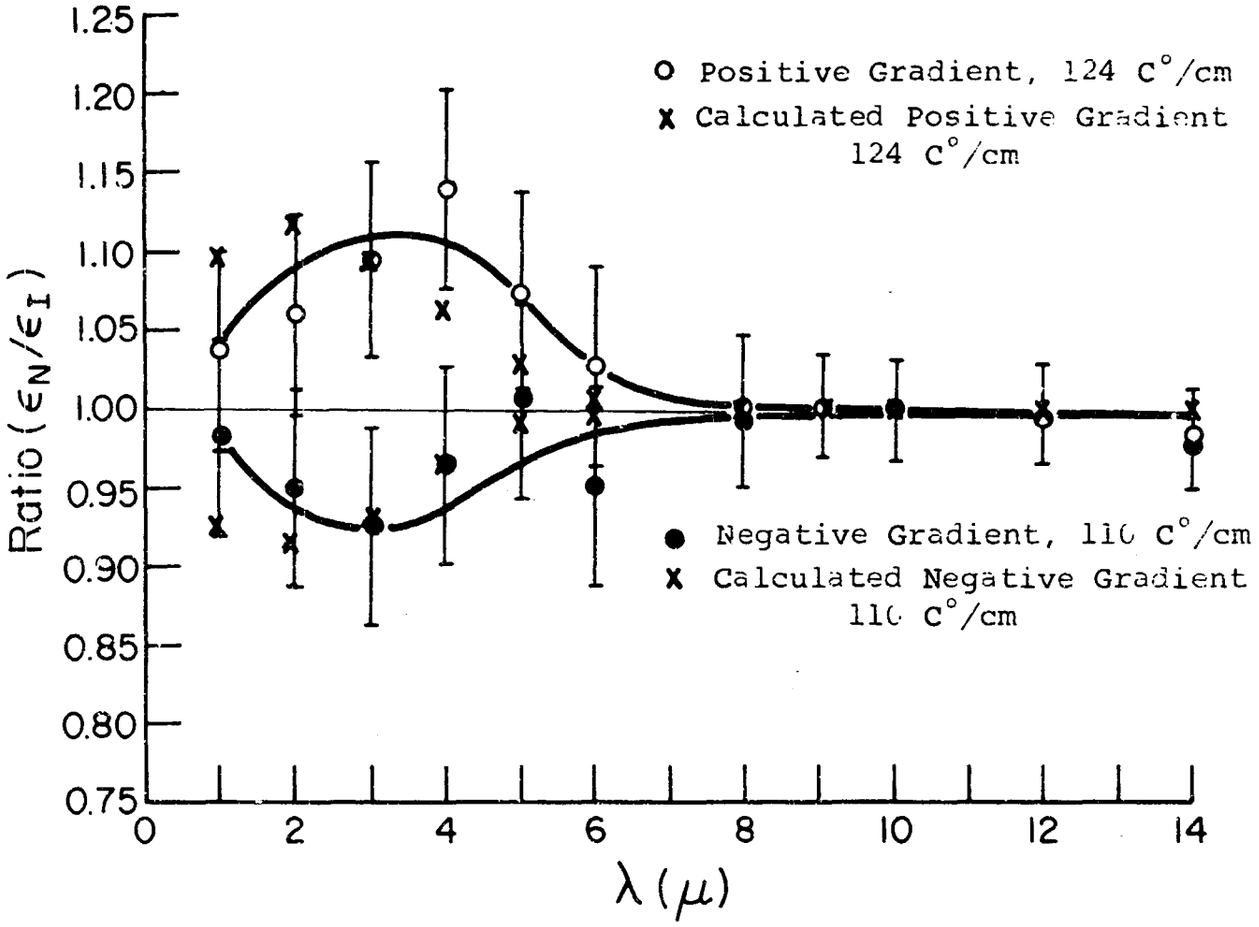

Figure 3.18 Emissivity Ratio vs. Wavelength for $SrTiO_3A$ at approximately 900°C.

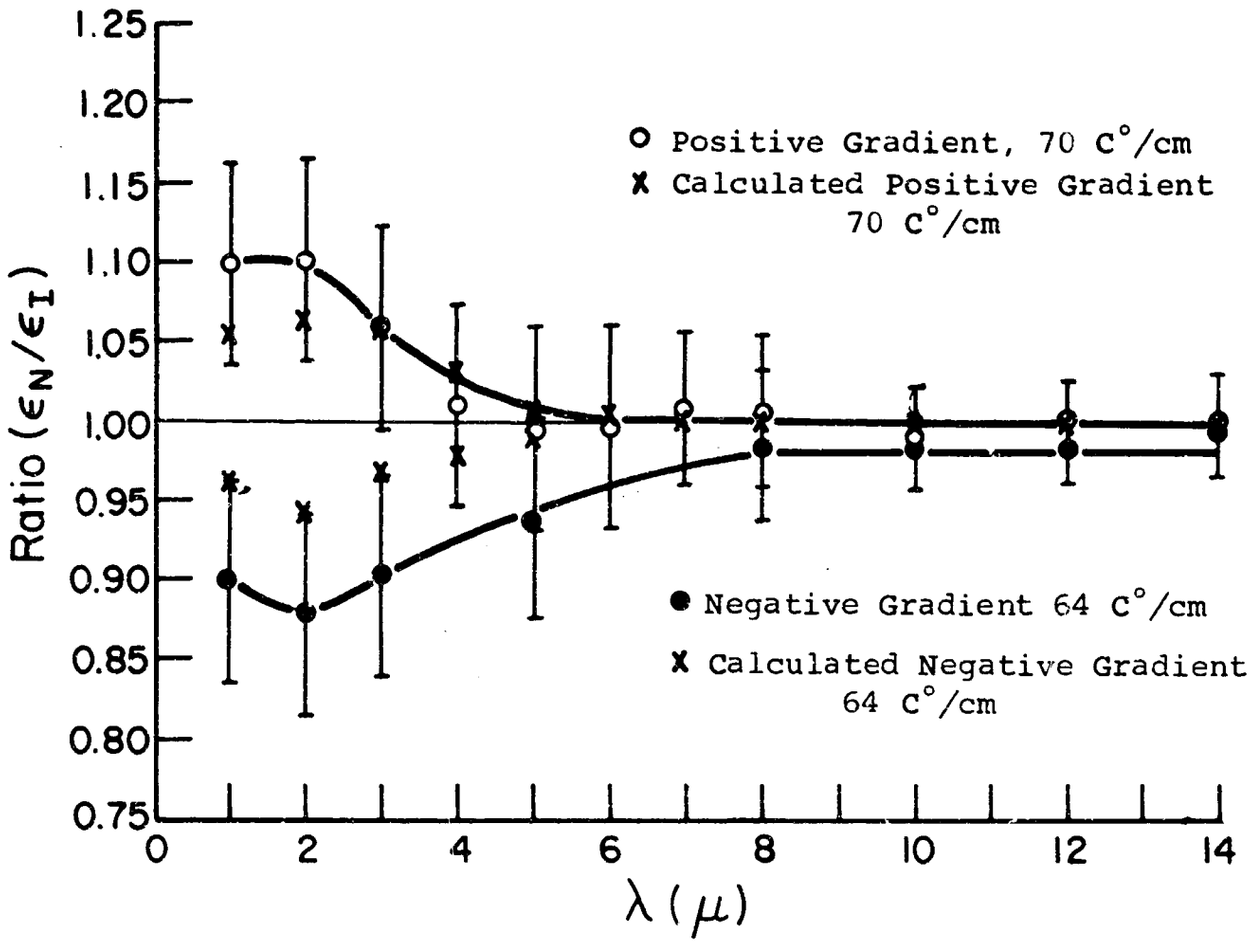

Figure 3.19 Emissivity Ratio vs. Wavelength for $SrTiO_3B$ at approximately 600°C.

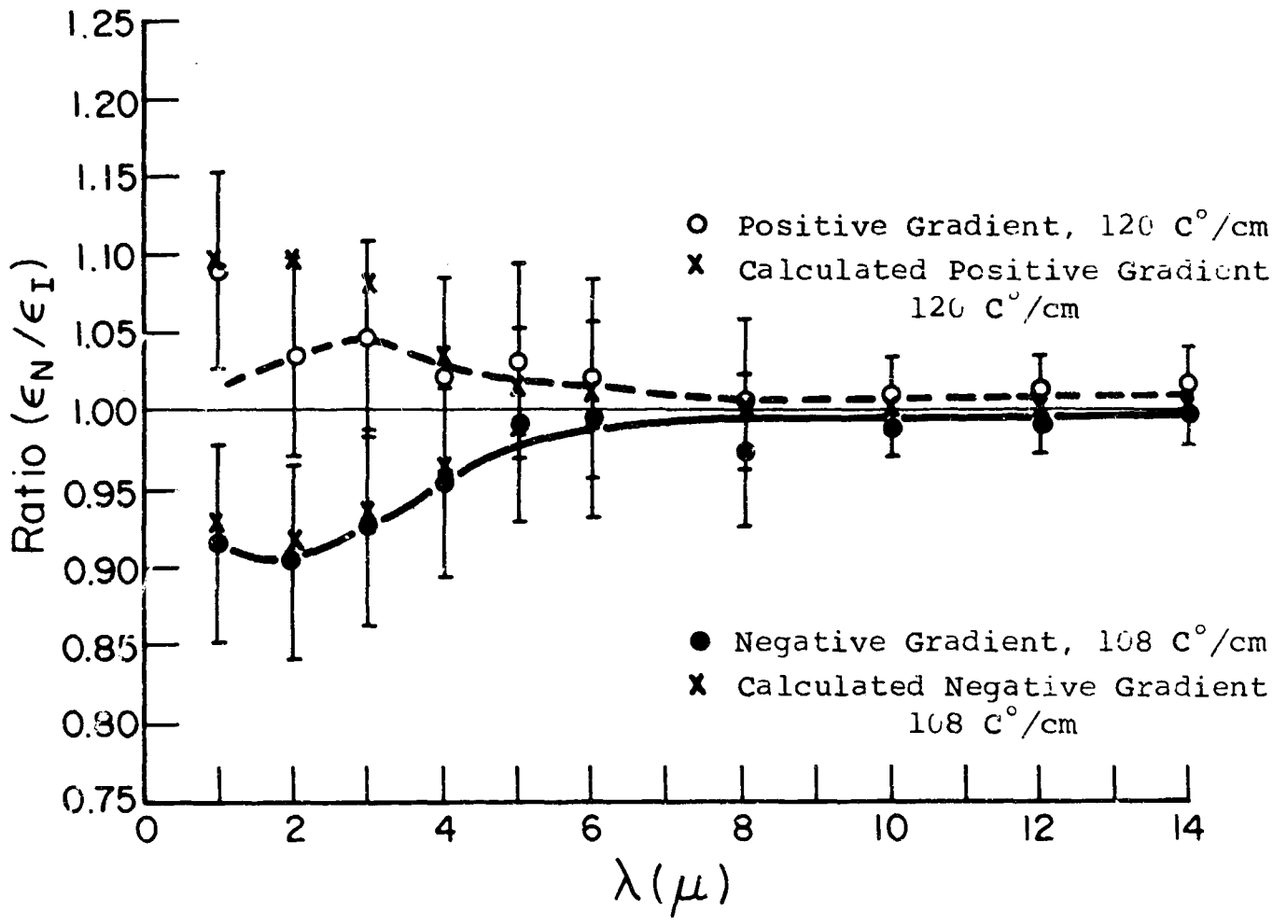

Figure 3.20 Emissivity Ratio vs. Wavelength for $SrTiO_3B$ at approximately 900°C.

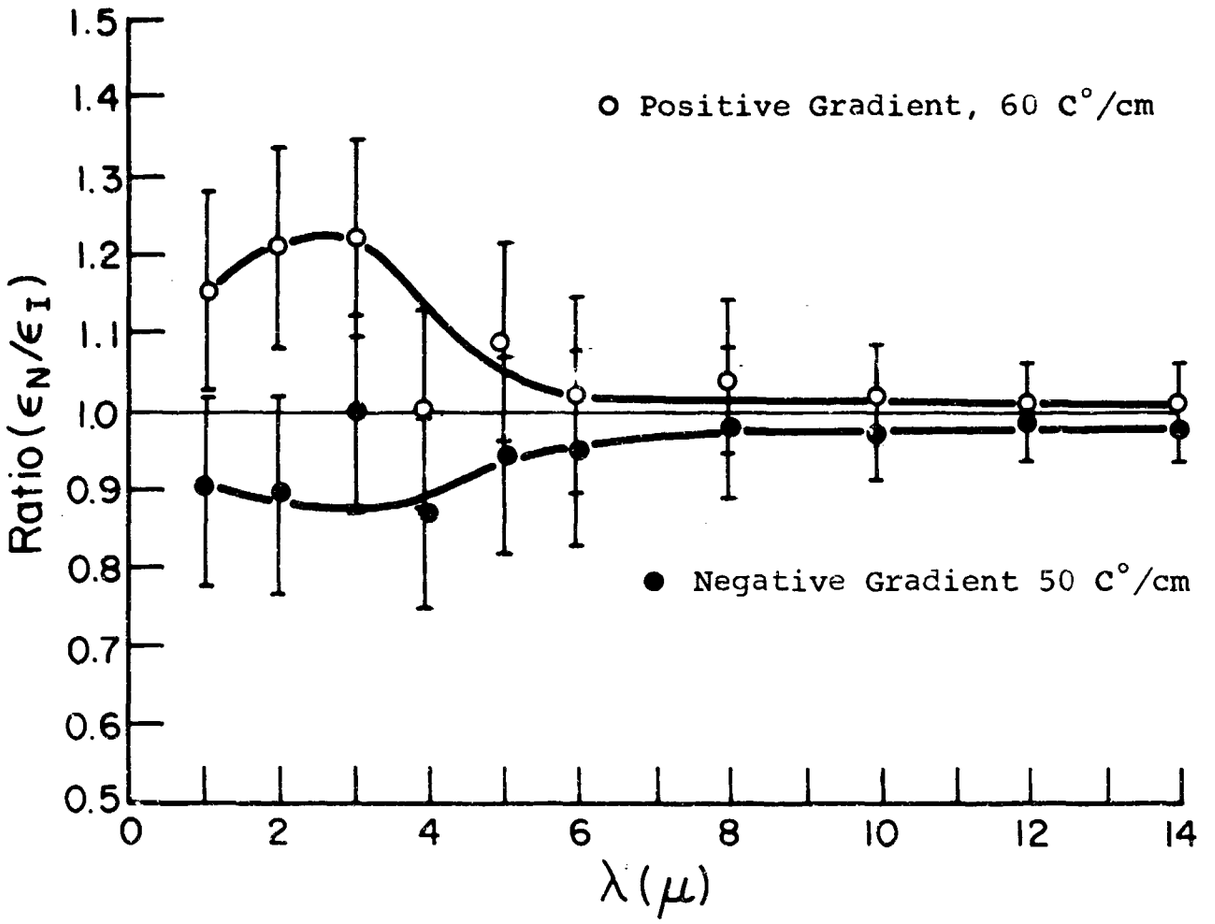

Figure 3.21 Emissivity Ratio vs. Wavelength for Pyroceram 9606 at approximately 600°C.

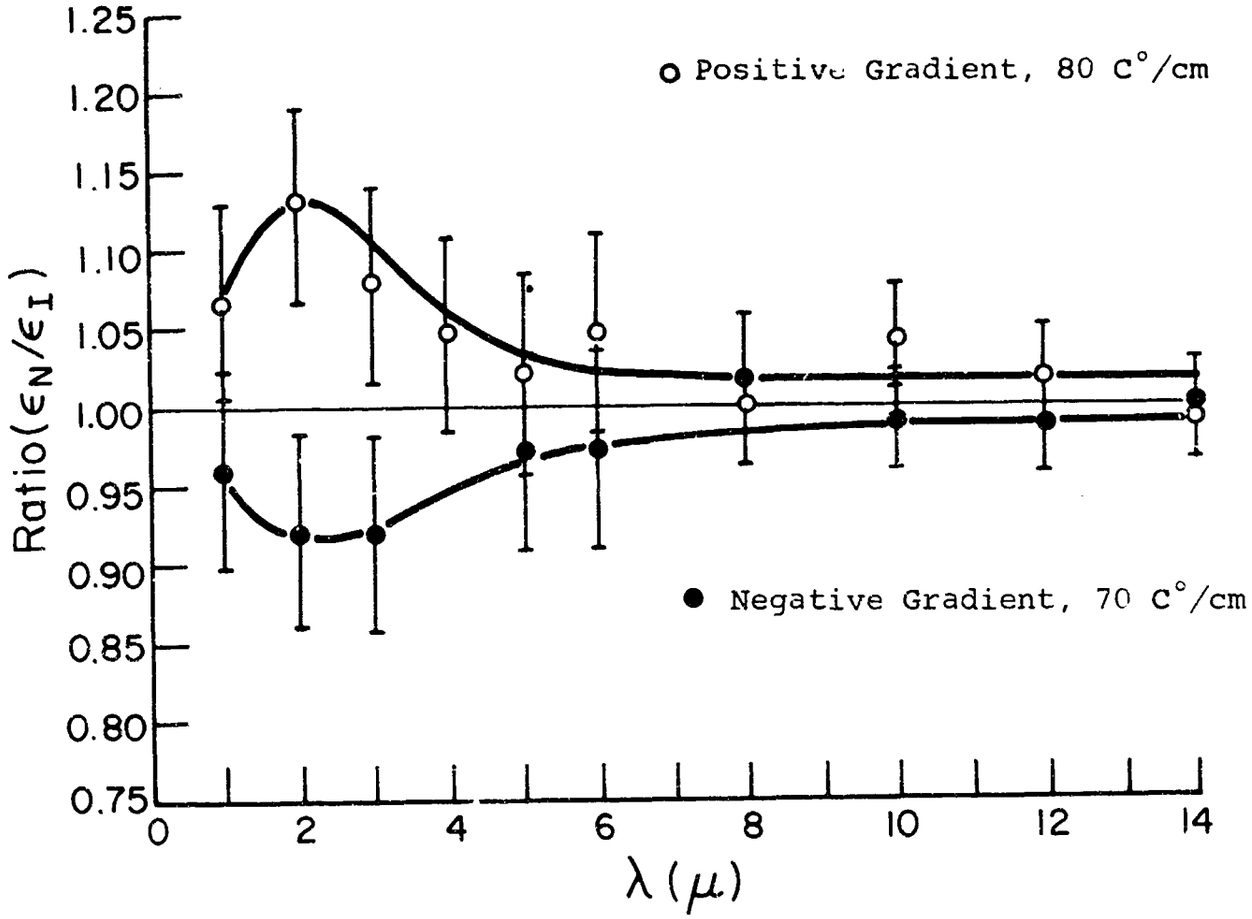

Figure 3.22 Emissivity Ratio vs. Wavelength for Pyroceram 9606 at approximately 900°C.

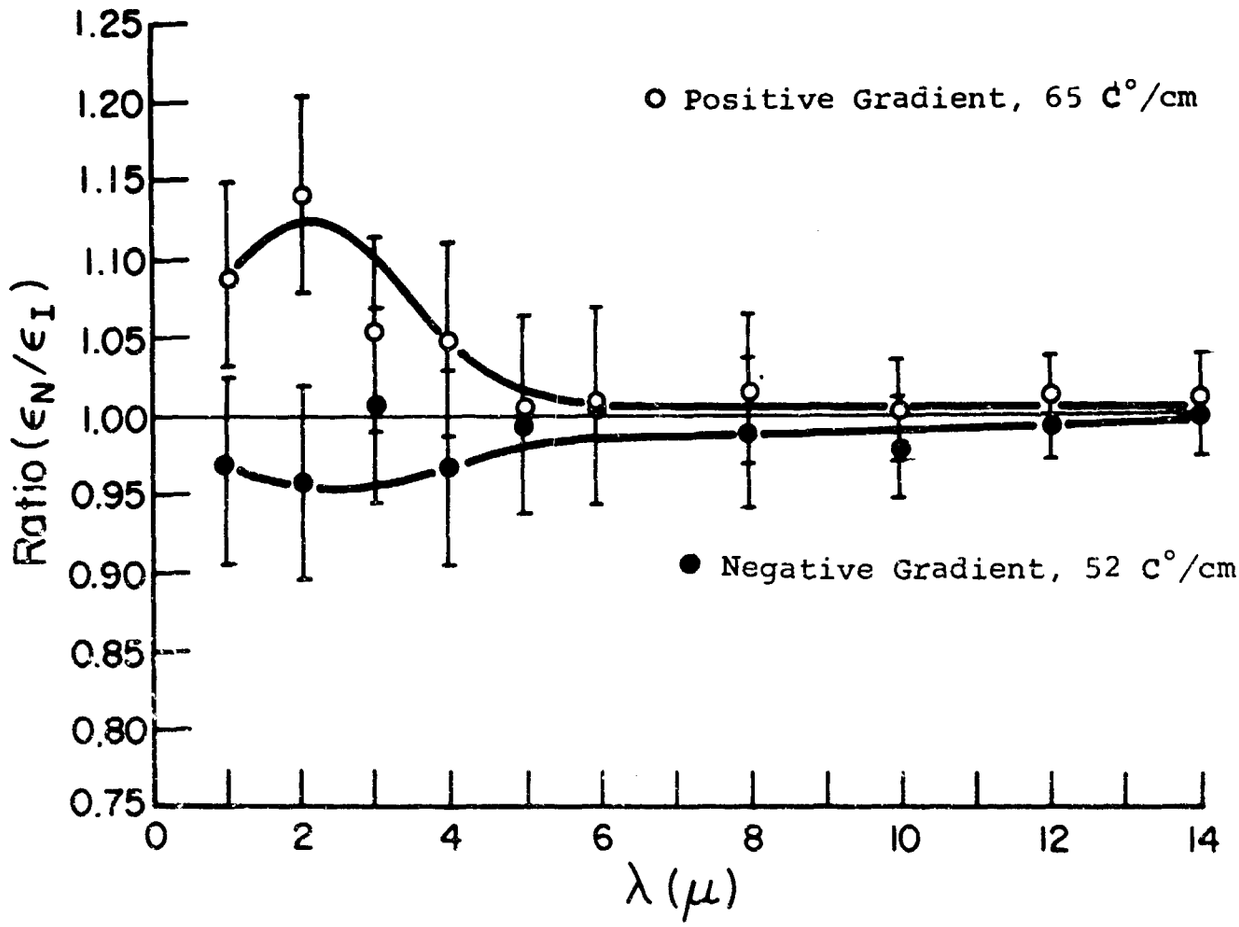

Figure 3.23 Emissivity Ratio vs. Wavelength for Pyroceram 9608 at approximately 600°C.

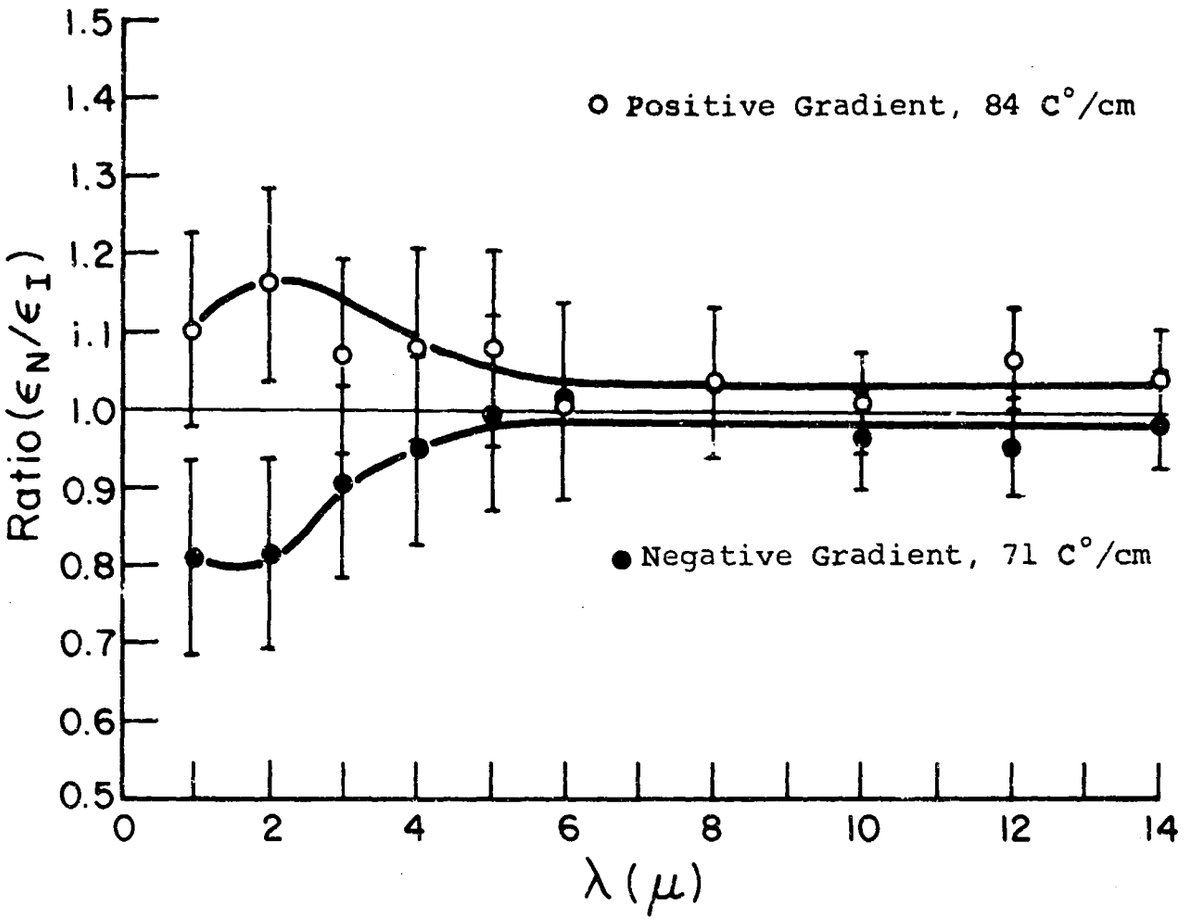

Figure 3.24 Emissivity Ratio vs. Wavelength for Pyroceram 9608 at approximately 900°C.

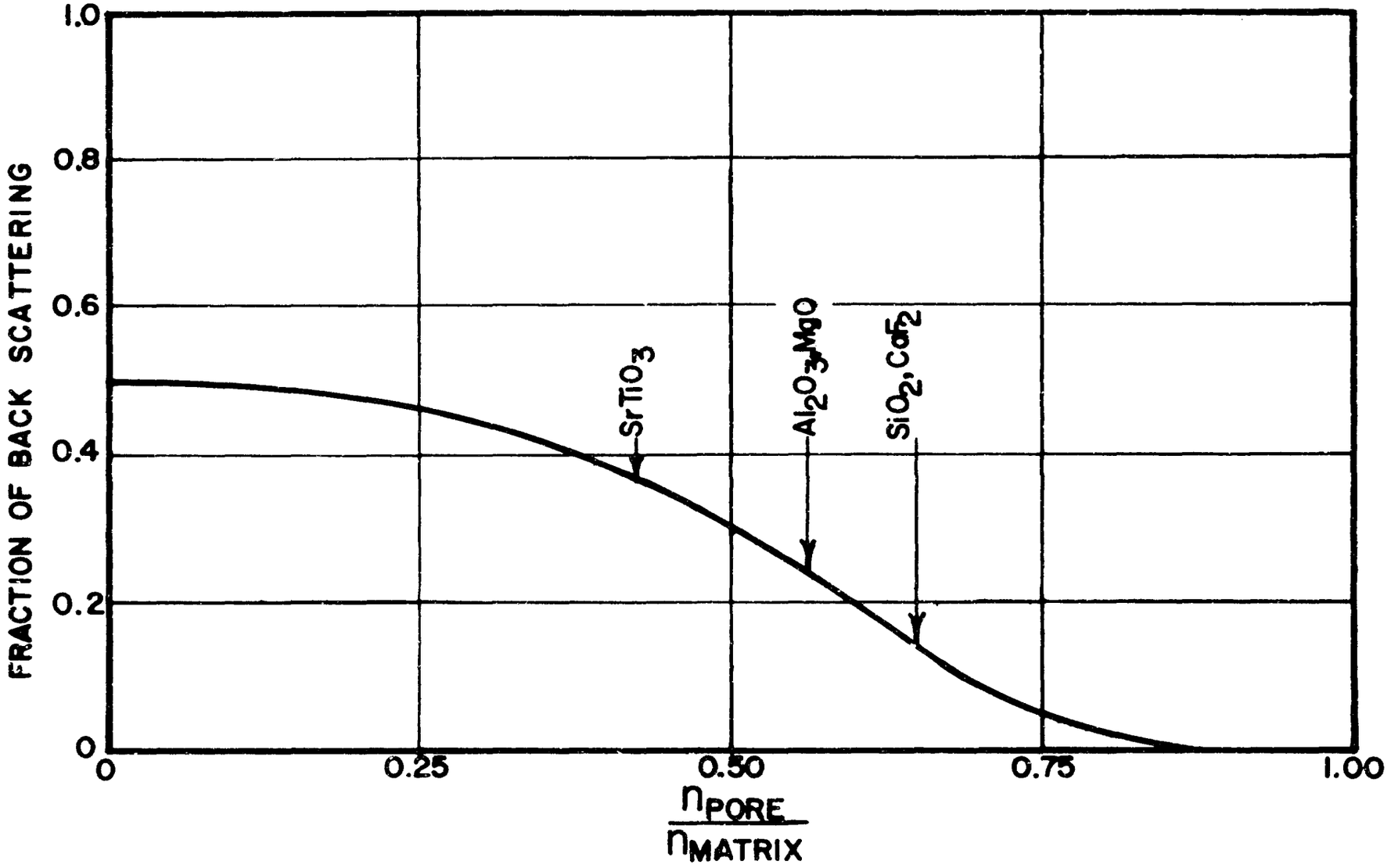

Figure 3.25 Relative Fraction of Back Scattering for Pores of Large Size in a Solid Matrix.

4.0 TRANSMISSION OF RADIANT ENERGY THROUGH A MATERIAL WITH ABSORPTION AND SCATTERING

When a beam of parallel light is incident normally upon a thin slab containing scattering centers, the emerging light may consist of both parallel and diffuse light. The differential equations describing this system have been formulated and solved by Ryde[3]. Some of Ryde's equations have been reproduced here to have them available in the notation used in this report.

The equations for the forward and backward diffuse flux are:

$$\frac{dI}{dx} = f' I_p - (a + s) I + sJ \tag{4.1}$$

$$-\frac{dJ}{dx} = s' I_p - (a + s) J + sI \tag{4.2}$$

and for the forward and backward parallel flux:

$$\frac{dI_p}{dx} = -(a + s' + f') I_p = -g' I_p \tag{4.3}$$

$$-\frac{dJ_p}{dx} = -(a + s' + f') J_p = -g' J_p \tag{4.4}$$

The solutions to these equations obtained by Ryde[3] are:

$$I_p = K \exp(-g'x) \tag{4.5}$$

$$J_p = M \exp(g'x) \tag{4.6}$$

$$I = A(1 - \beta_o)\exp(\sigma_o x) + B(1 + \beta_o)\exp(-\sigma_o x) - U \exp(-g'x) \tag{4.7}$$

$$J = A(1 + \beta_o)\exp(\sigma_o x) + B(1 - \beta_o)\exp(-\sigma_o x) - V \exp(-g'x) \tag{4.8}$$

where $$U = \frac{ss' + f'(a + s + g')}{g'^2 - \sigma_o^2} \tag{4.9}$$

$$V = \frac{sf' + s'(a + s - g')}{g'^2 - \sigma_o^2} \qquad (4.10)$$

and K, M, A, and B are determined by the boundary conditions.

If the amount of parallel light passing through the specimen is large (i.e., very thin sample and very small scattering coefficient), then equations 4.1 and 4.2 are not correct, but must contain a term representing the scattering from the parallel flux in the negative x-direction. This flux in the (-x) direction is caused by reflection from the sample-air interface where the beam is emerging from the sample. These conditions and the differential equations are treated in Appendix III.

For the case where the sample is sufficiently thick and the scattering coefficient large, the intensity of the transmitted diffuse and parallel light beams may be solved as follows:

1) Consider the case wherein the index of refraction of the medium containing the scattering centers is the same as the index outside the medium. Then there are no reflections, and the boundary conditions for diffuse light for a beam of parallel light of unit intensity incident normally on the medium are

1) at $x = o$, $I = o$, $J = R'$ (4.11)

2) at $x = d$, $I = T' - I_p$, $J = o$ (4.12)

where T' is the total light transmitted both parallel and diffuse and R' is the amount reflected. Then a system of four equations in terms of A, B, T', and R' may be solved for A, B, T', and R'. These equations are:

$$A(1 - \beta_o) + B(1 + \beta_o) = U \qquad (4.13)$$

$$A(1 + \beta_o) + B(1 - \beta_o) - R' = V \qquad (4.14)$$

$$A(1 - \beta_o)\exp(\sigma_o d) + B(1 + \beta_o)\exp(-\sigma_o d) - T' =$$

$$(U - 1)\exp(-g'd) \qquad (4.15)$$

$$A(1 + \beta_o)\exp(\sigma_o d) + B(1 - \beta_o)\exp(-\sigma_o d) =$$

$$V\exp(-g'd) \qquad (4.16)$$

Therefore:

$$\Delta = 2(1 + \beta_o^2)\ \sinh \sigma_o d + 4\beta_o \cosh \sigma_o d \qquad (4.17)$$

$$A = \frac{1}{\Delta}\{U(1 - \beta_o)\exp(-\sigma_o d) - V(1 + \beta_o)\exp(-g'd)\} \qquad (4.18)$$

$$B = \frac{1}{\Delta}\{V(1 - \beta_o)\exp(-g'd) - U(1 + \beta_o)\exp(\sigma_o d)\} \qquad (4.19)$$

It is not necessary to solve for T' and R', since equation (4.6) does not contain either R' or T'. Substituting A and B into equation (4.7) - (4.7)

$$I_{x=d} = \frac{1}{\Delta}\{(1 - \beta_o)\ U(1 - \beta_o)\exp(-\sigma_o d)\exp(\sigma_o d) -$$

$$(1 - \beta_o)\ V(1 + \beta_o)\exp(-g'd)\exp(\sigma_o d) +$$

$$(1 + \beta_o)\ V(1 - \beta_o)\exp(-g'd)\ \exp(-\sigma_o d) -$$

$$(1 + \beta_o)\ U(1 + \beta_o)\exp(\sigma_o d)\exp(-\sigma_o d)\} -$$

$$U\exp(-g'd) \qquad (4.20)$$

$$I_{x=d} = \frac{1}{\Delta}\{4\beta_o U + V(1 - \beta_o^2)\exp(-g'd)\ \sinh \sigma_o d\} -$$

$$U\exp(-g'd) \qquad (4.21)$$

and for parallel light

$$I_{p_{x=d}} = \exp(-g'd) \qquad (4.22)$$

2) Next, consider the case where there are reflections from the surfaces of the specimen. For the parallel segment, the boundary conditions are (Fig. 4.1):

1) $x = d,\ J_p = I_p \rho_{ni} \approx 0$ (4.23)

2) $x = o,\ I_p = (1 - \rho_{no})$ (4.24)

$\therefore\ I_{p_{x=d}} = (1 - \rho_{no}) \exp(-g'd)$ (4.25)

For the diffuse portion:

$$I_{x=d} = (1 - \rho_{no}) \left[\frac{1}{\Delta} \{4\beta_o U + V(1 - \beta_o^2) \exp(-g'd) \sinh \sigma_o d\} - U \exp(-g'd)\right] \quad (4.26)$$

The intensity of the light emerging from the surface is:

1) For parallel light $I^*_{p_{x=d}} = (1 - \rho_{ni}) I_{p_{x=d}} =$

$$(1 - \rho_{ni})(1 - \rho_{no}) \exp(-g'd) \quad (4.27)$$

or $I^*_{p_{x=d}} = (1 - \rho_{ni})^2 \exp(-g'd)$ (4.28)

2) For diffuse light $I^*_{x=d} = (1 - \rho_i) I_{x=d}$ (4.29)

or $I^*_{x=d} = (1 - \rho_i)(1 - \rho_{no}) \left[\frac{1}{\Delta} \{4\beta_o U + V(1 - \beta_o^2) \exp(-g'd) \sinh \sigma_o d\} - U \exp(-g'd)\right]$ (4.30)

Since the intensity of the incident light was taken as unity, $I^*_{p_{x=d}}$ and $I^*_{x=d}$ are the transmissivities, τ_p and τ_d of the material for parallel and diffuse light.

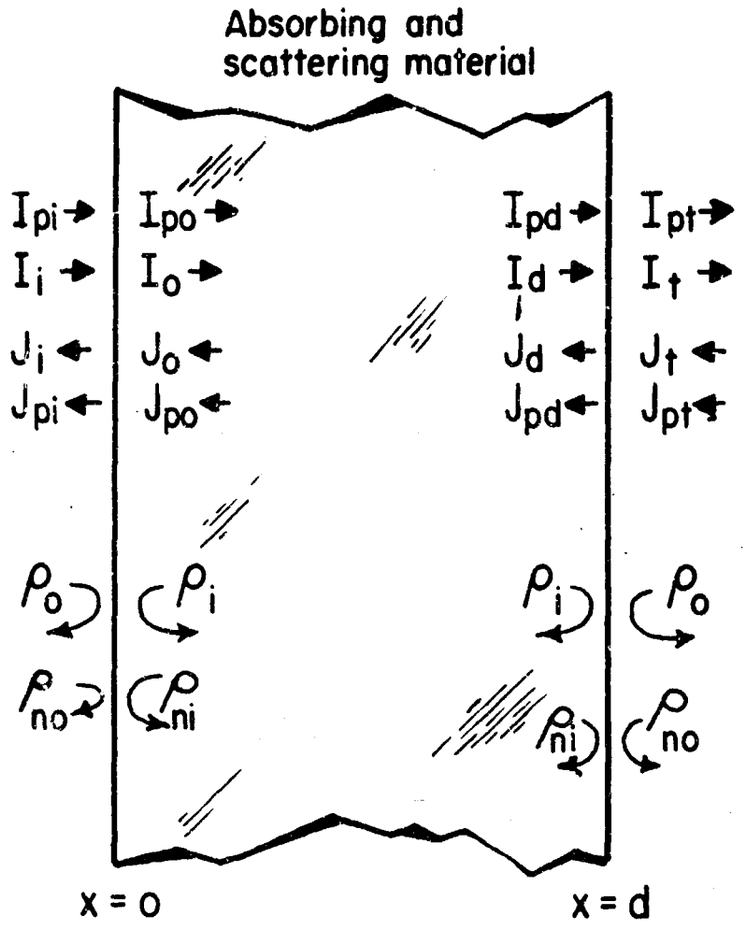

Fig. 4.1 Heat flow by combined radiation and conduction.

The materials investigated under this contract all have large scattering coefficients (see Appendix A). For a specimen thickness of 0.006" (0.015 cm) and scattering coefficients s' and f' of 90 and 260 cm^{-1}, with a = 0.8 and $\rho_{ni} \approx 0.07$ (corresponding to AD-85 Al_2O_3 @ $\lambda = 1\mu$ and T = 500°C), a calculation of $I^*_{p_{x=d}}$ reveals that:

$$I_{p_{x=d}} = (0.93)\exp(-5.26) = 0.005 \tag{4.31}$$

$$I^*_{p_{x=d}} = (0.93)^2\exp(-5.26) = 0.004 \tag{4.32}$$

or a transmission for parallel light of less than one percent. From equation 4.23,

$$J_{p_{x=d}} = (0.07)\ (0.005) = 0.0004 \tag{4.33}$$

which justifies neglecting the scattering from the backward parallel flux in calculating the diffuse flux. Equations (4.28) and (4.30) have been used to calculate the transmission of the thin sections described in the next section.

5.0 THIN SAMPLE TRANSMISSION MEASUREMENTS

Thin sample transmission measurements, when made on single crystal specimens, allow evaluation of the absorption coefficient (α) of the single crystal. The equation

$$\tau_p = I^*_{p_{x=d}} = (1 - \rho_{ni})^2 \exp(-g'd) \qquad (5.1)$$

allows evaluation of (g'), the extinction coefficient for polycrystalline thin sections. This extinction coefficient is the sum of twice the single crystal absorption coefficient plus the forward and backward scattering coefficients for parallel light.

5.1 Apparatus

It was originally planned that the single crystal transmission furnace and optics[1] be used so that measurements could be taken at elevated temperatures. The low transmission of energy through the sample prevented the use of both the furnace and the special optics. Instead, the sample was inserted into the normal optical path of the spectrophotometer (Fig. 5.1). Room temperature measurements only were run because there was no furnace which was small enough to fit into the limited space available on the spectrophotometer.

5.2 Transmission Measurements

The amount of parallel energy passed through the sample was very small. As calculated in section 4, the amount of parallel light (wavelength 1μ) passed by a .006" sample of AD-85 at 500°C is 0.4%. Thus, measurements were being taken at the extreme limits of the spectrophotometer precision.

In order to obtain measurements, the following technique was used:

1. A curve was run with both optical paths open (referred to as "100% line").

2. A curve was run with the sample path completely blocked ("zero percent" line).

3. A curve was run with the sample inserted into the sample optical path.

4. The reference beam was partially blocked so that the energy ratio was smaller.

5. The sample curve was re-run at this amplifier setting.

6. The curves (1, 2, 3, and 5) were normalized to give transmission data for the thin sections.

This process was tried using the single crystal furnace and optical system, but was unsuccessful because of energy losses by the optics.

For diffuse transmission measurements it is desirable to measure the transmitted radiation over a solid angle of 180°; for parallel transmission measurements the ideal arrangement would be a collimated measurement system assuring that only the parallel beam reaches the instrument collector. In the present measurements the optical system collects transmitted radiation on a solid angle of 15° fixed by the minimum energy input necessary for barely acceptable precision. Thus, the intensities measured are that of the parallel radiation plus the diffuse radiation falling within a 15° solid angle to the parallel axis.

5.3 Results

Transmission curves were run on the alumina samples, two strontium titanate samples, and two Pyroceram samples. These results (extinction coefficient vs. wavelength) are plotted in Figs. 5.2 to 5.8. Two samples of alumina AD-995 were run, one sample being 0.006" thick and the other specimen 0.004" thick. The results (Fig. 5.2) indicate that experimentally the extinction coefficient is not the same for both samples. Physically, the extinction coefficient should be independent of thickness. The difference between the extinction coefficients is thus an indication of the magnitude of the errors involved in the transmission measurements. Deviations between the two curves range from 12% to 84%.

For the AD-995 specimens, the transmission at one micron for the 0.006" specimen is 0.0507, or 5.07%, and for the 0.004" specimen it is 0.0568, or 5.68%. Data on the spectrophotometer[4] give an accuracy of 0.5% and a reproducibility of 0.25% for the ordinate scale of the instrument. This would mean an estimated maximum error for the instrument of 0.50% of full scale when comparing two specimens of the same

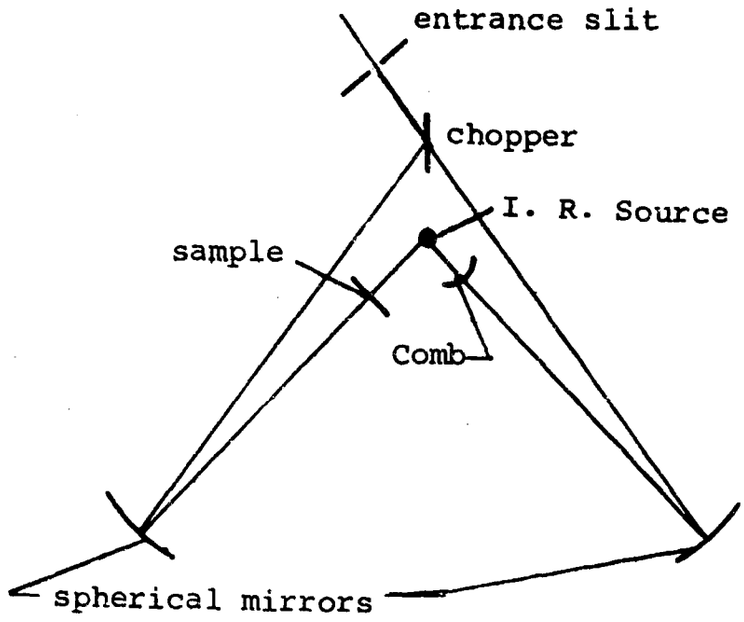

Figure 5.1 Optical Diagram for Transmission Measurements.

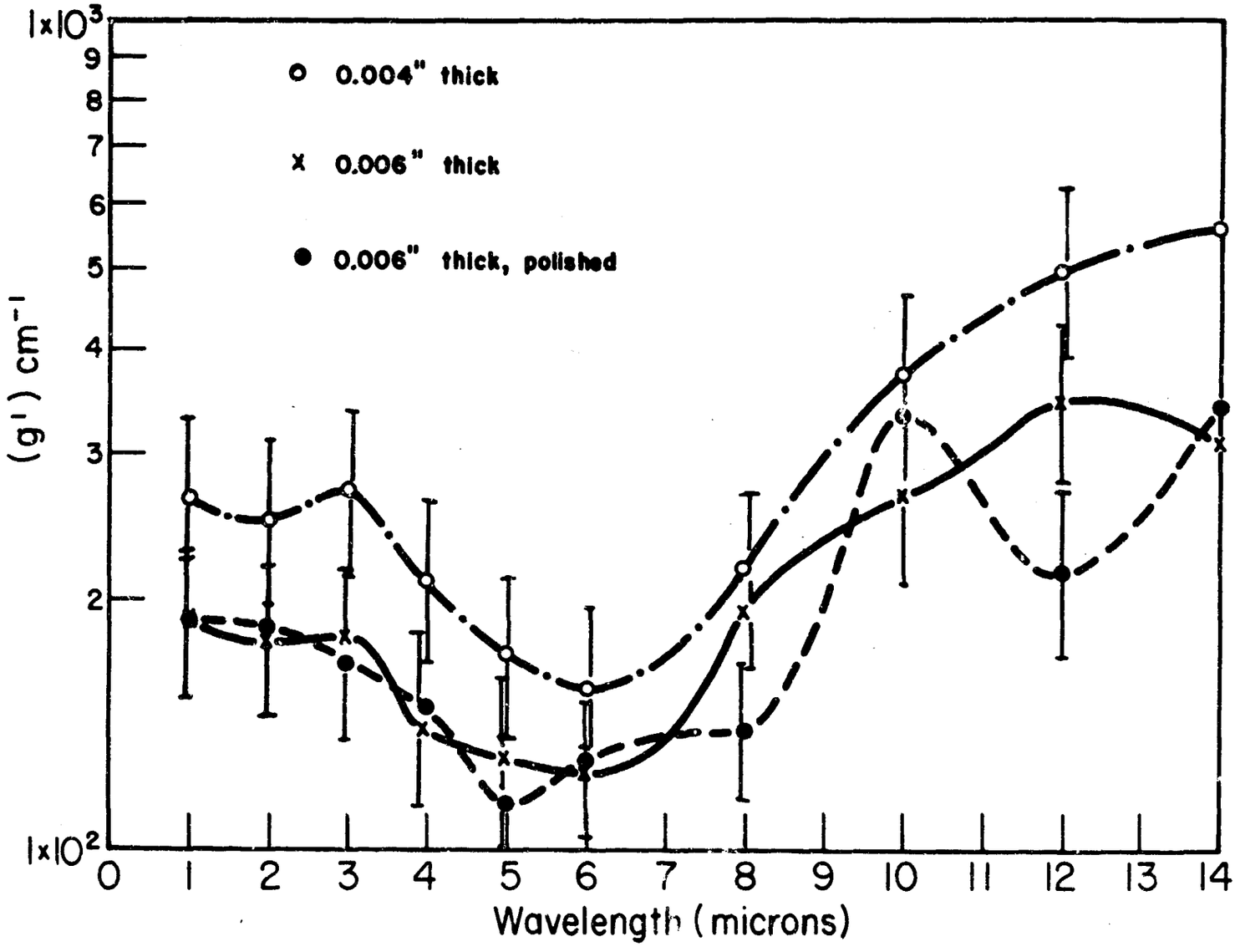

Figure 5.2 Extinction Coefficient vs. Wavelength for AD-995.

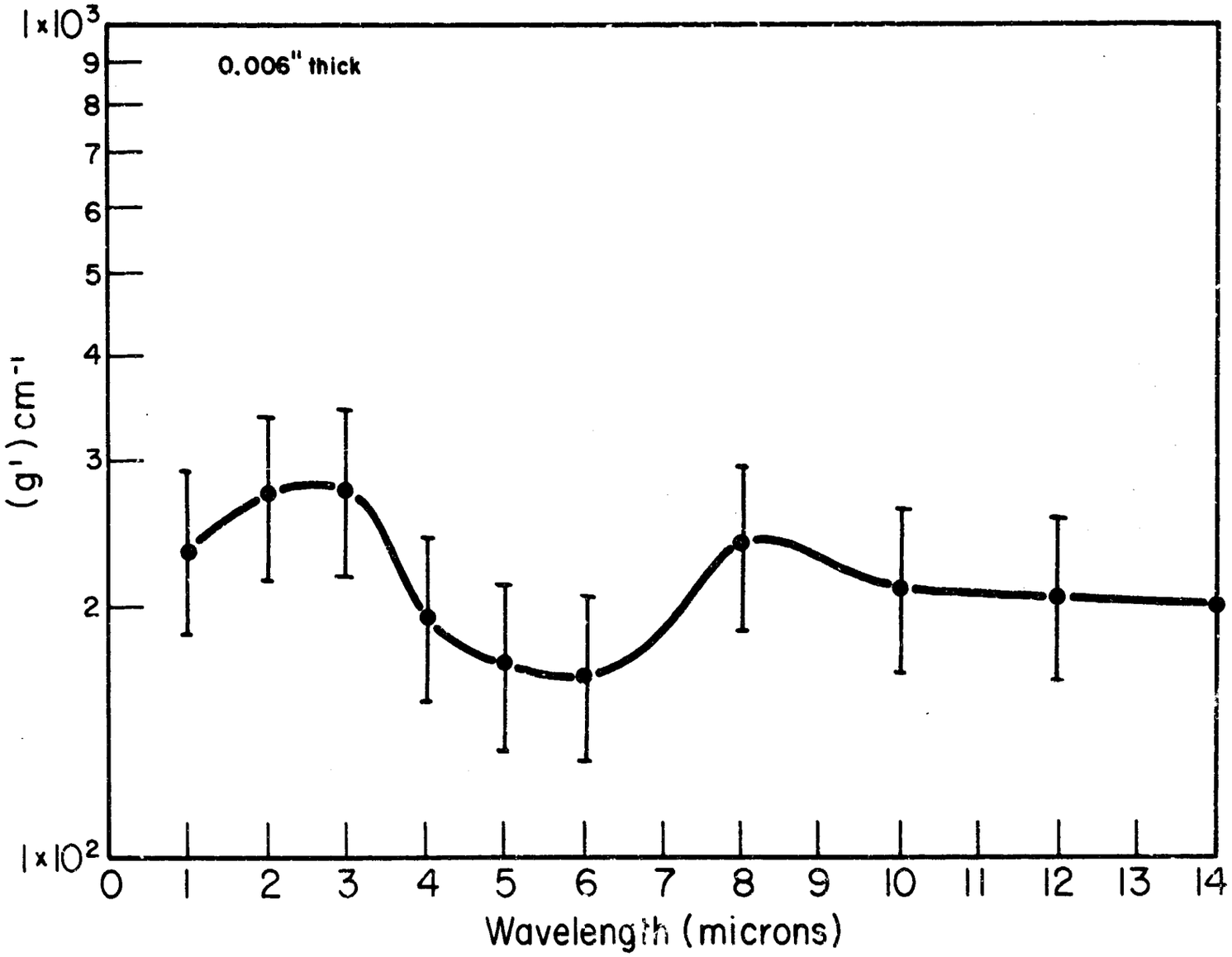

Figure 5.3 Extinction Coefficient vs. Wavelength for AD-85.

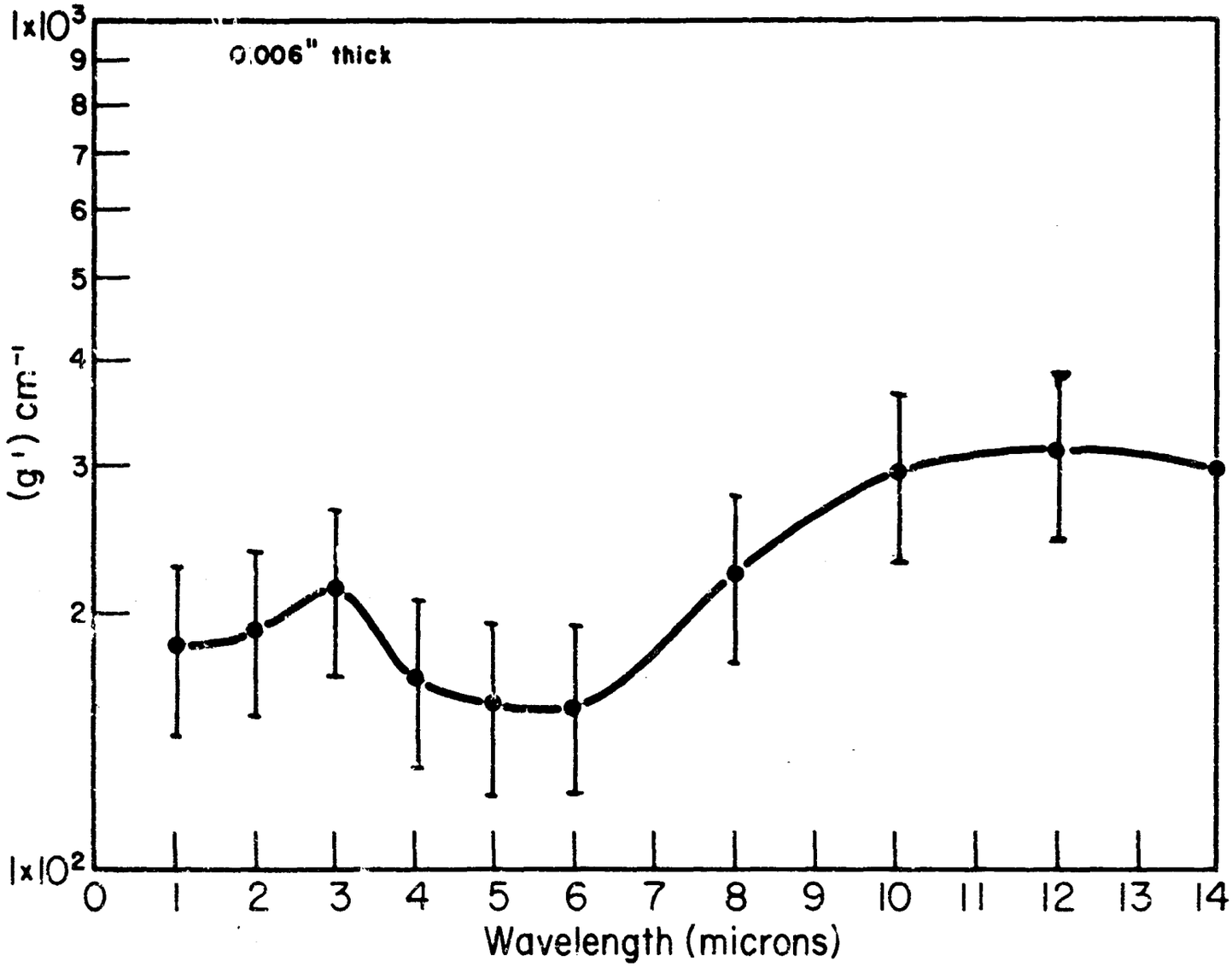

Figure 5.4 Extinction Coefficient vs. Wavelength for Aℓ-1.

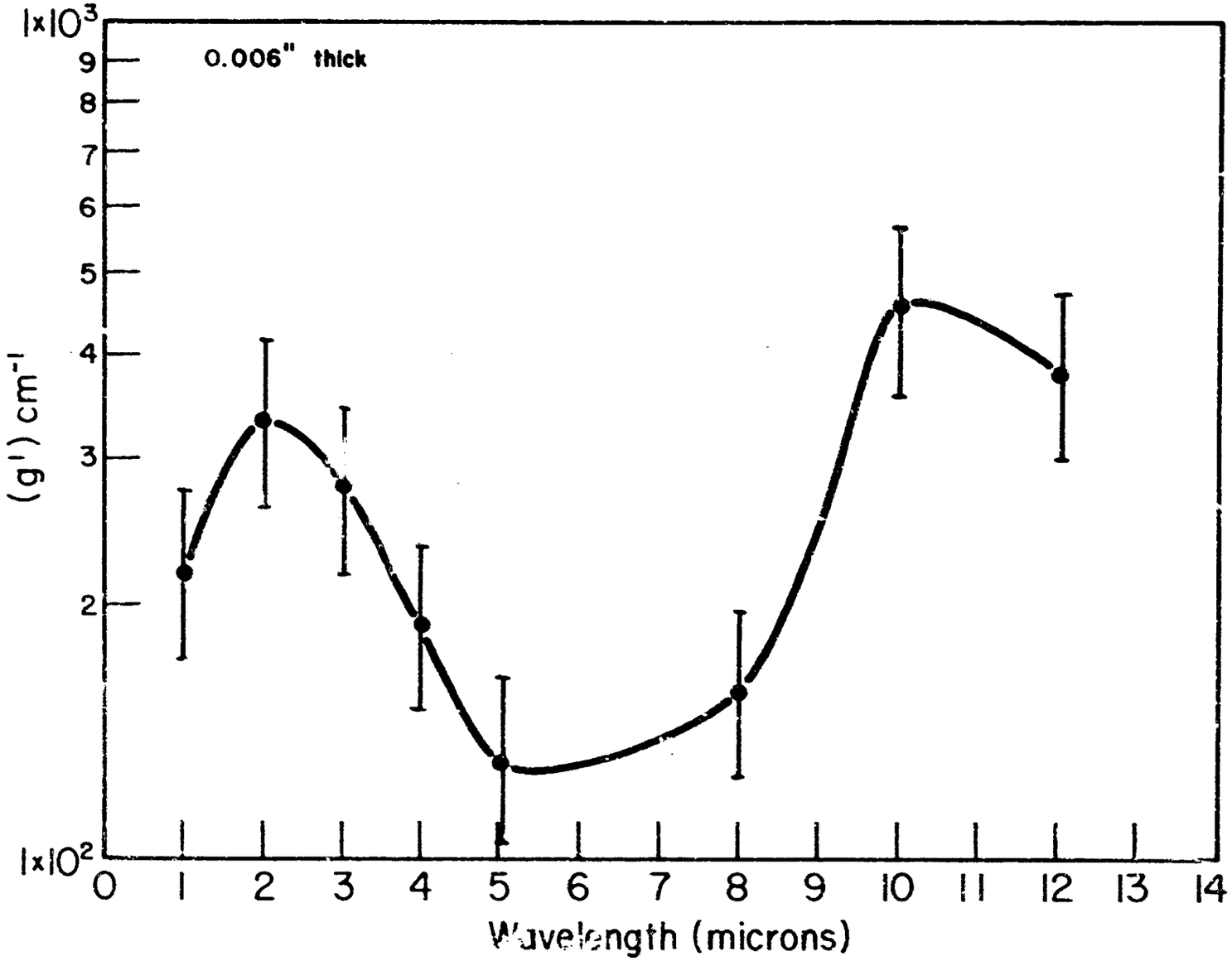

Figure 5.5 Extinction Coefficient vs. Wavelength for Ai-4.

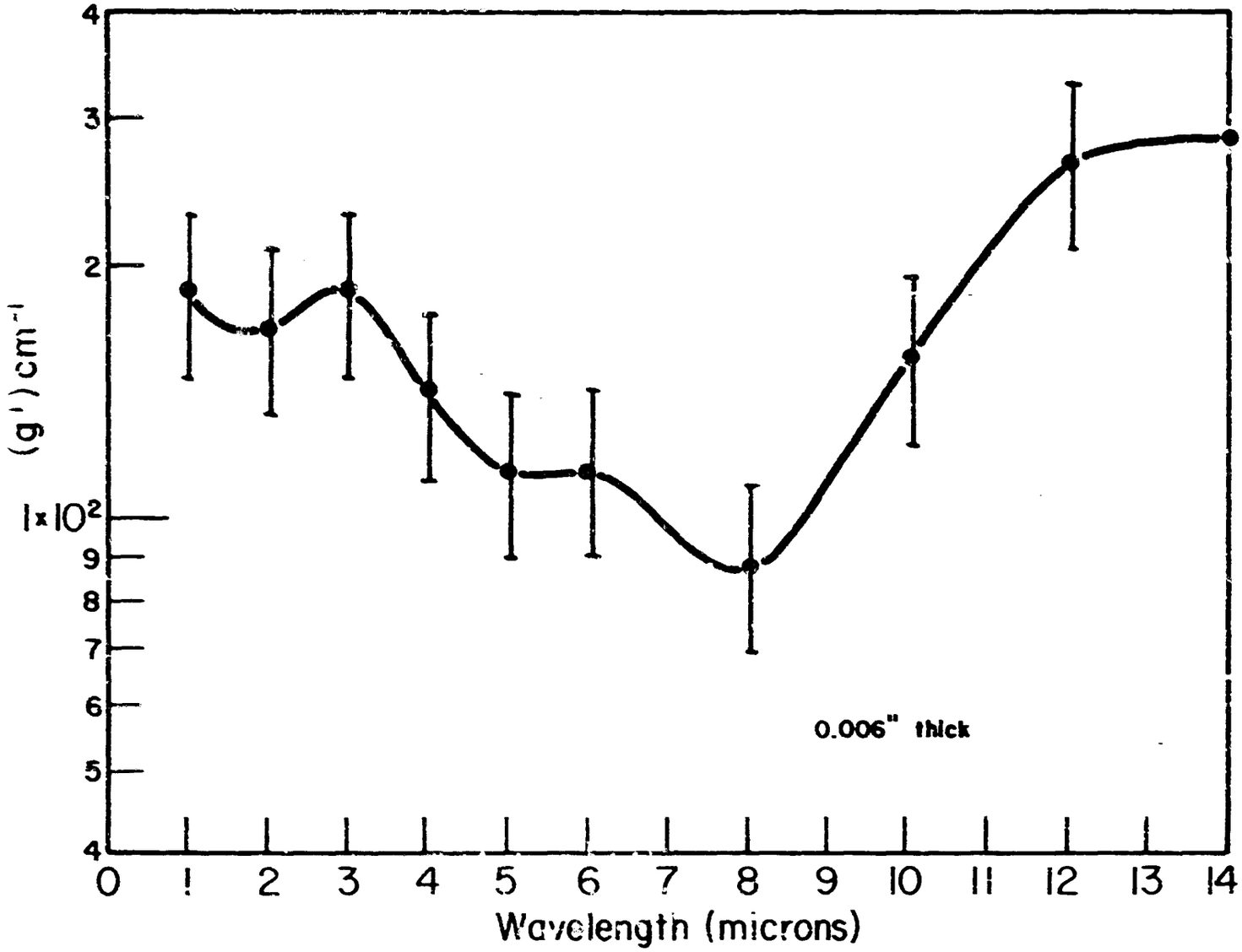

Figure 5.6 Extinction Coefficient vs. Wavelength for $SrTiO_3$A.

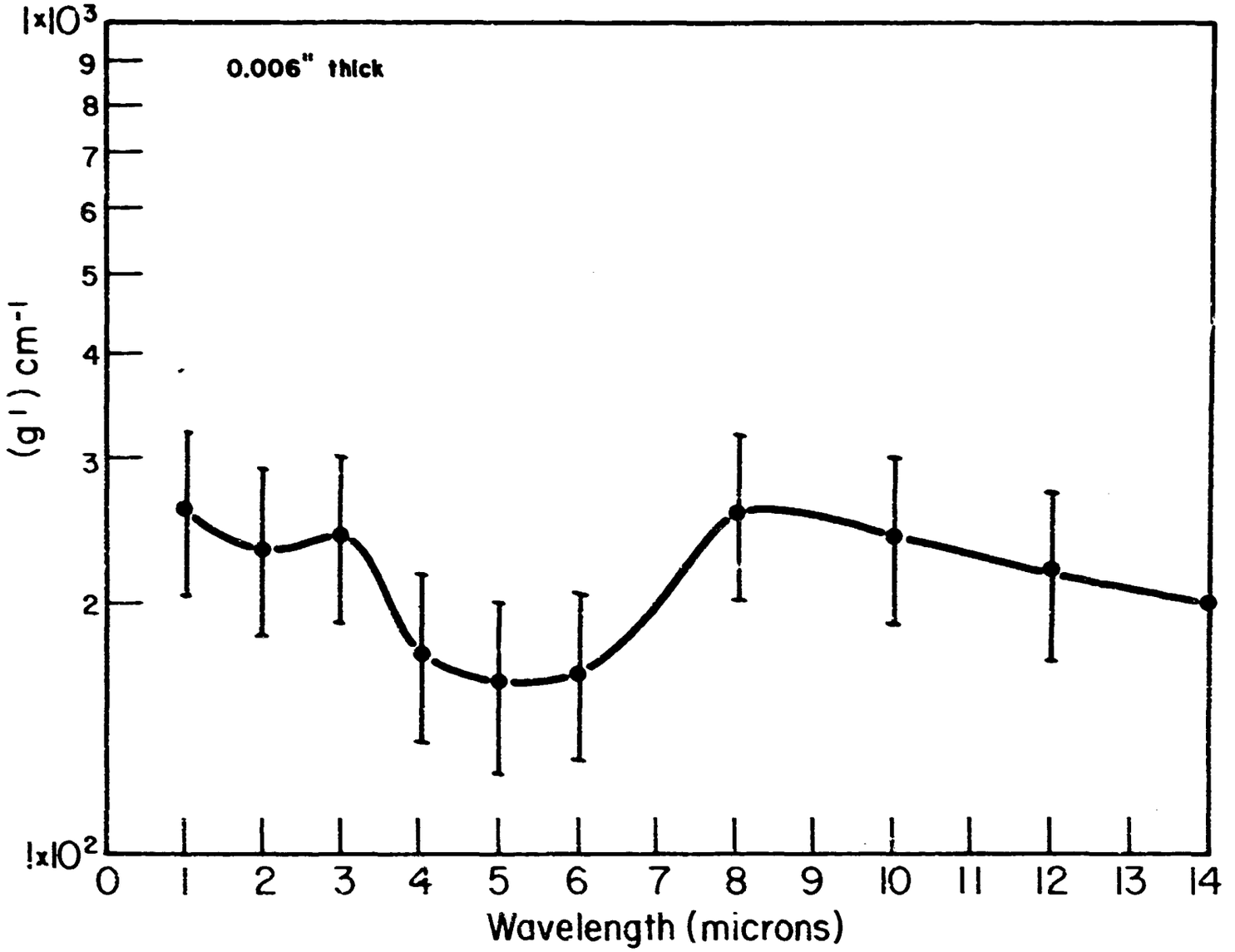

Figure 5.7 Extinction Coefficient vs. Wavelength for Pyroceram 9616.

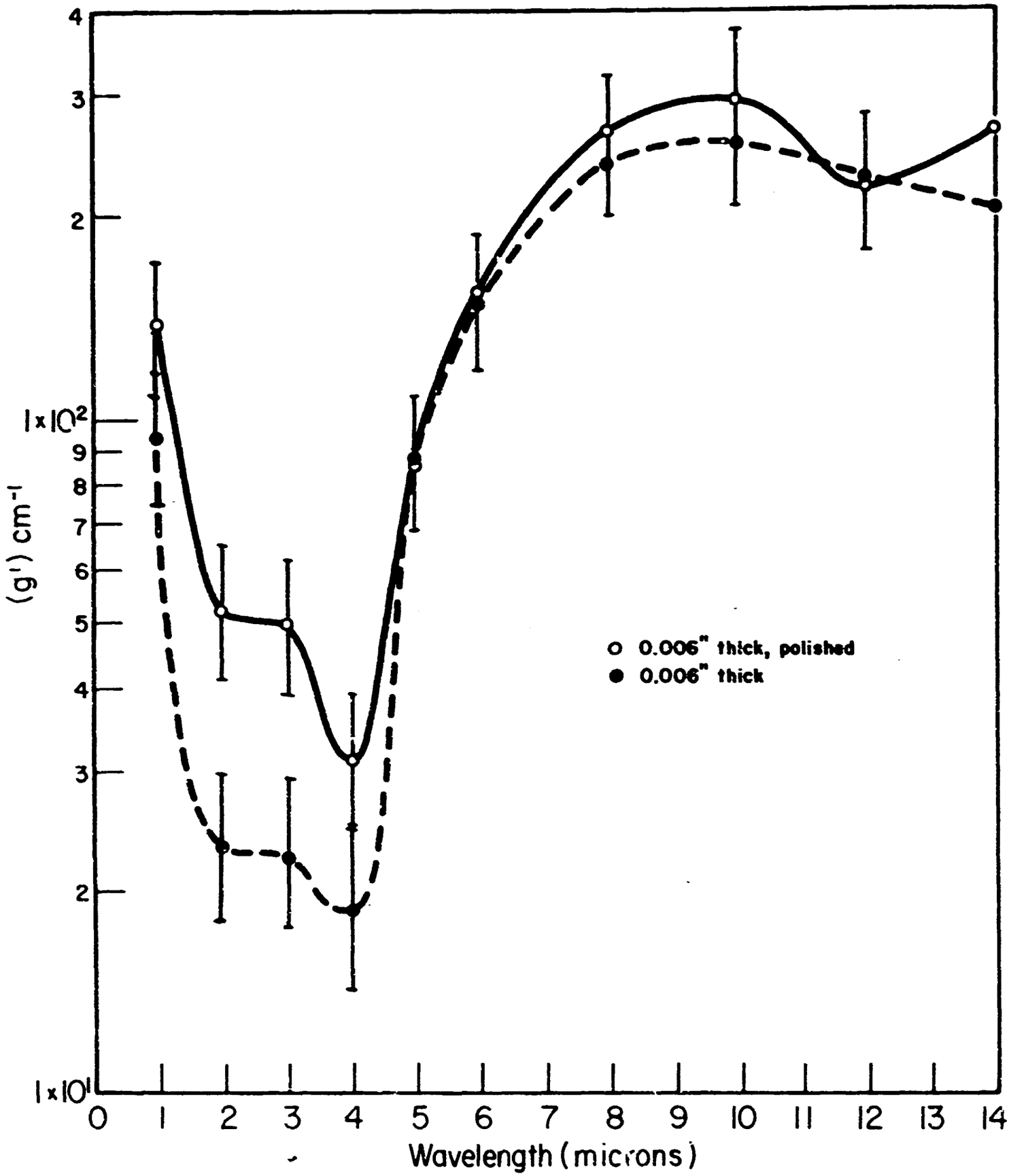

Figure 5.8 Extinction Coefficient vs. Wavelength for Pyroceram 9608.

material under the same conditions. For energy transmissions of less than 15% (full scale), this would be minimum error of 3%, and could be 50% or greater whenever the transmission is less than 1%.

The properties of the materials tested were such that we were taking measurements in the region of 15% or less for the total parallel transmitted energy. Therefore, it does not seem unreasonable to assume an error of 50% for the measured coefficient of extinction of the polycrystalline specimens.

5.4 Comparison with Calculated Results

Values of the diffuse transmissivity and parallel transmissivity were calculated from equations (4.28) and (4.30), using the IBM 7090 computer at The Aeronautical Systems Division, Wright-Patterson Air Force Base, Ohio.

The extinction coefficient g' was calculated from material properties. By definition (equation 4.3 and 4.4)

$$g' = a + s' + f' \tag{5.2}$$

where a, s', and f' are as previously defined (see equation 5.1). The normal scattering coefficient, S, bears the following relationships to the forward and backward scattering coefficients for parallel light, f' and s' respectively:

$$S = f' + s' \tag{5.3}$$

And from Folweiler and Mallio[2], for alumina

$$f' \approx 3\, s' \tag{5.4}$$

The scattering coefficient, S, is related to the number of pores per unit volume, N, and the pore radius, r, and the scattering factor, K, by the relation

$$S = KN(\pi r^2) \tag{5.5}$$

If the volume fraction porosity is P, then

$$S = \frac{3}{4} K \frac{P}{r} \tag{5.6}$$

The scattering factor K varies between zero and four and depends on the pore radius, r, the wavelength of radiation,

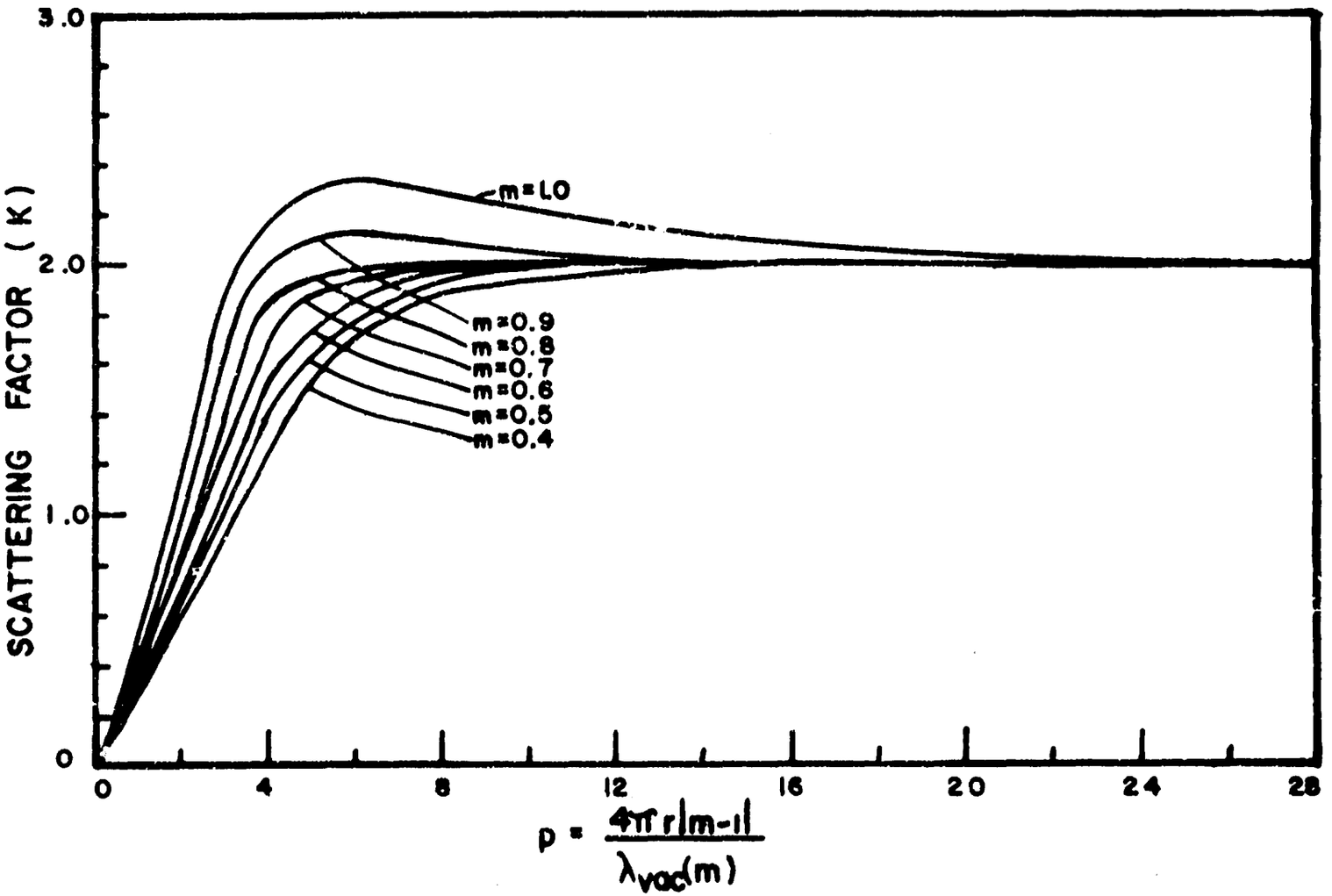

Figure 5.9 Values of the Scattering Factor K vs. p for Various Values of the Relative Index m, when $m < 1$.

λ, and the relative index of the scattering center and medium, m.

The scattering factor, K, has been summarized as a function of the dimensionless parameter,

$$p = \frac{4\pi r\,|m-1|}{\lambda m} \tag{5.7}$$

by Van de Hulst[5], as shown in Fig. 5.9, for values of $m \leq 1$.

Using equation (5.6) and the relation that a, the absorption coefficient appropriate to the Ryde equation, is equal to twice α, the single crystal absorption coefficient, it is possible to compute the extinction coefficient.

Calculation of values of the extinction coefficient were included in the computer program to evaluate the expression for the diffuse transmission (equation 4.29). These calculations indicate that the extinction coefficients are greater than the values measured with the spectrophotometer. Table 5-I is a tabulation of calculated and measured extinction coefficients for alumina, strontium titanate, and Pyroceram samples.

For most of the sample conditions investigated, it was sufficiently accurate to set the extinction coefficient, g', equal to $(s' + f')$, or S, because the absorption coefficient a, was very small compared to S, especially in the region 1-4 microns. It may be concluded, therefore, that the annihilation of a beam of parallel light by a body having an absorption constant $a << S$, the scattering coefficient, is caused by scattering.

If the extinction coefficient g' were not great enough or the sample was not thick enough to neglect the parallel beam, difficulties about the uniformity of the diffuse beam would arise. That is, the scattered light would not be homogeneously dispersed in either the forward or backward direction.

The measured transmissivity, and the calculated parallel and diffuse transmissivities for the alumina and strontium titanate samples are shown in Figs. 5.10 - 5.15. As can be seen, the measured transmissivities are greater than the parallel transmissivity (equation 5.1), but less than the diffuse transmissivity (equation 4.29). The measured transmissivity approaches the total transmissivity $(\tau_D + \tau_p)$ as

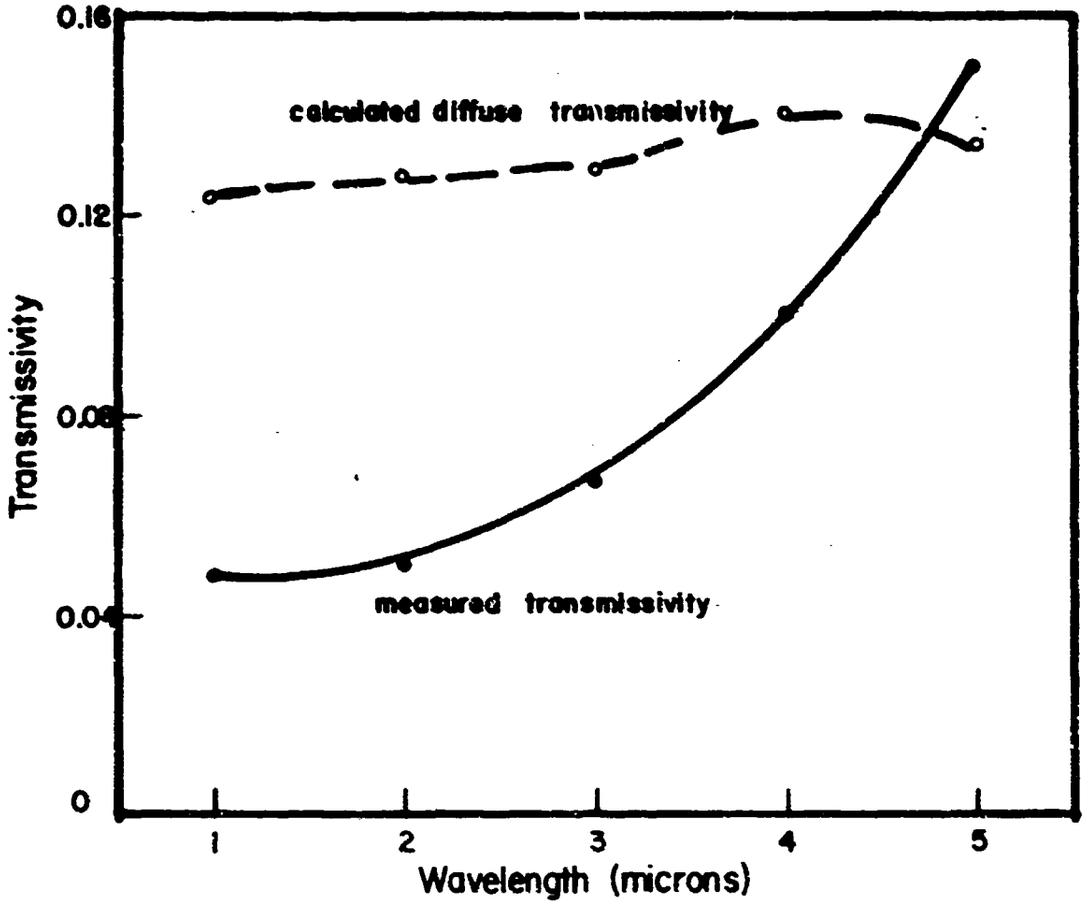

Figure 5.10 Measured and Calculated Transmissivity vs. Wavelength for AD-995.

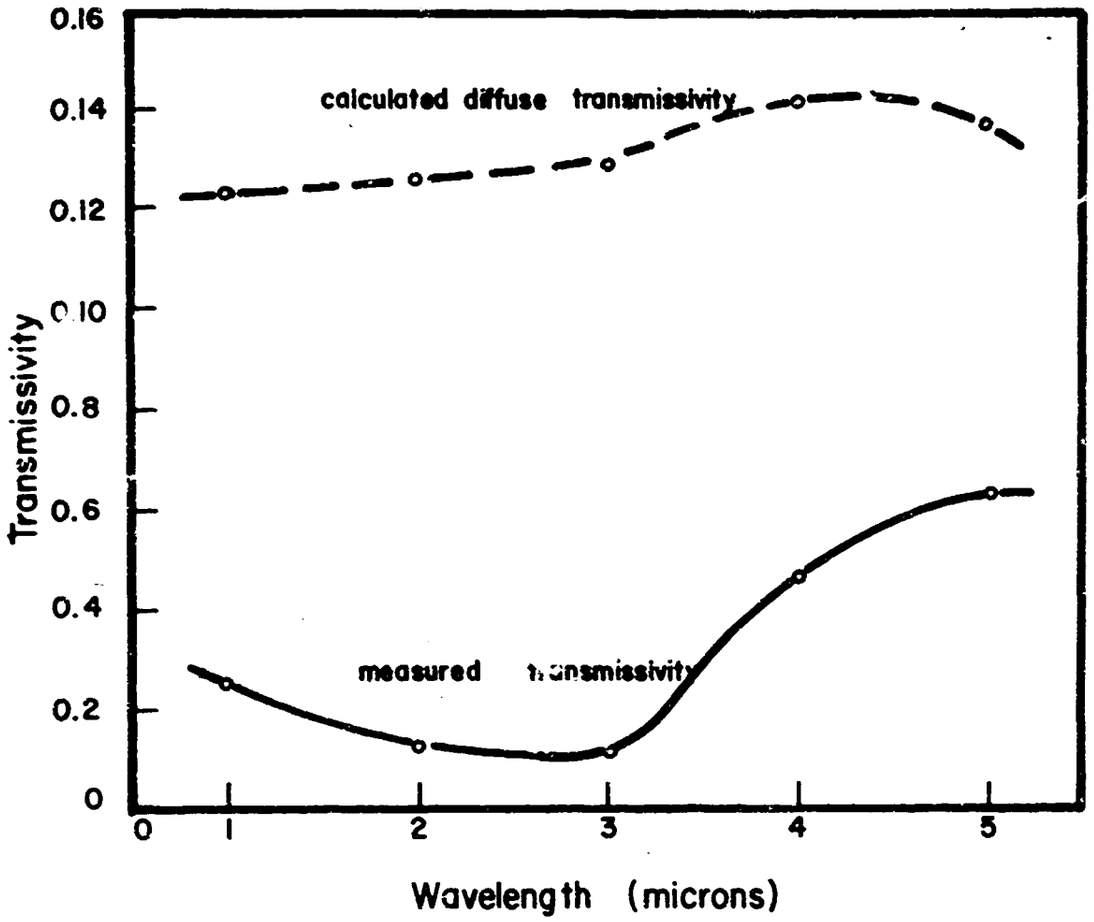

Figure 5.11 Measured and Calculated Transmissivity vs. Wavelength for AD-85.

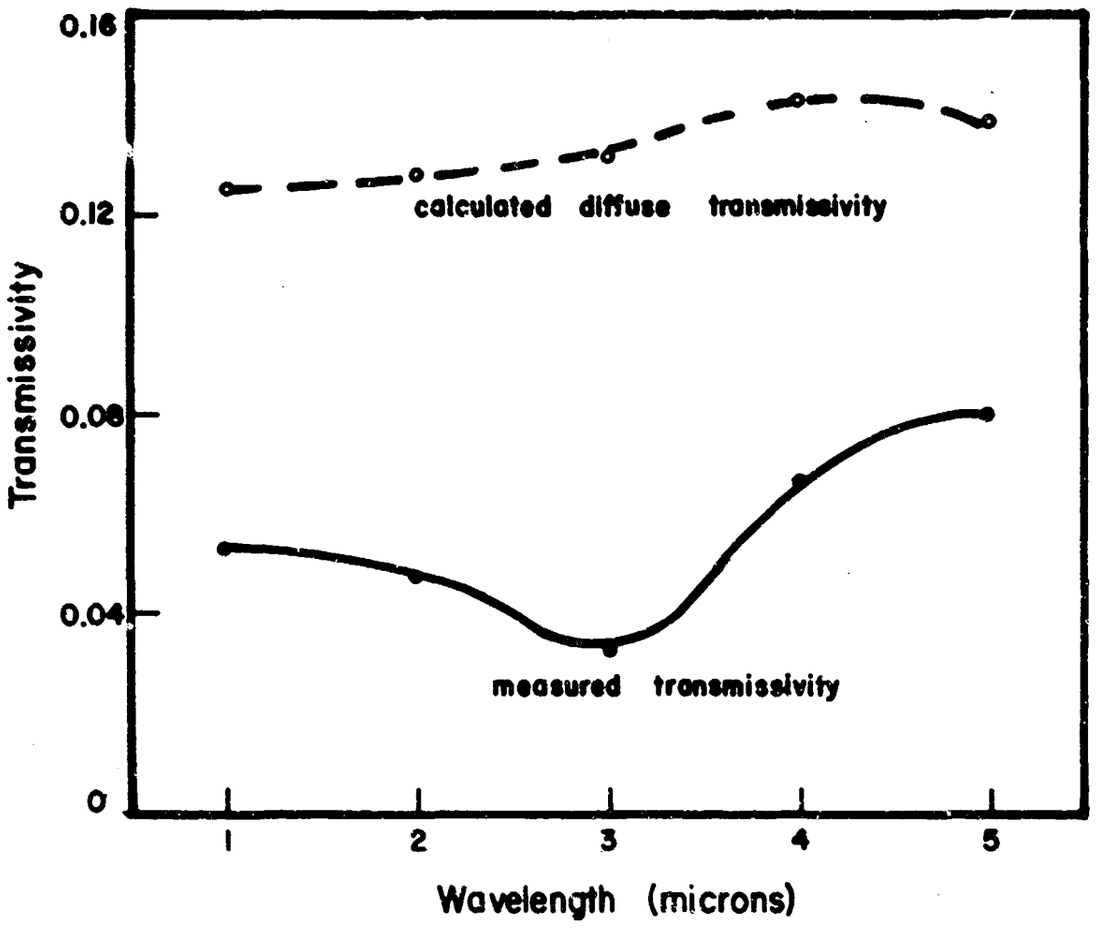

Figure 5.12 Measured and Calculated Transmissivity vs. Wavelength for Aℓ-1.

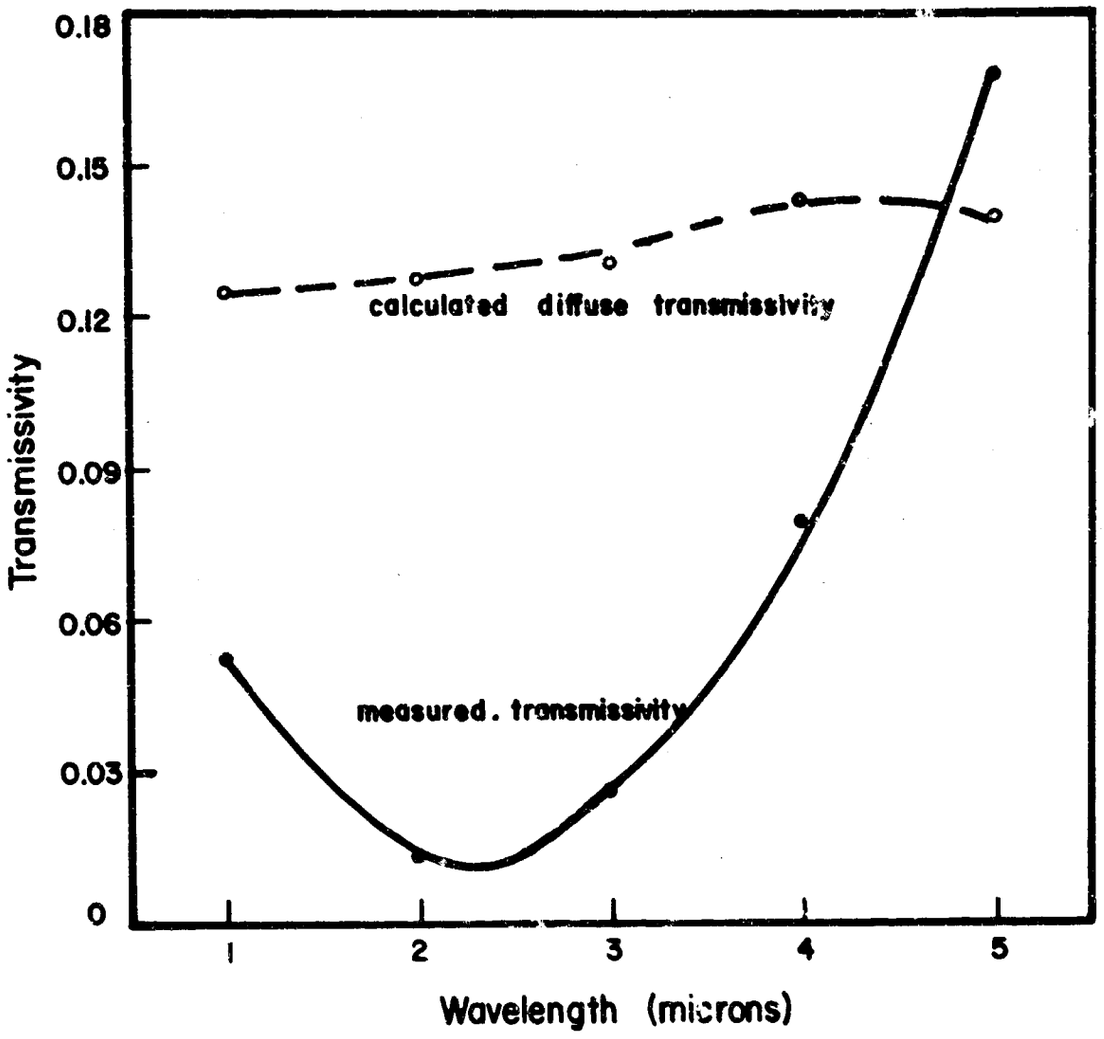

Figure 5.13 Measured and Calculated Transmissivity vs. Wavelength for Aℓ-4.

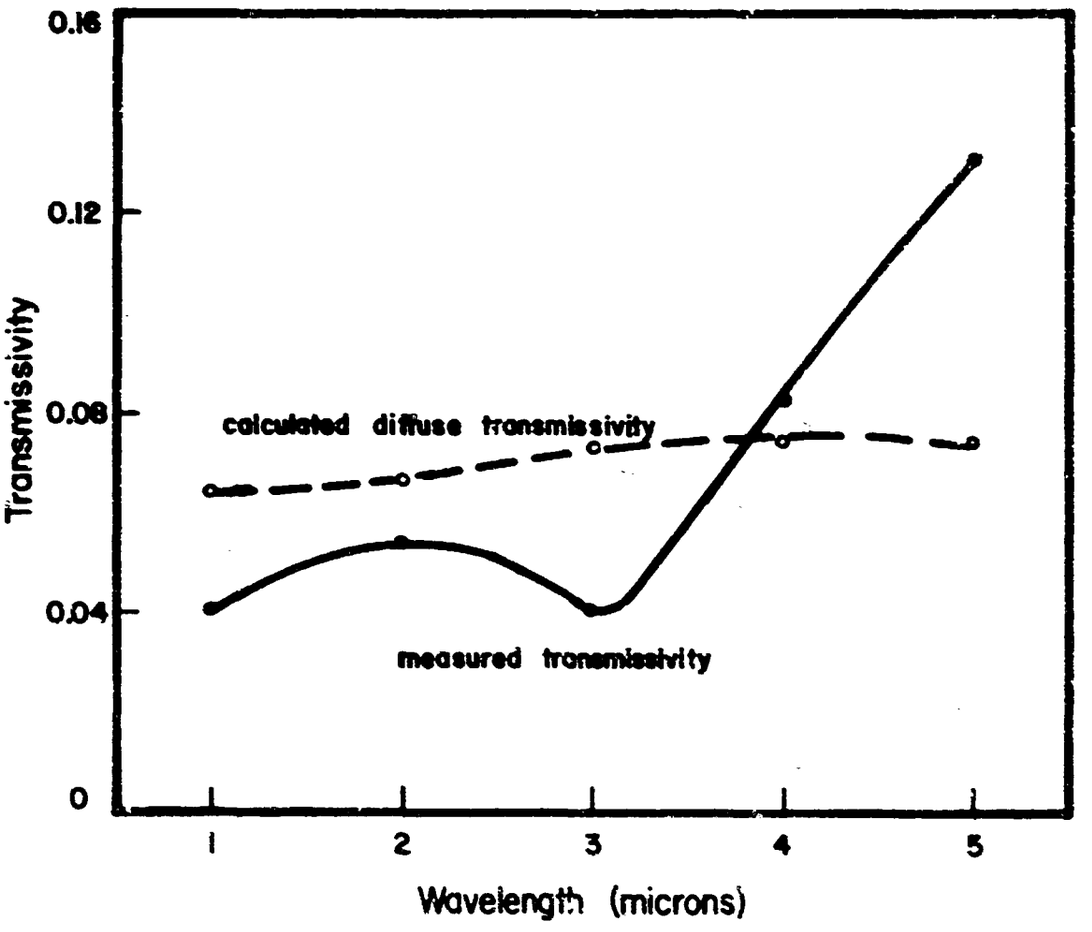

Figure 5.14 Measured and Calculated Transmissivity vs. Wavelength for $SrTiO_3$A.

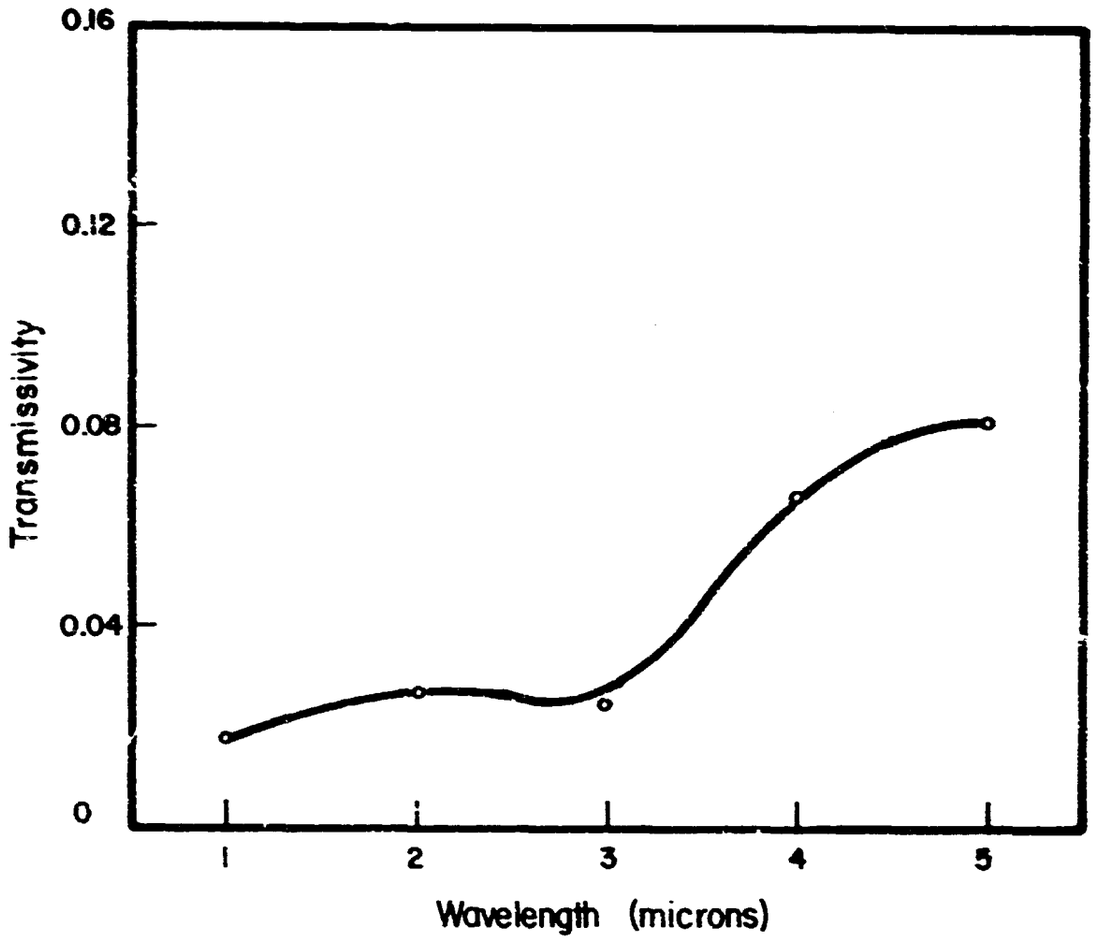

Figure 5.15: Measured Transmissivity vs. Wavelength for Pyroceram 9606.

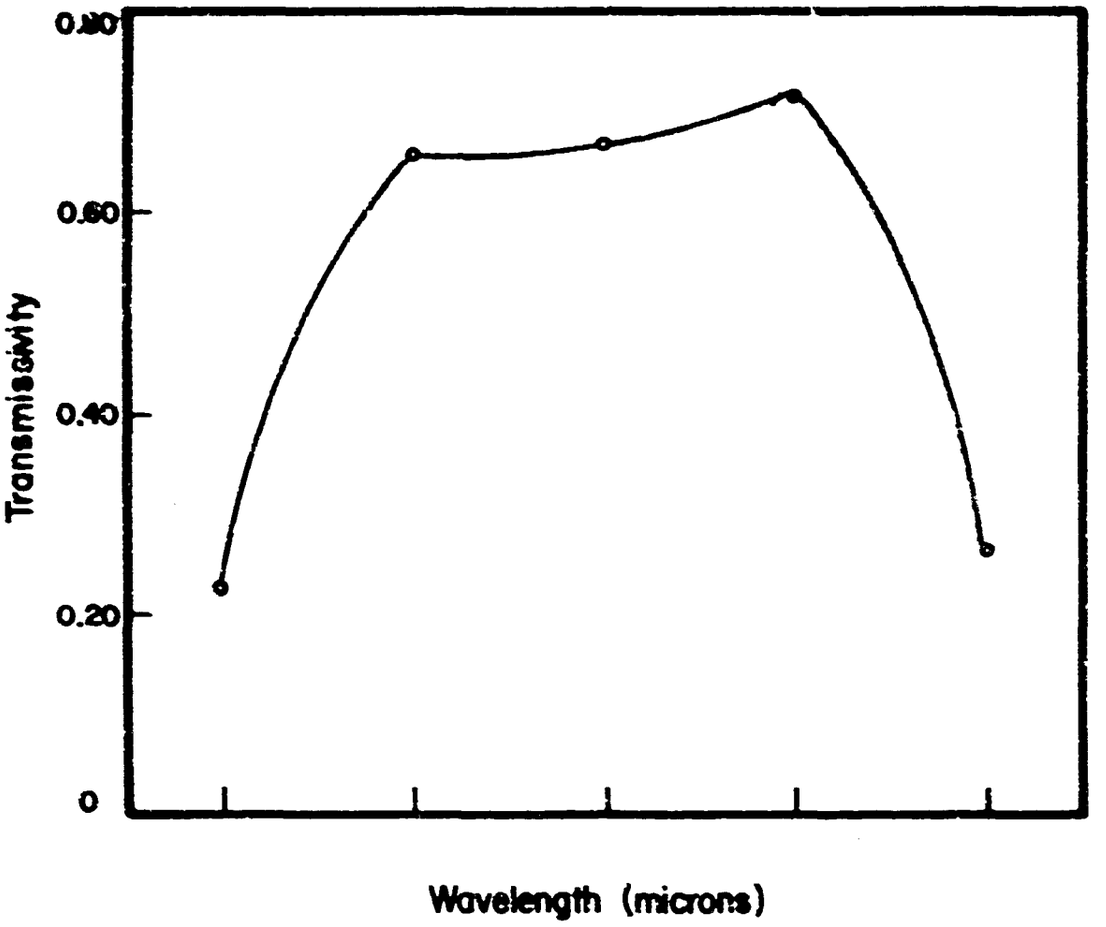

Figure 5.16: Measured Transmissivity vs. Wavelength for Pyroceram 9608.

the wavelength increases. This means that the angular distribution of transmitted light is not ideally diffuse (i.e., does not follow a cosine law), but has an angular distribution in the forward direction such that more is transmitted in the area subtended by the optical system than in the high angle region. The infrared scattering work of Love and Wheasler[6], using an aerosol of six micron alumina-particles as the scattering medium show that the amount of the scattered light in the angular range 0-10 degrees is 60 to 85% of the total amount scattered in the forward direction, depending on the wavelength of the incoming light. The theoretical work of Mie (see Ref. (5), Appendix E) indicated that as a function of wavelength, the intensity at low angles (0-20°) decreases with the wavelength when the scattering media contains absorbing particles. The opposite is true for our system of a scattering media with non-absorbing particles. This difference in the angular intensity distribution with wavelength is slight, however.

TABLE 5-I: Calculated and Measured Extinction Coefficients (cm^{-1})
All samples 6 mils thick except where noted.

	AD-85		AD-995				A1-1	
			6 mil		6 mil Meas.	4 mil		
λ	Calc.	Meas.	Calc.	Meas.	Pol.*	Meas.	Calc.	Meas
1	348	233	385	186	187	266	973	184
2	348	272	372	176	184	249	947	190
3	352	276	357	178	167	270	907	217
4	351	194	327	140	148	211	813	166
5	340	171	277	128	114	173	734	157

	A1-4		$SrTiO_3$				Pyroceram	
			A		B	9606	Meas.9608	
	Calc.	Meas.	Calc.	Meas.	Calc.	Meas.	Pol.*	Meas.
1	2373	219	1004	186	549	260	139	94
2	2133	331	1004	167	549	233	52.2	23
3	1787	279	1004	187	549	240	50	22
4	1200	189	803	142	513	175	31	18
5	787	129	683	114	495	162	85	86

*Polished specimens have metallographic polish on surfaces.

6.0 COMPARISON BETWEEN THE EXACT AND HAMAKER SOLUTIONS FOR HEAT TRANSMISSION BY COMBINED CONDUCTIVE AND RADIATIVE TRANSFER

The exact equations for describing the transmission of heat by combined conductive and radiative transfer in a homogeneous medium are (for the one-dimensional case and the steady state):

$$k \frac{d^2T}{dx^2} - 2 a n^2 \sigma' T^4 + a(I + J) = 0 \qquad (6.1)$$

$$\frac{dI}{dx} = a n^2 \sigma' T^4 - (a + s)I + sJ \qquad (6.2)$$

$$\frac{dJ}{dx} = (a + s)J - sI - a n^2 \sigma' T^4 \qquad (6.3)$$

where I and J are the radiant fluxes in the +x and -x direction, T is the absolute temperature, σ' is the Boltzmann constant, n is the refractive index, k is the thermal conductivity, a is the absorption coefficient for diffuse radiation, and s is the back-scattering coefficient for diffuse radiation.

It is convenient to reduce the set of Eq. (6.1), (6.2), and (6.3), to a single second-order equation. Eq. (6.2) and Eq. (6.3) are added and the sum integrated once to give:

$$I + J = -(a + 2s)(H x + kT) + A \qquad (6.4)$$

in which A is a constant of integration and H is the constant heat flux defined by:

$$H = I - J - k \frac{dT}{dx} \qquad (6.5)$$

Substituting in Eq. 6.1 we obtain:

$$k \frac{d^2T}{dx^2} - 2 a n^2 \sigma' T^4 - a(a + 2s)(Hx + kT) + a A = 0 \qquad (6.6)$$

For simplicity we consider the one-dimensional flow of heat by conduction and radiation inside a medium as shown in Fig. 4.1. Once the material constants, k, a, s, and n^2 are specified, there remain four independent initial conditions to be fixed; i.e., T_o, $(dT/dx)_o$, I_o, and J_o. For various

values of these initial conditons we have constructed a family of solutions by numerical integration of Eq. (6.6).

The calculation consists of (1) selection of material constants and initial conditions; (2) evaluation of A and H from Eqs. (6.4) and (6.5); (3) calculation of T(x) by numerical integration of Eq. (6.6); (4) calculation of k(dT/dx); and (5) calculation of I(x) and J(x) from the relations:

$$I = \frac{1}{2}\left[-(a + 2s)\ (Hx + kT) + a + H + k\left(\frac{dT}{dx}\right)\right] \qquad (6.7)$$

$$J = \frac{1}{2}\left[-(a + 2s)\ (Hx + kT) + C - H - k\left(\frac{dT}{dx}\right)\right] \qquad (6.8)$$

Hamaker's approximation consists of replacing the first term in Eq. (6.1) $k(d^2T/dx^2)$ by $k/T_o^3\ d^2(T^4)/dx^2$ in which T_o is some average temperature in the material. This replacement makes the set of Eqs. (6.1), (6.2), and (6.3) linear and homogeneous in the quantities I, J, and T^4 so that a solution in closed form can be obtained readily.

The Hamaker solutions for the radiant fluxes are given in terms of the lumped material constants:

$$b = 4n^2\ \sigma'\ T_o^3 \qquad (6.9)$$

$$\sigma = \sqrt{\frac{2ab}{k} + a(a + 2s)} = \sigma_o\sqrt{(1 + \kappa)} \qquad (6.10)$$

$$\beta = \sigma/(a + 2s) \qquad (6.11)$$

$$\kappa = 2b/k\ (a + 2s) = 2b\beta/k\sigma \qquad (6.12)$$

Then, the radiant energy fluxes and temperature are given by:

$$I = A(1 - \beta)\ e^{\sigma x} + B(1 + \beta)\ e^{-\sigma x} + C(\sigma x - B) + D \qquad (6.13)$$

$$J = A(1 + \beta)\ e^{\sigma x} + B(1 - \beta)\ e^{-\sigma x} + C(\sigma x + \beta) + D \qquad (6.14)$$

$$E = -A\kappa e^{\sigma x} - B\kappa e^{-\sigma x} + C\sigma x + D \qquad (6.15)$$

$$T = T_o + \frac{1}{b}\ (E - E_o) \qquad (6.16)$$

where

$$A = \frac{J_o\,\sigma(1+\beta) - E_o(2\beta\sigma) - \left(\frac{dE}{dx_o}\right) 2\beta}{4\beta\,\sigma(\kappa+1)} \tag{6.17}$$

$$B = \frac{-J_o\,\sigma(1-\beta) - E_o(2\beta\sigma) + \left(\frac{dE}{dx_o}\right) 2\beta}{4\beta\,\sigma(\kappa+1)} \tag{6.18}$$

$$C = \frac{J_o\,2\kappa\sigma + \left(\frac{dE}{dx_o}\right) 2\beta}{4\beta\,\sigma(\kappa+1)} \tag{6.19}$$

$$D = \frac{J_o\,2\beta\kappa\sigma + E_o(4\beta\sigma)}{4\beta\sigma(\kappa+1)} \tag{6.20}$$

The calculation consists of (1) selection of material constants and initial conditions; (2) evaluation of b, σ, β, and κ from Eq. (6.9), (6.10), (6.11), and (6.12); (3) evaluation of A, B, C, and D from Eqs. (6.17), (6.18), (6.19), and (6.20); and (4) calculation of I, J, E, and T for various values of x from Eqs. (6.13), (6.14), (6.15), and (6.16).

A comparison has been made between numerical integration of the exact equation and numerical evaluation of the Hamaker solution for the system described for a range of initial conditions and material constants corresponding to previously measured values of a, s, and n. Computations were done on an IBM 7090 computer at the Aeronautical Systems Division, Wright-Patterson Air Force Base.

For all calculations I_o was set equal to zero; physically this corresponds to radiation from the surface into a semi-infinite media with the same index as the test section (no surface reflection) and having perfect transmissivity (no scattering or absorption). Values of J_o ranged from 0.26-125 cal cm^{-2} sec^{-1}, values of (dT/dx) were 100°K cm^{-1} and values of T_o were 1000 and 2000°K. Material constants were selected to correspond to measured values of a, s, n and K for Al_2O_3, MgO, SiO_2 and $SrTiO_3$. Tabulated input data and a comparison of results between the exact and Hamaker solutions are given in Table 6.1, and Figs. 6.1 and 6.2, are typical results.

The depth of the sample contributing to the emissivity characteristics is that part that is optically "near" the

TABLE 6.1

Input Constants and Comparison of Results of Exact and Hamaker Equations for Various Conditions

Condition	k	a	S	n^2	$(\frac{dT}{dx})_o$	T_o	J_o	I_o	at $x = (a + 2S)^{-1}$			at $x = 2(a + 2s)^{-1}$		
									$\frac{J_H}{J_E}$	$\frac{I_H}{I_E}$	$\frac{T_H}{T_E}$	$\frac{J_H}{J_E}$	$\frac{I_H}{I_E}$	$\frac{T_H}{T_E}$
1	0.020	0.23	260	3	100	1000	5	0	1.000	1.000	1.000	1.000	1.000	1.000
2	0.010	0.23	260	3	100	2000	35	0	1.000	1.000	1.000	1.000	1.000	1.000
3	0.020	0.23	279	3	100	2000	35	0	1.000	1.000	1.000	1.000	1.000	1.000
4	0.010	0.23	279	3	100	1000	5	0	1.000	1.000	1.000	1.000	1.000	1.000
5	0.020	7.44	208	3	100	2000	35	0	1.000	1.000	1.000	1.000	1.000	1.000
6	0.010	7.44	208	3	100	1000	5	0	1.000	1.000	1.000	1.000	1.000	1.000
7	0.020	0.23	710	3	100	1000	5	0	1.000	1.000	1.000	1.000	1.000	1.000
8	0.010	0.23	710	3	100	2000	35	0	1.000	1.000	1.000	1.000	1.000	1.000
9	0.020	0.23	1600	3	100	1000	5	0	1.000	1.000	1.000	1.000	1.000	1.000
10	0.010	0.23	1600	3	100	2000	35	0	1.000	1.000	1.000	1.000	1.000	1.000
11	0.020	7.44	590	3	100	1000	5	0	1.000	1.000	1.000	1.000	1.000	1.000
12	0.010	7.44	590	3	100	2000	35	0	1.000	1.000	1.000	1.000	1.000	1.000
13	0.005	2.58	3280	2	100	1000	35	0	1.000	1.000	1.000	1.000	1.000	1.000
14	0.005	94	540	2	100	1000	5	0	1.000	1.000	1.000	1.000	1.000	1.000
15	0.020	0.31	800	3	100	1000	5	0	1.000	1.000	1.000	1.000	1.000	1.000
16	0.010	0.31	800	3	100	2000	35	0	1.000	1.000	1.000	1.000	1.000	1.000
17	0.015	1.80	450	5	100	1000	5	0	1.000	1.000	1.000	1.000	1.000	1.000
18	0.008	1.80	450	5	100	2000	35	0	1.000	1.000	1.000	1.000	1.000	1.000
19	0.015	1.80	2000	5	100	1000	5	0	1.000	1.000	1.000	1.000	1.000	1.000

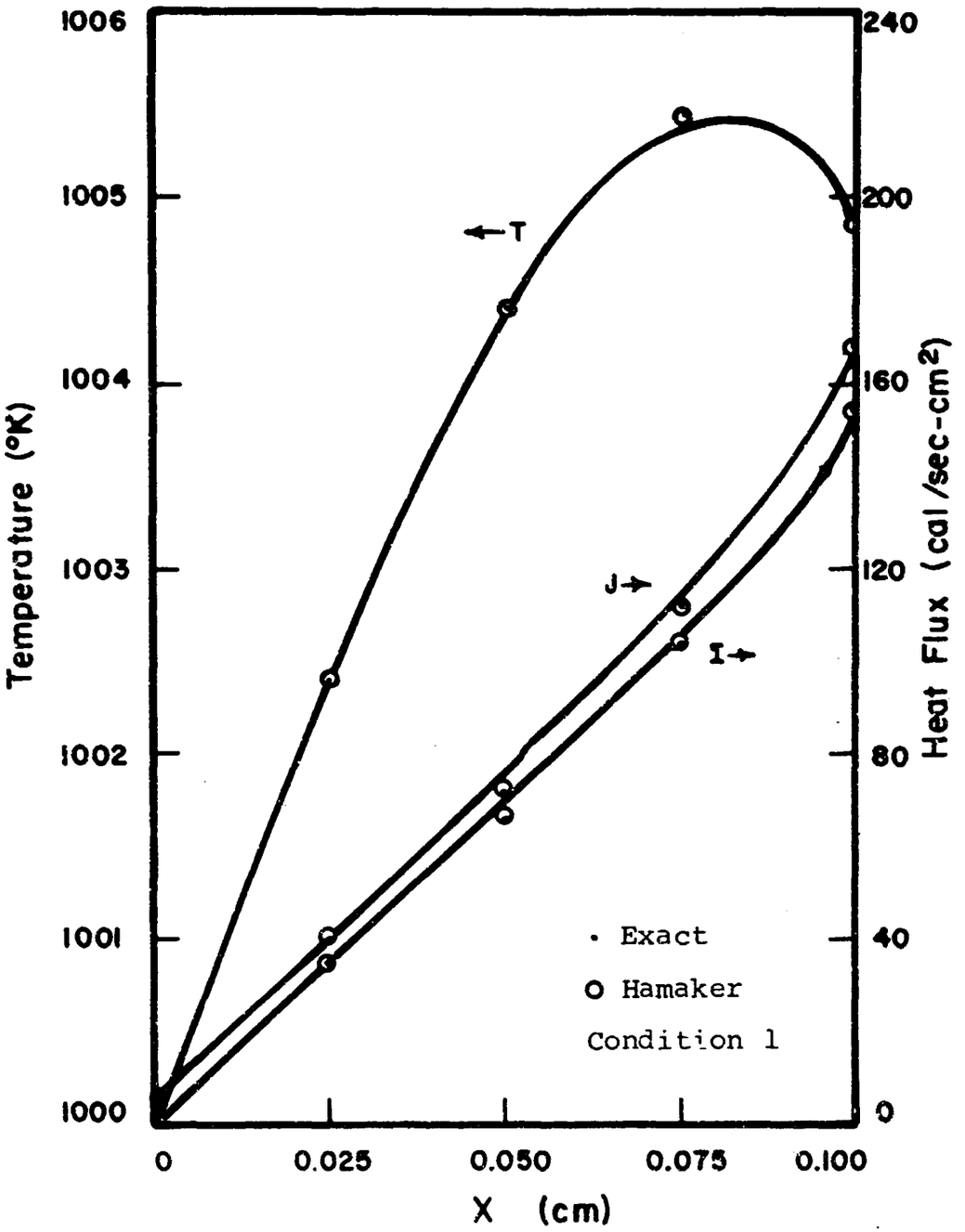

Figure 6.1 Comparison Between Exact and Hamaker Solution Using Conditions Approximating Test Material Properties. $k = 0.020$; $a = 0.23$; $S = 260$; $n^2 = 3$; $\left(\frac{dT}{dx}\right)_o = 100$; $T_o = 1{,}000$; $J_o = 5$; $I_o = 0$

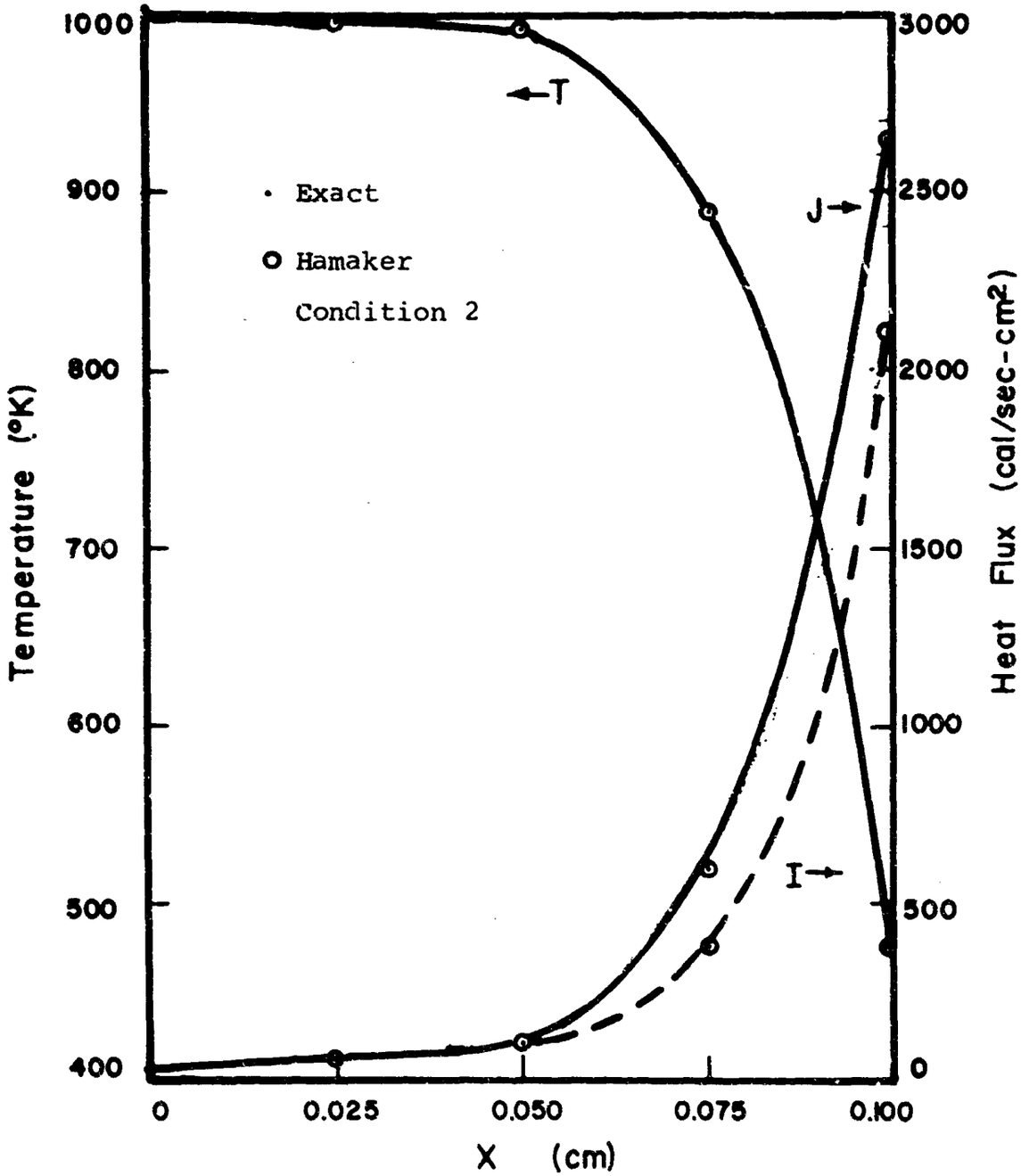

Figure 6.2 Comparison Between Exact and Hamaker Solution Using Conditions Approximating Test Material Properties. $k = 0.010$; $a = 0.23$; $S = 710$; $n^2 = 3$; $\left(\frac{dT}{dx}\right)_o = 100$; $T_o = 2{,}000$; $J_o = 35$; $I_o = 0$

surface. Thus, even though calculations were carried out to a greater sample depth in most cases, we have compared results at $x = (a + 2s)^{-1}$ and $x = 2(a + 2s)^{-1}$ in Table 6.1. As shown there for the entire range of conditions selected agreement between the exact and the Hamaker equations was within 0.1%.

7.0 SUMMARY

At wavelengths in the range from one to six microns, oxide materials are at least partially transparent. As a result thermal emissivity is a volume process dependent on the sample's radiant energy absorption and scattering characteristics. In Parts I[1] and II[2] of the present study, the influence of these material and specimen properties in isothermal emissivity was evaluated analytically and measured experimentally. Results showed that the behavior of these materials could be analyzed satisfactorily by means of the Hamaker approximation, and that calculations based on optical characteristics and microstructure features were in satisfactory agreement with experimental measurements.

In the present report, we have extended these analyses to specifically deal with the question of radiant energy emission from a non-isothermal body. In Section 2.0, analytical evaluations of the problem for total energy emission (assuming material constants independent of wavelength) and for the more important problem of spectral radiant energy emission (which allows one to account for the variation of refractive index, absorption coefficient and scattering coefficient) are reported. On the basis of this development it is possible to calculate, and we have calculated, the influence of temperature gradients on radiant energy emission.

In Section 3.0, a device for measurement of non-isothermal emissivity has been described and experimental results are compared with our calculations. This comparison is based on individual measurements precise to 0.01 emissivity units. At the wavelengths of most interest we are concerned with low emissivity values-in the range 0.05-0.25. As a result, even with this small absolute error, the precision of the comparison is not high. However, calculated and measured values agree within our rather broad error limits. The methods of material characterization and emissivity evaluation presented are clearly applicable to non-isothermal as well as isothermal conditions. As predicted, the influence of temperature gradients on radiant energy emission is found to be substantial and of real importance for heat transfer calculations.

Thus, it is confirmed that in this 1-5 micron range radiant energy emissivity can in no way be regarded as a material, or even as a sample characteristic. It is influenced by the microstructure (mostly porosity); but it is also influenced by

the temperature gradients in the solid as well as the surface temperature. To a certain extent one can academically circumvent this difficulty by always including the word "isothermal" in definitions, but this merely avoids the problem. In the present work we have unequivocably shown that the effect of temperature gradients is large, and we have tried to show how to cope with it.

Calculations of the transmission of radiant energy are presented in Section 4.0 of the present report. Comparisons of these calculations with experimental measurements (Section 5.0) offer still greater problems than for emissivity because of the low values of transmission we are dealing with and consequent low precision. Within the limits of experimental precision, calculations and experiment are in agreement. However the difficulty of measuring all the diffuse transmission (through a solid angle of 180°) and the extremely low fraction of parallel transmission make an exact analysis of the parallel and diffuse components, and a clear separation of the two, unattainable with the apparatus and techniques employed here.

It was hoped that evaluation of the parallel and diffuse transmission would lead to a basis for determining the effective absorption coefficient in oxide samples as a separable variable distinguished from the scattering coefficient. That hope has not been realized primarily because scattering overwhelms radiant energy absorption. Aside from either preparing a sample free from scattering centers, or by analysis of emissivity (or reflectivity) measurements, we have not achieved a simple reliable method of determining the effective absorption coefficient. Since, as reported in Part II[2] the absorption coefficient is a function of both wavelength and temperature, determination of isothermal emissivity (or reflectivity) remains the most effective way of fixing that variable. Once this is done however, we now have a sound basis for evaluating the effects of both microstructure and temperature gradients on the radiant energy emission over a range of conditions tested by both analytical calculations and experimental measurements.

As a final underpinning to confident application of this approach we have compared the Hamaker approximation and an exact solution for radiant energy emission for a range of thermal conditions and real material constants in Section 6.0. We have found that the Hamaker approximation is suitable (within 0.1%) for the conditions tested.

8.0 REFERENCES

1) Folweiler, R. C., "Thermal Radiation Characteristics of Transparent, Semi-Transparent and Translucent Materials Under Non-Isothermal Conditions", ASD-TDR-62-719, April, 1964.

2) Folweiler, R. C. and Mallio, W. J., "Thermal Radiation Characteristics of Transparent, Semi-Transparent and Translucent Materials Under Non-Isothermal Conditions", ASD-TDR-62-719, Part II, June, 1964.

3) Ryde, J. W., "Scattering of Light by Turbid Media: I", Proc. Roy. Soc., Ser A131, 451-465 (1931).

4) Baird-Atomics, Inc., Technical Data Sheet 460.

5) Van de Hulst, H. C.,"Light Scattering by Small Particles", J. Wiley & Sons, New York, (1957).

6) Love, T. J., and Wheasler, R. A., "An Experimental Study of Infra-Red Scattering by Clouds of Particles", ARL-64-109, June, 1964.

7) Chandrasekhar, S. "Radiative Transfer", Oxford University Press, Oxford (1950), Chapters II and III.

8) Abramowitz, M. and Stegun, I. A., Handbook of Mathematical Functions, U. S. Department of Commerce, 1964, p. 886, formula 25.4.15.

9) Kourganoff, V., "Basic Methods in Transfer Problems", Dover Edition, 1963.

APPENDIX I

1. Characterization of the Material Specimens Used for Transmissivity and Emissivity Measurements

In order to calculate the emissivity and transmissivity of a material, certain material properties must be characterized. These properties fall into two types: (1) properties which are unique to the material and (2) properties which are unique to the sample. The index of refraction, n, is an example of a material property, while the scattering coefficient S, is a property which is unique for each sample.

1.1 Al_2O_3

Emissivity and transmissivity measurements were made on four alumina samples, characterized as follows:

1.1.1 AD-995

Volume Fraction Porosity (P)* 0.044
Pore Radius (r)* 2.31μ

λ	Index of Refraction (n)*	Absorption Coefficient (cm^{-1})		Scattering Coefficient (cm^{-1})
		α*	a*= 2α	S*
1	1.75	0.38	0.76	385
2	1.74	0.12	0.24	372
3	1.72	0.10	0.20	357
4	1.65	0.24	0.48	327
5	1.60	2.6	5.2	277

*These symbols are the same as used throughout the text.

Figures 1.1 and 1.2 are photomicrographs of AD-995 alumina before and after testing.

1.1.2 AD-85

Volume Fraction Porosity (P) 0.103
Pore Radius (r) 2.31μ

λ	n	α	S
1	1.75	0.38	348
2	1.74	0.12	348
3	1.72	0.10	331
4	1.65	0.24	278
5	1.60	2.6	178

Figures 1.3 and 1.4 are photomicrographs of AD-85 before and after emissivity measurements were run.

1.1.3 Al-1

Volume Fraction Porosity (P) 0.119
Pore Radius (r) 2.5μ

λ	n	$\alpha(cm^{-1})$	$S(cm^{-1})$
1	1.75	0.38	973
2	1.74	0.12	943
3	1.72	0.10	907
4	1.65	0.24	813
5	1.60	2.6	734

Figures 1.5 and 1.6 are photomicrographs of Al-1 taken before and after emissivity measurements were run.

1.1.4 Al-4

Volume Fraction Porosity (P) 0.145
Pore Radius (r) 1.17μ

λ	n	$\alpha(cm^{-1})$	$S(cm^{-1})$
1	1.75	0.38	2373
2	1.74	0.12	2133
3	1.72	0.10	1787
4	1.65	0.24	1200
5	1.60	2.6	787

Figures 1.7 and 1.8 are photomicrographs of the sample before and after emissivity testing.

1.2 $SrTiO_3$

Two specimens of strontium titanate with different densities were fabricated by American Lava Company. After thermally annealing, these were ground to the required shapes for emissivity and transmissivity measurements.

1.2.1 $SrTiO_3$-A and $SrTiO_3$-B	A	B
Volume Fraction Porosity (P)	0.069	0.043
Pore Radius (r)	1.61μ	2.8μ

λ	n	α(cm^{-1})	A S(cm^{-1})	B S(cm^{-1})
1	2.31	0.58	1004	549
2	2.27	0.90	1004	549
3	2.23	0.32	1004	549
4	2.18	0.29	803	513
5	2.11	2.4	663	495

Figures 1.9 - 1.12 are before and after photomicrographs of the strontium titanate samples.

1.3 Pyroceram

Samples of Pyroceram 9606 and Pyroceram 9608 for emissivity and transmissivity measurements were supplied by Corning Glass Works. The 9606 and 9608 Pyrocerams were both fully dense (i.e., no porosity), and of optically indeterminate grain size so that no characterization of them could be made by the parameters used for the alumina and strontium titanate specimens. Figures 1.13 and 1.14 are photomicrographs of Pyroceram 9606 and 9608, but there is no detail visible.

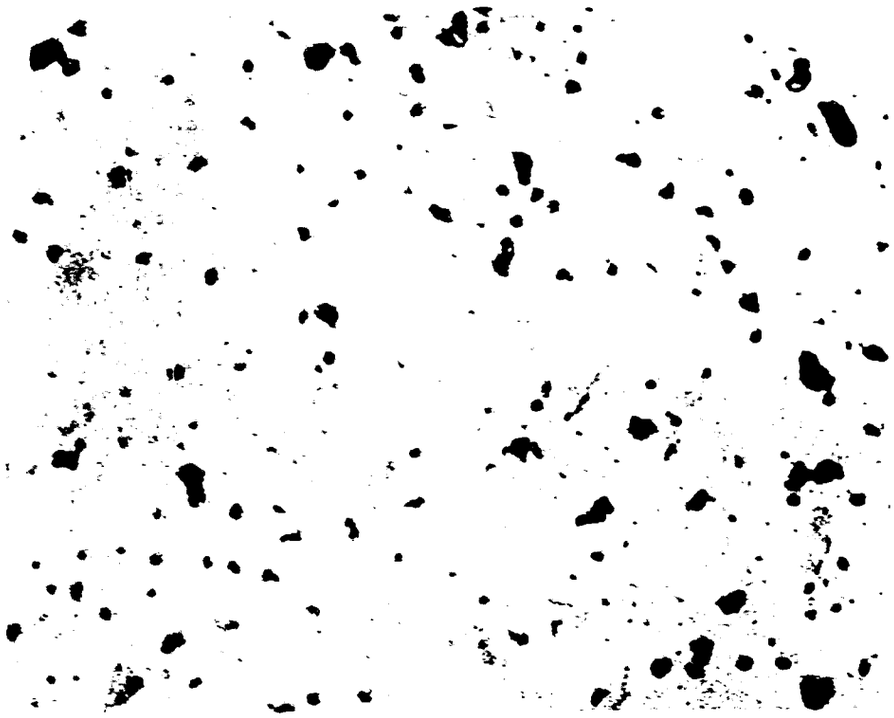

Figure I.1 Photomicrograph of AD-995 Before Non-Isothermal Test (400x).

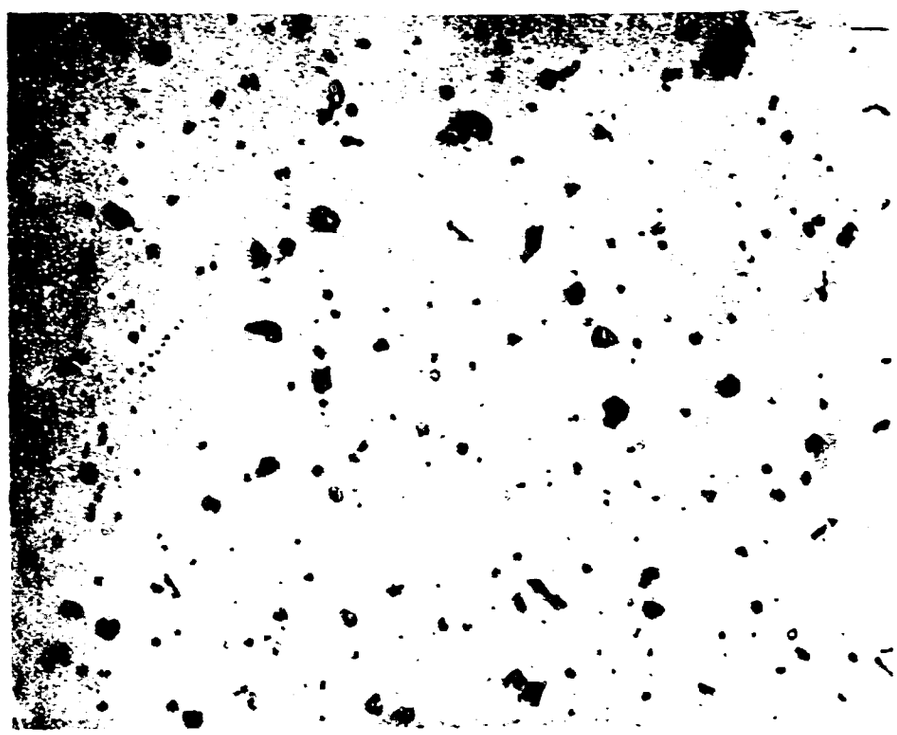

Figure I.2 Photomicrograph of AD-995 After Non-Isothermal Test (400x).

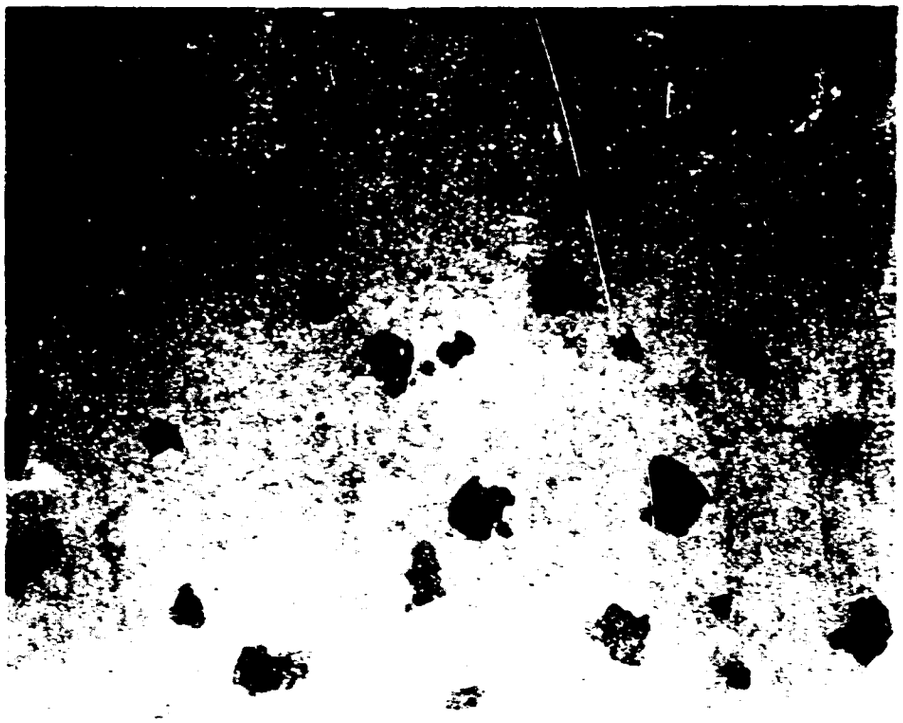

Figure I.3 Photomicrograph of AD-85 Before Non-Isothermal Test (400x).

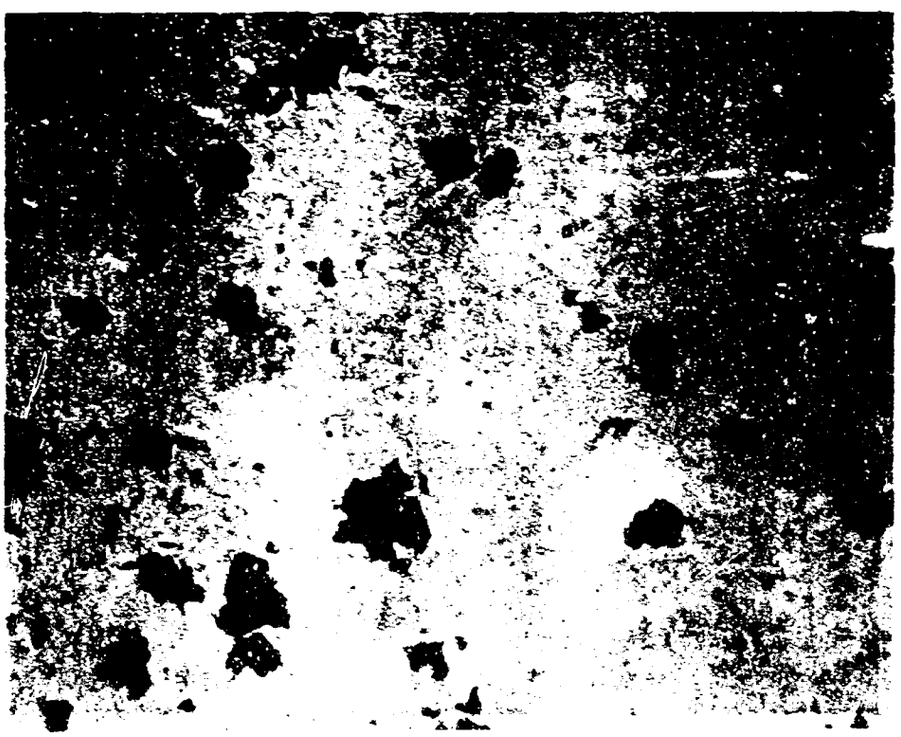

Figure I.4 Photomicrograph of AD-85 After Non-Isothermal Test (400x).

Figure I.5 Photomicrograph of Aℓ-1 Before Non-Isothermal Test (400x).

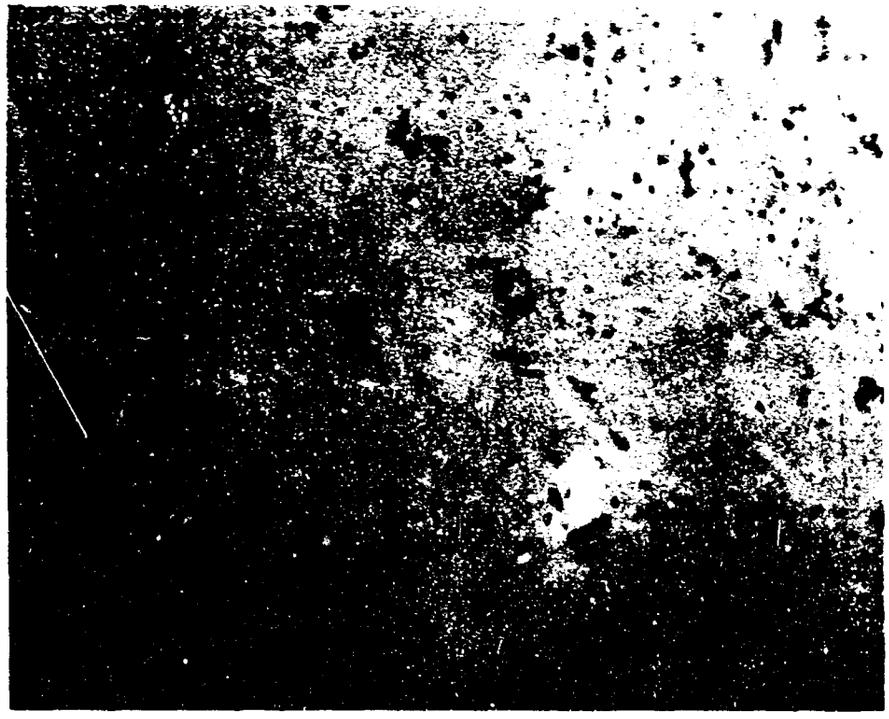

Figure I.6 Photomicrograph of Aℓ-1 After Non-Isothermal Test (400x).

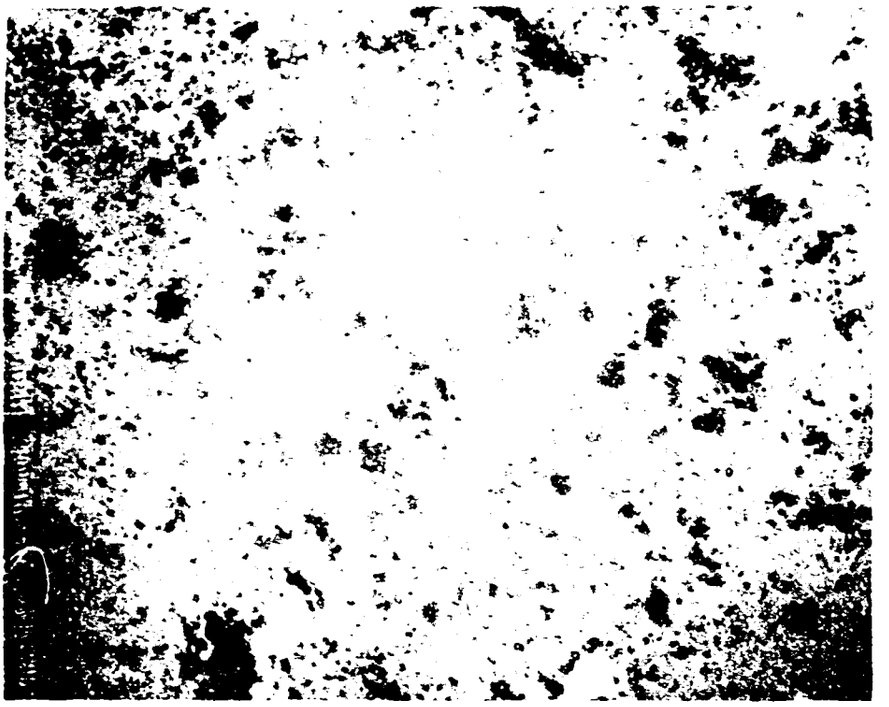

Figure I.7 Photomicrograph of Aℓ-4 Before Non-Isothermal Test (400x).

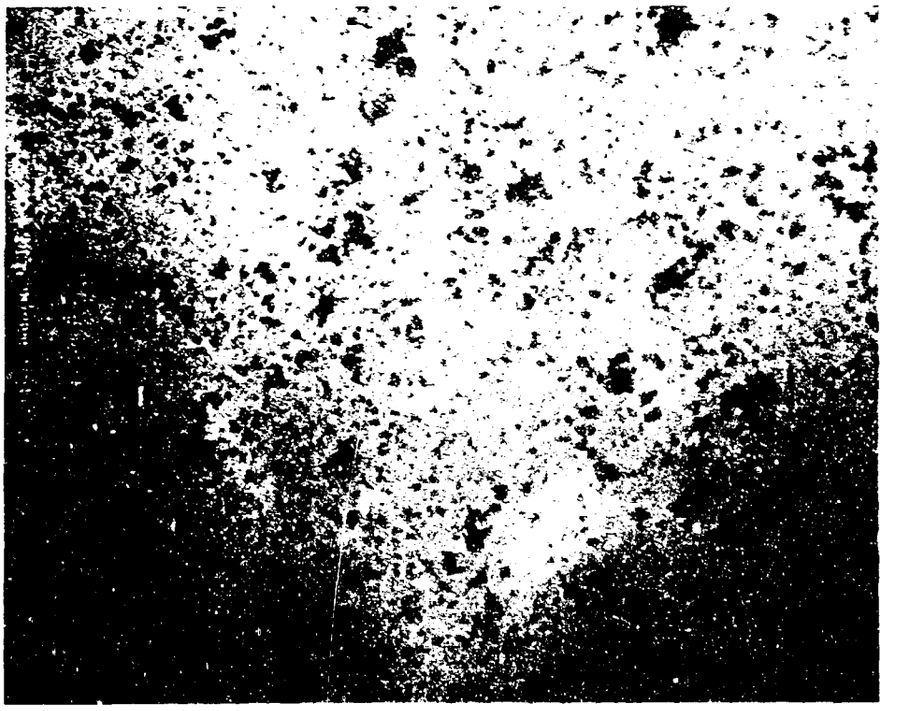

Figure I.8 Photomicrograph of Aℓ-4 After Non-Isothermal Test (400x).

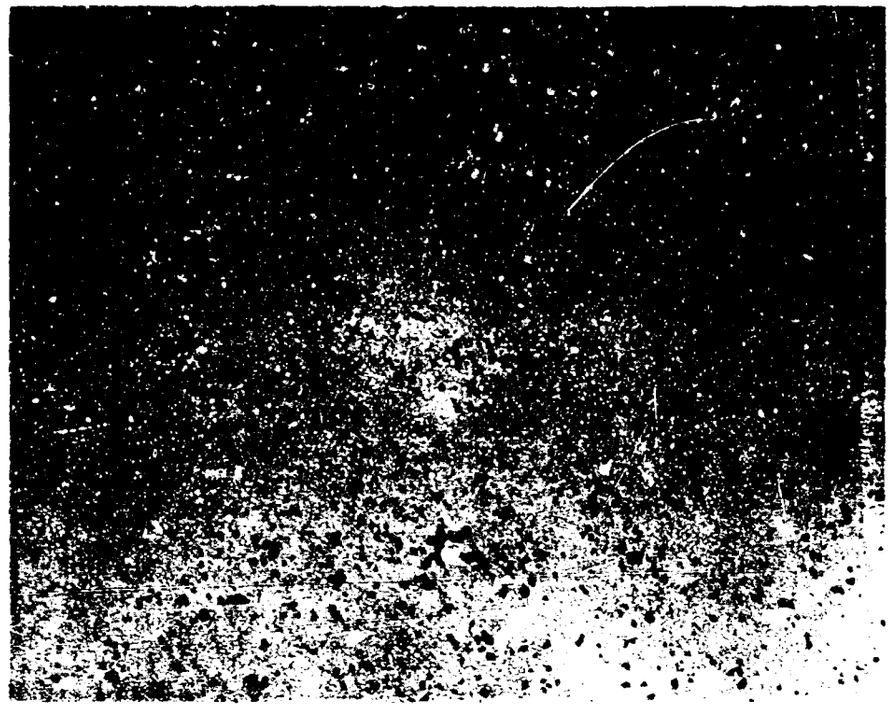

Figure I.9 Photomicrograph of $SrTiO_3A$ Before Non-Isothermal Test (400x).

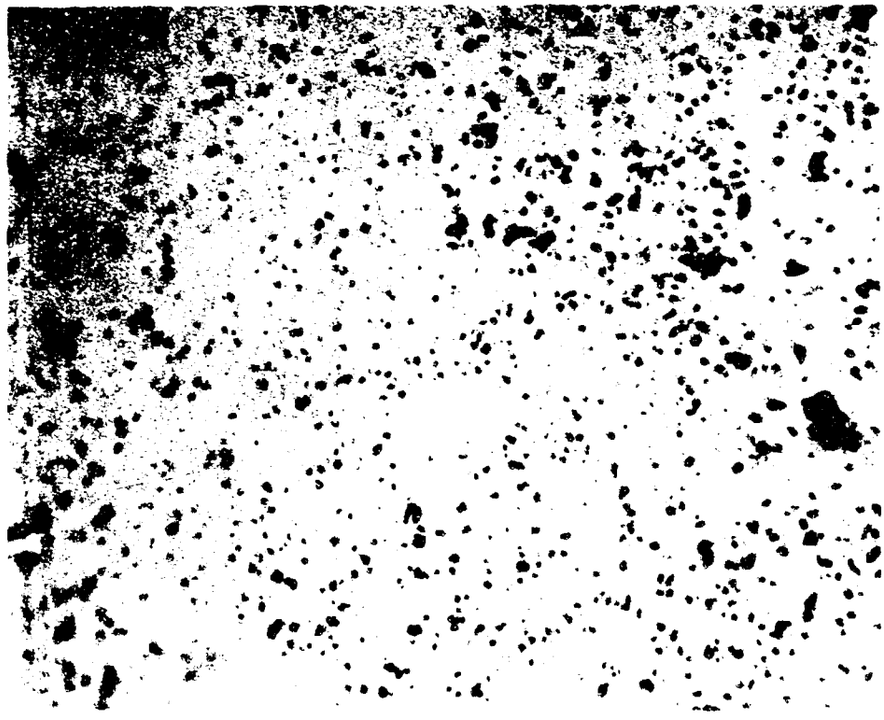

Figure I.10 Photomicrograph of $SrTiO_3A$ After Non-Isothermal Test (400x).

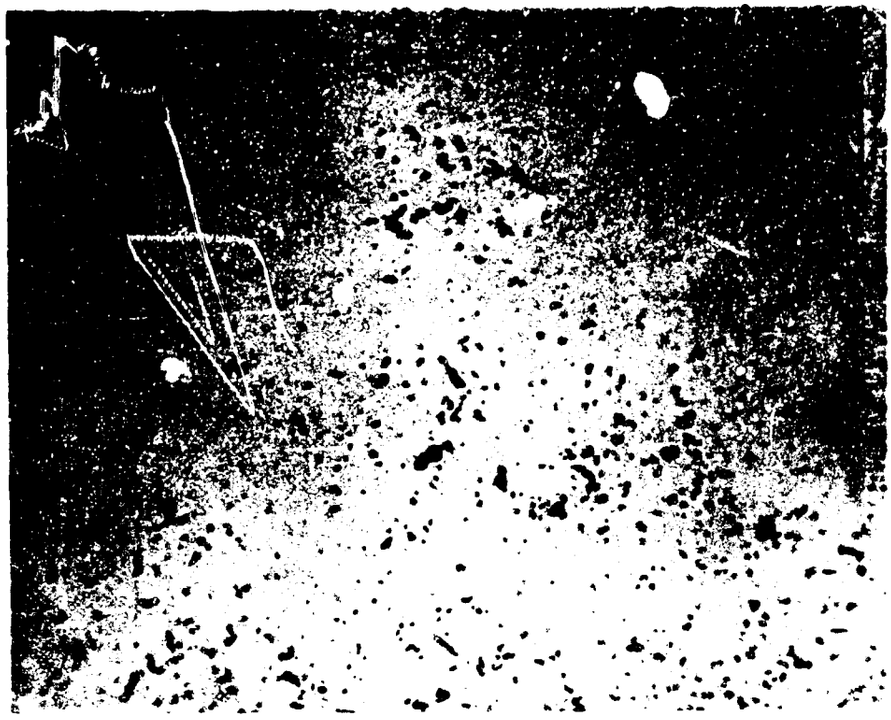

Figure I.11 Photomicrograph of $SrTiO_3B$ Before Non-Isothermal Test (400x).

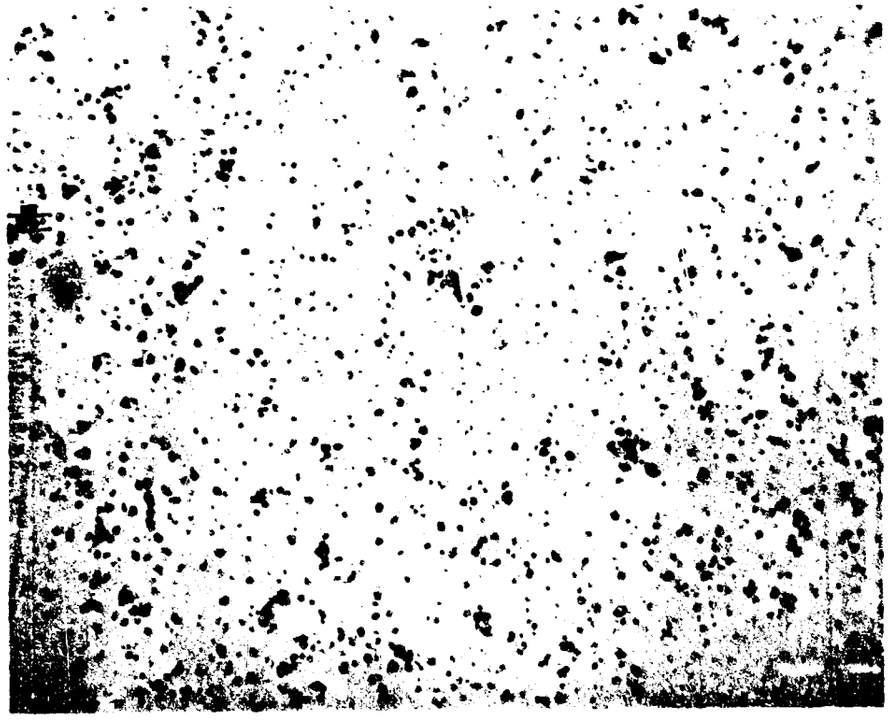

Figure I.12 Photomicrograph of $SrTiO_3B$ After Non-Isothermal Test (400x).

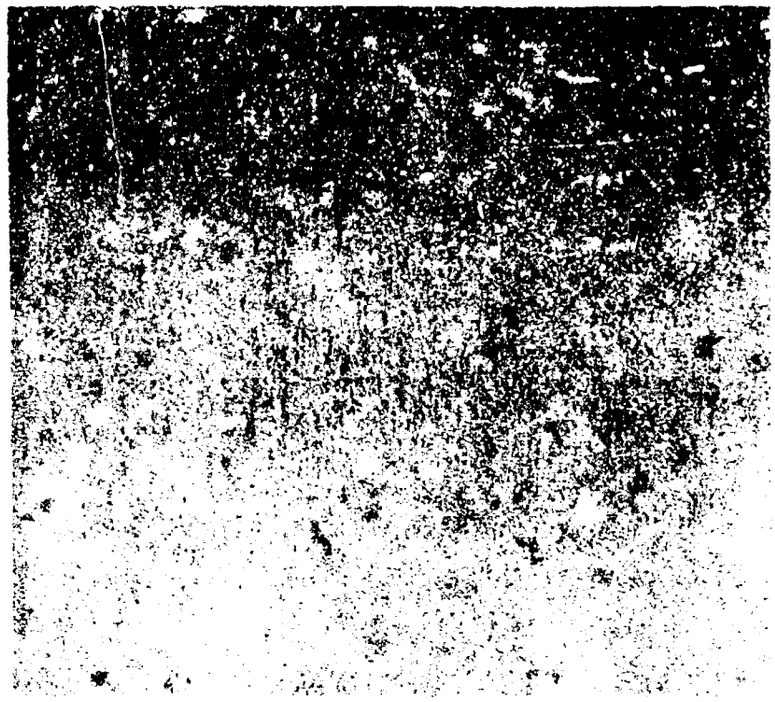

Figure I.13 Photomicrograph of Pyroceram 9606 Before Non-Isothermal Test (400x).

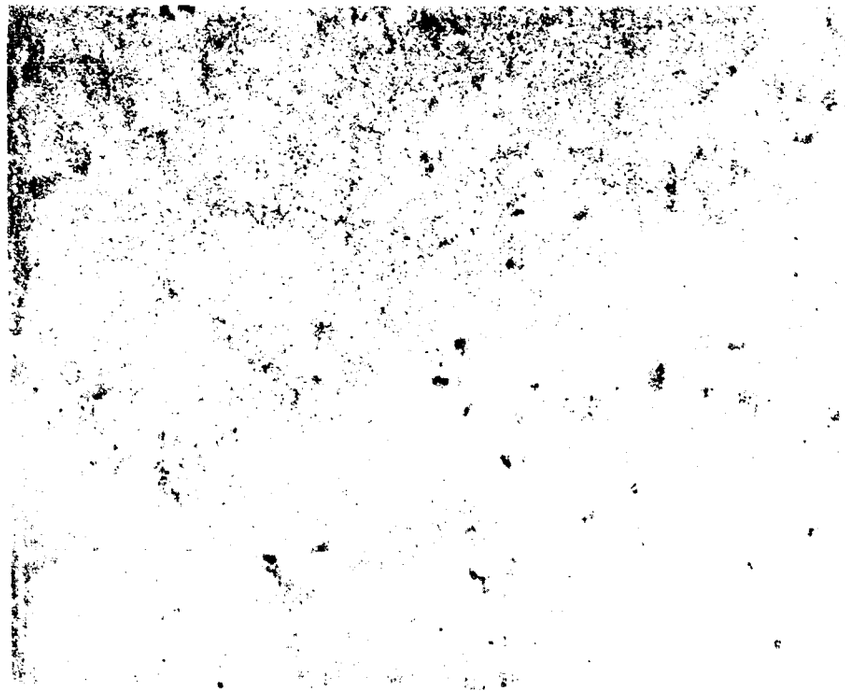

Figure I.14 Photomicrograph of Pyroceram 9608 Before Non-Isothermal Test (400x).

APPENDIX II

Spectral Emissivity of Radiating Energy from a Radiating Material with an Unknown Surface Temperature and a Known Gradient in the Body

We shall assume that a sample of radiating material has a temperature distribution given by

$$T(x) = T_o + \left(\frac{dT}{dx}\right)_o x \qquad (1)$$

in the interior, i.e. sufficiently far from the boundary. x measures the distance into the material from the boundary. We wish to determine the temperature distribution near x = 0 and also ascertain that Eq. 1 is a valid representation of T in the interior. For now assume that the absorption coefficient α, the scattering coefficient S, and the index of refraction n are independent of frequency. We have the following equations for the flux $\pi F(x)$ and the mean intensity $\bar{I}'(x)$.

$$\frac{dF(x)}{dx} = -4\alpha\,\bar{I}'(x) + 4\alpha n^2\sigma' T^4(x); \qquad (2)$$

and

$$\frac{4}{3}\frac{d\bar{I}'(x)}{dx} = (\alpha + S)F(x). \qquad (3)$$

These equations may be combined to obtain

$$\frac{d^2\bar{I}'(x)}{dx^2} - 3\alpha(\alpha + S)\,\bar{I}'(x) = -3\alpha(\alpha + S)n^2\sigma' T^4(x). \qquad (4)$$

Now the sum of the energy flux due to conduction and the energy flux due to radiation must be a constant. Therefore

$$-k\frac{dT(x)}{dx} + \pi F(x) = H, \qquad (5)$$

where k is the thermal conductivity of the material and H is the total energy flux. Note that $H < 0$ for energy coming out of the material. Substituting $F(x)$ from equation 3 into equation 5 we find

$$-k \frac{dT(x)}{dx} + \frac{4\pi}{3(\alpha + S)} \frac{d\bar{I}'(x)}{dx} = H \qquad (6)$$

with the immediate first integral

$$-kT(x) + \frac{4\pi}{3(\alpha + S)} \bar{I}'(x) = Hx + A, \qquad (7)$$

where A is a constant. Therefore,

$$\bar{I}'(x) = \frac{+3(\alpha + S)}{4\pi} \left[Hx + kT(x) + A \right]. \qquad (8)$$

Substituting from equation 8 in equation 4, we obtain

$$k\left[\frac{d^2T}{dx^2} - 3\alpha(\alpha + S)T\right] = -4\pi\alpha n^2 \sigma' T^4 + 3\alpha(\alpha + S)(Hx + A). \qquad (9)$$

First check that equation 1 is a valid interior solution for the temperature field. Let

$$T^4 = T_o^4 + 4T_o^3 \left(\frac{dT}{dx}\right)_o \cdot x \qquad (10)$$

is the interior, consistent with equation 1. Then equation 9 becomes

$$-3\alpha(\alpha + S)k\left[T_o + \left(\frac{dT}{dx}\right)_o x\right] = -4\pi\alpha n^2 \sigma' \left[T_o^4 + 4T_o^3 \left(\frac{dT}{dx}\right)_o x\right] + 3\alpha(\alpha + S)(Hx + A). \qquad (11)$$

Therefore

$$H = -k\left(\frac{dT}{dx}\right)_o + \frac{16\pi}{3(\alpha + S)} n^2 \sigma' T_o^3 \left(\frac{dT}{dx}\right)_o \tag{12}$$

and

$$A = - KT_o + \frac{4\pi}{3(\alpha + S)} n^2 \sigma' T_o^4 \tag{13}$$

Hence the observation of T at two interior points of the material determine A and H, since two observations give T_o and $\left(\frac{dT}{dx}\right)_o$. We have verified that equation (1) is a valid interior solution for T. Now we wish to find out how T varies near x = 0. Let the total temperature field T be written as the sum of an interior and a boundary contribution. Write

$$T = T^* + T_o + \left(\frac{dT}{dx}\right)_o x \tag{14}$$

Substituting equation (14) for T in equation (9), and using equations (12) and (13) for H and A, we obtain the following equation for T^*.

$$\frac{d^2T^*}{dx^2} - \left[3\alpha(\alpha + S) - \frac{16\pi\alpha n^2 \sigma' T_o^3}{k}\right] T^* = 0 \tag{15}$$

We have neglected terms which are quadratic in the quantities T^* and $\left(\frac{dT}{dx}\right)_o$, which are assumed to be small. The validity of this approximation must be verified <u>a posteriori</u>. If $L^2 = 3\alpha(\alpha + S) - \frac{16\pi\alpha n^2 \sigma' T_1^3}{k}$ is positive, then the solution of equation (15) which approaches 0 as $x \longrightarrow \infty$ is $T^* = Ce^{-Lx}$, where C is any constant. So the temperature field is given by

$$T(x) = T_o + \left(\frac{dT}{dx}\right)_o x + Ce^{-Lx} \tag{16}$$

Using equation 8, we find

$$\bar{I}'(x) = \frac{3(\alpha + S)}{4\pi} \left\{H_x + A + K\left[T_o + \left(\frac{dT}{dx}\right)_o x + Ce^{-Lx}\right]\right\}, \quad (17)$$

and from equations (3) and (17) we find

$$F'(x) = \frac{1}{\pi} \left\{H + K\left[\left(\frac{dT}{dx}\right)_c - CLe^{-Lx}\right]\right\} \quad (18)$$

Now C may be evaluated by imposing the boundary condition

$$I'^{+}(o) = \bar{\rho}\, I'^{-}(o), \quad (19)$$

where $\bar{\rho}$ is a mean reflection coefficient. Now

$$I'^{+}(x) = \bar{I}'(x) + \frac{F(x)}{2} \quad (20)$$

and

$$I'^{-}(x) = \bar{I}'(x) - \frac{F(x)}{2} . \quad (21)$$

So (19) is

$$\bar{I}'(o) + \frac{F(o)}{2} = \bar{\rho}\,\left(\bar{I}'(o) - \frac{F(o)}{2}\right),$$

or $$(1 - \bar{\rho})\bar{I}'(o) + \left(\frac{1 + \bar{\rho}}{2}\right)F(o) = 0 \quad (22)$$

Using (17) and (18), (22) becomes

$$(1 - \bar{\rho})\, \frac{3(\alpha + S)}{4\pi} \left\{A + K\,[T_o + C]\right\} +$$

$$\left(\frac{1 + \bar{\rho}}{2}\right)\, \frac{1}{\pi} \left\{H + K\left[\left(\frac{dT}{dx}\right)_o - CL\right]\right\} = 0$$

This equation gives

$$C = \frac{\frac{2}{3(\alpha + S)} \left(\frac{1 + \bar{\rho}}{1 - \bar{\rho}}\right) \left[\left(\frac{dT}{dx}\right)_o + \frac{H}{K}\right] + T_o + \frac{A}{K}}{\frac{2}{3(\alpha + S)} \left(\frac{1 + \bar{\rho}}{1 - \bar{\rho}}\right) L - 1} \qquad (23)$$

Now we use this temperature distribution (16) to investigate the radiation field as a function of frequency.

We shall assume that a sample of radiating material has a specified temperature distribution given by

$$T(x) = T_o + \left(\frac{dT}{dx}\right)_o x + Ce^{-Lx} \qquad (16)$$

where C is given by equation (23).
Let the sample have absorption coefficient α_ν, scattering coefficient S_ν, and index of refraction n_ν. These may all be frequency dependent. Let $I'_\nu(x, \vartheta)$ be the specific intensity of radiation at frequency ν in the material, where ϑ is the polar angle with respect to the +x axis. Assume axial symmetry. The equation of transfer for the radiation in the material is

$$\cos\vartheta \frac{dI'_\nu(x, \vartheta)}{dx} = -(\alpha_\nu + S_\nu)I'_\nu(x, \vartheta) + j_\nu(x). \qquad (24)$$

$j_\nu(x)$ is the emission coefficient for radiation at frequency ν in the material. $j_\nu(x)$ has two terms, one due to thermal emission at frequency ν and the other due to scattering of radiation at frequency ν. $j_\nu(x)$ is given by

$$j_\nu(x) = \alpha_\nu n_\nu^2 B_\nu(T(x)) + \frac{S_\nu}{2}\int_o^\pi I'_\nu(x, \vartheta)\sin\vartheta d\vartheta \qquad (25)$$

$B_\nu(T)$ is the Planck function given by

$$B_\nu(T) = \frac{2h\nu^3}{c^2}\frac{1}{e^{h\nu/\underset{\sim}{K}T} - 1} \qquad (26)$$

where h = Planck's constant, $\underset{\sim}{K}$ = Boltzmann's constant, and c is the velocity of light in vacuo.

In accordance with $T(x) = T_o + \left(\frac{dT}{dx}\right)_o x + Ce^{-Lx}$ we write

$$B_\nu(T(x)) = B_\nu(T_o) + \left(\frac{\partial B_\nu}{\partial T}\right)_{T_o}\left[\left(\frac{dT}{dx}\right)_o x + Ce^{-Lx}\right] \qquad (27)$$

It is convenient to replace the variable ϑ by $\mu = \cos\vartheta$ in the following analysis. So we will now write $I_\nu(x, \mu)$ to denote the specific intensity of radiation at frequency ν, at a depth x in the material, in the direction $\vartheta = \cos^{-1}\mu$. The equation of transfer (24) may now be written in the form

$$\mu \frac{dI'_\nu(x, \mu)}{dx} = -(\alpha_\nu + S_\nu) I'_\nu(x, \mu) + \alpha_\nu n_\nu^2 B_\nu(T(x)) +$$

$$\frac{S_\nu}{2} \int_{-1}^{1} I'_\nu(x, \mu) d\mu \qquad (28)$$

From now on we will suppress the subscript ν on α_ν, S_ν, n_ν, and $B_\nu(T)$. But it is important to remember that whenever α, S, n, and B(T) appear they refer to these quantities at the particular frequency ν with which we are dealing. We now solve the equation of transfer (28) by the method of discrete ordinates [see Chandrasekhar, R. T., Chapters II and III] (7). Divide the radiation field into 2m streams in the directions μ_i ($i = \pm 1, \pm 2, \ldots \pm m$ and $\mu_i = -\mu_{-i}$). Let any integral of the form $\int_{-1}^{1} f(\mu) d\mu$ be approximated by

$$\int_{-1}^{1} f(\mu) d\mu \simeq \sum_{\substack{j=-m \\ j \neq o}}^{m} a_j f(\mu_j). \qquad (29)$$

We will use a Newton-Cotes quadrature formula, with $\mu_j = \left(\frac{2j-1}{2m-1}\right)$, $j = 1, \ldots m$. The a_j are chosen so that the formula

$$\int_{-1}^{1} f(\mu) d\mu = \sum_{\substack{j=-m \\ j \neq o}}^{m} a_j f(\mu_j) \qquad (30)$$

is exact whenever $f(\mu)$ is a polynomial of degree less than m. In general we will have $a_j = -a_{-j}$, and

$$\sum_{j=1}^{m} a_j = 1.$$

For m = 3, $\mu_1 = 1/5$, $\mu_2 = 3/5$, $\mu_3 = 1$, and $a_1 = 50/144$, $a_2 = 75/144$, and $a_3 = 19/144$. (See Abramowitz and Stegun (8), page 886, formula 25.4.15). For m = 4, $\mu_1 = 1/7$, $\mu_2 = 3/7$, $\mu_3 = 5/7$, $\mu_4 = 1$, and $a_1 = 0.34595$, $a_2 = 0.15313$, $a_3 = 0.41400$, $a_4 = 0.08692$ (See Kourganoff, page 112)(9). Writing the

equation of transfer for the direction μ_i we have

$$\mu_i \frac{dI'_\nu(x, \mu_i)}{dx} = -(\alpha + S)I'_\nu(x, \mu_i) + \alpha n^2 B(T(x)) + \frac{S}{2} \sum_{\substack{j=-m \\ j \neq o}}^{m} a_j I'_\nu(x, \mu_j)$$

$$i = \pm 1, \pm 2, \ldots \pm_m. \quad (31)$$

These are 2m first order linear differential equations for the 2m quantities $I'_\nu(x, \mu_i)$, $i = \pm 1, \ldots \pm m$.

$$\text{Define } B^o = B(T_o) \text{ and } B' = \left(\frac{\partial B}{\partial T}\right) T_o \quad (32)$$

Using the shortened notation, $I'_\nu(x, \mu_i) = I_i$, these equations may be written as

$$\mu_i \frac{dI_i}{dx} = -(\alpha + S)I_i + \alpha n^2 \left\{ B^o + B' \left[\left(\frac{dT}{dx}\right)_o x + Ce^{-Lx} \right] \right\} + \frac{S}{2} \sum_{\substack{j=-m \\ j \neq o}}^{m} a_j I_j. \quad (33)$$

A particular solution is

$$I_i = n^2 \left\{ \left[B^o + B' \left(\frac{dT}{dx}\right)_o \left(x - \frac{\mu_i}{\alpha + S}\right) \right] + \alpha B' Ch_i e^{-Lx} \right\} \quad (34)$$

where $h_i = D/\alpha + S - L\mu_j$ and $D = 1/\left[1 - \frac{S}{2} \sum_{j=-m}^{m} \frac{a_j}{\alpha + S - L\mu_j}\right]$

To this must be added the general solution of the homogeneous system

$$\mu_i \frac{dI_i}{dx} = -(\alpha + S)I_i + \frac{S}{2} \sum_{\substack{j=-m \\ j \neq o}}^{m} a_j I_j \quad (35)$$

We seek solutions of the form

$$I_i = g_i e^{+K_p(\alpha + S)x} \qquad i = \pm 1, \ldots \pm m. \quad (36)$$

Substituting this expression (36) for I_i into the differential equation (35), we find

$$g_i(\alpha + S)(1 + K_p\mu_i) = \frac{S}{2} \sum_{\substack{j=-m \\ j \neq o}}^{m} a_j g_j \tag{37}$$

The right hand side of this equation is a constant independent of i. Therefore

$$g_i = \frac{A}{1 + K_p \mu_i}, \quad i = \pm 1, \pm 2, \cdots \pm m, \tag{38}$$

where A is some constant. Substituting this back into the equation (37) for g_i and dividing by A we obtain

$$\alpha + S = \frac{S}{2} \sum_{\substack{j=-m \\ j \neq o}}^{m} \frac{a_j}{1 + K_p \mu_j} \tag{39}$$

This may be written as

$$1 = \frac{1}{2} \frac{S}{\alpha + S} \sum_{\substack{j=-m \\ j \neq o}}^{m} \frac{a_j}{1 + \mu_j K_p}, \tag{40}$$

recalling that $\mu_{-i} = -\mu_i$, $a_{-i} = a_i$, this becomes

$$1 = \frac{S}{\alpha + S} \sum_{j=1}^{m} \frac{a_j}{1 - K_p^2 \mu_j^2}. \tag{41}$$

This is the characteristic equation which must be solved for the constant K_p. If $\frac{S}{\alpha + S} < 1$, the equation

$$1 = \frac{S}{\alpha + S} \sum_{i=1}^{m} \frac{a_i}{1 - \mu_j^2 K_p^2} \tag{42}$$

has 2m non-zero distinct roots which occur in pairs $\pm K_p$ ($p = 1, \cdots m$). Suppressing the solutions which would let I_i become infinite exponentially as $x \to \infty$ we write

$$I_i = n^2 B' \left\{ \left(\frac{dT}{dx}\right)_o \left(x - \frac{\mu_i}{\alpha + S}\right) + \frac{B^o}{B'} + \sum_{p=1}^{m} \frac{L_p e^{-K_p(\alpha + S)x}}{1 - \mu_i K_p} + \alpha C h_i e^{-Lx} \right\} \qquad (43)$$

The m constants L_p are determined by the boundary conditions at $x = 0$. The boundary conditions at $x = 0$ are

$$I'_\nu(0, +\mu) = \rho(\theta) I'_\nu(0, -\mu), \text{ for } \sqrt{1 - \frac{1}{n^2}} \leq \mu \leq 1 \qquad (44)$$

and

$$I'_\nu(0, +\mu) = I'_\nu(0, -\mu) \text{ for } 0 \leq \mu \leq \sqrt{1 - \frac{1}{n^2}} \, . \qquad (45)$$

$\rho(\theta)$ is given by

$$\rho(\theta) = \frac{1}{2}\left[\frac{\sin^2(\theta - \theta')}{\sin^2(\theta + \theta')} + \frac{\tan^2(\theta - \theta')}{\tan^2(\theta + \theta')}\right], \qquad (46)$$

where $\mu = \cos\theta$ and $\sin\theta' = n \sin\theta$.

We now restrict the discussion to the case for which the four-point (m = 4) Newton-Cotes quadrature formula is used to evaluate integrals of the form $\int_{-1}^{1} f(\mu)\, d\mu$. In terms of the discrete angles μ_i the boundary conditions (44,45) are

$$I'_\nu(0, \mu_i) = \rho(\theta_i) I'_\nu(0, -\mu_i) \text{ for } \sqrt{1 - \frac{1}{n^2}} \leq \mu_i \leq 1, \qquad (47)$$

and

$$I_\nu'(0,\mu_i) = I_\nu'(0,-\mu_i) \text{ for } 0 \leq \mu_i \leq \sqrt{1 - \frac{1}{n^2}} \,. \tag{48}$$

For the Newton-Cotes four-point (m = 4) quadrature formula, we have $\mu_1 = 1/7$, $\mu_2 = 3/7$, $\mu_3 = 5/7$, $\mu_4 = 1$. If $n \geq 1.43$, we have

$$0 < \mu_1 < \mu_2 < \mu_3 \leq \sqrt{1 - \frac{1}{n^2}} \,.$$

Therefore

$$I_\nu'(0, \mu_i) = I_\nu'(0, -\mu_i) \quad i = 1, 2, 3, \tag{49}$$

and

$$I_\nu'(0, \mu_4) = \rho(0) I_\nu'(0, -\mu_4) \,. \tag{50}$$

This may be written

$$I_\nu'(0,1) = \rho(0) I_\nu'(0,-1) \,. \tag{51}$$

Note that

$$\rho(0) = \lim_{\theta \to 0} \rho(\theta) = \lim_{\theta \to 0} \frac{1}{2} \left[\frac{\sin^2(\theta - \theta')}{\sin^2(\theta + \theta')} + \frac{\tan^2(\theta - \theta')}{\tan^2(\theta + \theta')} \right]$$

$$= \lim_{\theta \to 0} \left[\left(\frac{\theta - \theta'}{\theta + \theta'} \right)^2 \right] = \lim_{\theta \to 0} \left[\frac{\theta^2 (1 - \frac{1}{n})^2}{\theta^2 (1 + \frac{1}{n})^2} \right]$$

$$= \left(\frac{n - 1}{n + 1} \right)^2 . \tag{52}$$

If $1.43 > n \geq 1.11$, $0 < \mu_1 < \mu_2 \leq \sqrt{1 - \frac{1}{n^2}}$ and

$\sqrt{1 - \frac{1}{n^2}} < \mu_3 < \mu_4 = 1.$

In this case the boundary conditions are

$$I_\nu'(0, \mu_i) = I_\nu'(0, -\mu_i) \quad i = 1, 2 \tag{53}$$

$$I_\nu'(0, \mu_3) = \rho(\theta_3) I_\nu'(0, -\mu_3), \tag{54}$$

and $$I_\nu'(C, \mu_4) = \rho(0) I_\nu'(0, -\mu_4). \tag{55}$$

Now from equation (43),

$$I_i(x, \mu_i) = n^2 B' \left\{ (x - \frac{\mu_i}{\alpha + S}) \left(\frac{dT}{dx}\right)_o + \frac{B^o}{B'} + \sum_{p=1}^{m} \frac{L_p e^{-K_p(\alpha + S)X}}{1 - \mu_i K_p} \right.$$

$$\left. + \frac{\alpha CD}{\alpha + S - L\mu_j} e^{-Lx} \right\} \tag{43}$$

So

$$I_i(0, \mu_i) = n^2 B' \left\{ \frac{B^o}{B'} - \frac{\mu_i \left(\frac{dT}{dx}\right)_o}{\alpha + S} + \sum_{p=1}^{m} \frac{L_p}{1 - \mu_i K_p} \right.$$

$$\left. + \frac{\alpha CD}{\alpha + S - L\mu_j} \right\} \tag{56}$$

We assume for now that $n \geq 1.43$. Then

$$I_i(C, \mu_i) = I_i(0, \mu_i) \quad i = 1, 2, 3 \tag{57}$$

$$I_i(0, 1) = \left(\frac{n - 1}{n + 1}\right)^2 I_i(0, -1). \tag{58}$$

Substituting from our expression (57) for $I_i(0, \mu_i)$ we have

$$n^2 B' \left[\frac{B^o}{B'} - \frac{\mu_i \left(\frac{dT}{dx}\right)_o}{\alpha + S} + \sum_{p=1}^{m} \frac{L_p}{1 - \mu_i K_p} + \frac{\alpha CD}{\alpha + S - L\mu_i} \right] =$$

$$n^2 B' \left[\frac{B^o}{B'} + \frac{\mu_i \left(\frac{dT}{dx}\right)_o}{\alpha + S} + \sum_{p=1}^{m} \frac{L_p}{1 + \mu_i K_p} + \frac{\alpha CD}{\alpha + S + L\mu_i} \right] \qquad (59)$$

for $i = 1, 2, 3$

and

$$n^2 B' \left[\frac{B^o}{B'} - \frac{\left(\frac{dT}{dx}\right)_o}{\alpha + S} + \sum_{p=1}^{m} \frac{L_p}{1 - K_p} + \frac{\alpha CD}{\alpha + S - L} \right] =$$

$$\left(\frac{n-1}{n+1}\right)^2 n^2 B' \left[\frac{B^o}{B'} + \frac{\left(\frac{dT}{dx}\right)_o}{\alpha + S} + \sum_{p=1}^{m} \frac{L_p}{1 + K_p} + \frac{\alpha CD}{\alpha + S + L} \right] \qquad (60)$$

These equations may be manipulated to obtain

$$\sum_{p=1}^{m} \frac{L_p K_p}{1 - \mu_i^2 K_p^2} = \frac{\left(\frac{dT}{dx}\right)_o}{\alpha + S} - \frac{\alpha CDL}{(\alpha + S)^2 - L^2 \mu_i^2} \qquad (61)$$

$$i = 1, 2, 3$$

and

$$\sum_{p=1}^{m} L_p \left[\frac{1}{1 - K_p} - \left(\frac{n-1}{n+1}\right)^2 \frac{1}{1 + K_p} \right] = \left(\frac{dT}{dx}\right)_o \frac{1 + \left(\frac{n+1}{n+1}\right)^2}{\alpha + S}$$

$$- \left[1 - \left(\frac{n-1}{n+1}\right)^2 \right] \frac{B^o}{B'} + \alpha CD \left[\frac{\left(\frac{n-1}{n+1}\right)^2}{\alpha + S + L} - \frac{1}{\alpha + S + L} \right] \qquad (62)$$

Of course in this case m= 4 and the K_p are the 4 positive roots of the equation

$$1 = \frac{S}{\alpha + S} \sum_{j=1}^{4} \frac{a_j}{1 - \mu_j^2 K_p^2} . \qquad (42)$$

We have $\mu_1 = 1/7$, $\mu_2 = 3/7$, $\mu_3 = 5/7$, $\mu_4 = 1$, and $a_1 = 0.34595$, $a_2 = 0.15313$, $a_3 = 0.41400$, and $a_4 = 0.08692$.

The values K_p depend on the ratio $\frac{S}{\alpha + S}$. Having chosen α and S we may solve for the K_p. Then the coefficients in the 4 linear equations (61,62) for the L_p are known, and we may solve for L_p. Then we may compute

$$I'_\nu(0,-1) = n^2 B' \left[\frac{\left(\frac{dT}{dx}\right)_o}{\alpha + S} + \frac{B^o}{B'} + \sum_{p=1}^{m} \frac{L_p}{1 + K_p} + \frac{\alpha CD}{\alpha + S + L} \right] \tag{63}$$

The intensity of radiation emerging from the sample in a narrow cone normal to the surface is

$$I_{emergent} = \frac{1 - \rho(0)}{\mu^2} I'_\nu(0,-1) \tag{64}$$

$$\therefore \quad I_{emergent} = \frac{4nB'}{(n+1)^2} \left[\frac{\left(\frac{dT}{dx}\right)_o}{\alpha + S} + \frac{B^o}{B'} + \sum_{p=1}^{m} \frac{L_p}{1 + K_p} + \frac{\alpha CD}{\alpha + S + L} \right] \tag{65}$$

The reason the analysis cannot be carried out explicitly in general is that the characteristic equation (42) for K_p is a polynomial of moderately high order. For our four-point method, equation (42) is a quartic in K_p^2. For each choice of $\frac{S}{\alpha + S}$ this equation must be solved numerically. In this connection we can make the following observations, Equation (42) may be written in the form

$$F(K_p) = 1 - \frac{S}{\alpha + S} \sum_{j=1}^{4} \frac{a_j}{1 - \mu_j^2 K_p^2} = 0 \tag{66}$$

It is clear the $F(K_p) = F(-K_p)$ and $F(0) = 1 - \frac{S}{\alpha + S} = \frac{\alpha}{\alpha + S} > 0$. Also, $F(K_p)$ is undefined when $K_p = \frac{1}{\mu_j}$, $j = 1, 2, 3, 4$.

In fact, $\lim_{K_p \to \frac{1}{\mu_j} -} F(K_p) = -\infty$, and $\lim_{K_p \to \frac{1}{\mu_j} +} F(K_p) = +\infty$.

Finally we note that

$$\frac{dF(K_p)}{dK_p} = -\frac{S}{\alpha + S} \sum_{j=1}^{4} \frac{2\alpha_i \mu_j^2 K_p}{(1 - \mu_j^2 K_p^2)^2} < 0 \text{ for } K_p > 0.$$

From these facts we conclude that $F(K_p)$ has the form

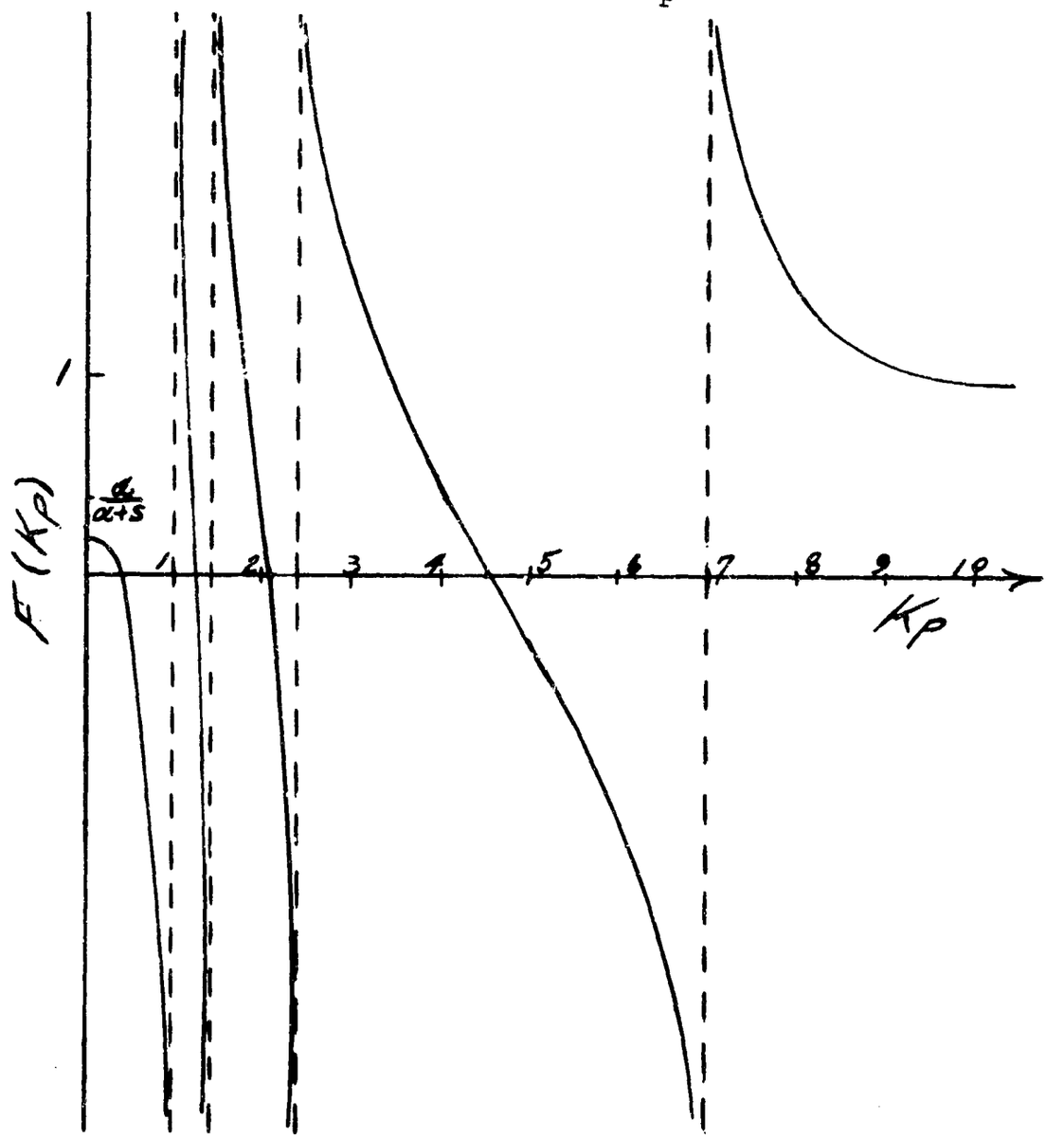

Thus we see $F(K_p)$ has four positive zeros, with

$$0 < K_1 < 1 < K_2 < \frac{7}{5} < K_3 < \frac{7}{3} < K_4 < 7. \tag{67}$$

That these are all the positive roots may be seen by multiplying equation (66) by

$$P(K_p) = \prod_{j=1}^{4} (1 - \mu_j^2 K_p^2). \tag{68}$$

$P(K_p)$ is a quartic equation in K_p^2. Multiplying (66) by $P(K_p)$ gives

$$P(K_p) - \frac{S}{\alpha + S} \sum_{j=1}^{4} \frac{a_j}{1 - \mu_j^2 K_p^2} \prod_{i=1}^{4} (1 - \mu_i^2 K_p^2) = 0 \tag{69}$$

This may be simplified to give

$$Q(K_p) = P(K_p) - \frac{S}{\alpha + \alpha} \sum_{j=1}^{4} a_j \prod_{\substack{i=1 \\ i \neq j}}^{4} (1 - \mu_i^2 K_p^2) = 0 \tag{70}$$

Now $\sum_{j=1}^{4} a_j \prod_{\substack{i=1 \\ i \neq j}}^{4} (1 - \mu_i^2 K_p^2)$ is the sum of four cubic polynomials in K_p^2. So $Q(K_p)$ is a quartic polynomial in K_p^2, and the equation

$$Q(K_p) = 0 \tag{71}$$

has four real or complex roots for K_p^2. But the roots of $Q(K_p) = 0$ are the same as the roots of $F(K_p) = 0$, and we have shown that $F(K_p)$ has four positive roots K_p. So the eight roots K_p of $Q(K_p) = 0$ are just $\pm K_p'$, where K_p' are the positive roots of $F(K_p') = 0$. To find the actual roots numerically

equation (66) should be reduced to the form of equation (70). Then any of the standard numerical techniques for quartic equations may be used. (See, for example, Abramowitz and Stegun, page 20, Example 6.) The inequalities (67) will be useful in any iterative procedure used to solve (70). Once the K_p are known, solution of the system of equations (61 and 62) for L_p is quite straight-forward. It requires only the inversion of one 4 x 4 matrix.

In solving (62) it is useful to note that B^o and B' are given by

$$B^o = \frac{2h\nu^3}{c^2} \frac{1}{e^{h\nu/\underset{\sim}{K}T_o} - 1} \tag{72}$$

and

$$\frac{B'}{B^o} = \frac{\frac{h\nu}{\underset{\sim}{K}T_o^2}}{1 - e^{-h\nu/\underset{\sim}{K}T_o}} \tag{73}$$

APPENDIX III

Exact Solution for the Transmissivity of an Absorbing and Scattering Material

For a beam of parallel light of unit intensity that is incident normally on the surface of a specimen, the equations for the flux are:

$$\frac{dI}{dx} = sJ + s'J_p - (a + s)I + f'I_p \tag{1}$$

$$-\frac{dJ}{dx} = sI + s'I_p - (a + s)J + f'J_p \tag{2}$$

$$\frac{dI_p}{dx} = -(a + s' + f')I_p = -g'I_p \tag{3}$$

$$-\frac{dJ_p}{dx} = -(a + s' + f')J_p = -g'J_p \tag{4}$$

Solutions of these equations are:

$$I_p = I_{po}\exp(-g'x) \tag{5}$$

$$J_p = J_{po}\exp(g'x) \tag{6}$$

$$I = A(1 - \beta_o)\exp(\sigma_o x) + B(1 + \beta_o)\exp(-\sigma_o x) - U\,I_{po}\exp(-g'x) - V\,J_{po}\exp(g'x) \tag{7}$$

$$J = A(1 + \beta_o)\exp(\sigma_o x) + B(1 - \beta_o)\exp(-\sigma_o x) - V\,I_{po}\exp(-g'x) - U\,J_{po}\exp(g'x) \tag{8}$$

where A and B are constants determined by the boundary conditions and U and V are as defined in section 4.1.

The boundary conditions are:

$$x = o,\ I_p = (1 - \rho_{no}) + J_p\rho_{ni}$$

$$I = J\rho_i$$

$$x = d,\ J_p = I_p\rho_{ni}$$

$$J = I\rho_i$$

Applying the parallel radiation boundary conditions,

$$x = d,\ J_{po}\exp(g'd) = \rho_{ni}I_{po}\exp(-g'd) \tag{9}$$

$$x = o,\ I_{po} = (1 - \rho_{no}) + J\rho_{ni} \tag{10}$$

$$\therefore \quad I_{po} = \frac{(1-\rho_{no})}{1 - \rho_{ni}^2\exp(-2g'd)} \tag{11}$$

$$J_{po} = \frac{(1 - \rho_{no})\ \rho_{ni}\exp(-2g'd)}{1 - \rho_{ni}^2\ \exp(-2g'd)} \tag{12}$$

Applying the diffuse radiation boundary conditions

$$x = o,\ A(1 - \beta_o) + B(1 + \beta_o) - U\ I_{po} - V\ J_{po} =$$

$$\rho_i\left\{A(1 + \beta_o) + B(1 - \beta_o) - U\ J_{po} - V\ I_{po}\right\} \tag{13}$$

$$x = d,\ A(1 + \beta_o)\exp(\sigma_o d) + B(1 - \beta_o)\exp(-\sigma_o d) - V\ I_{po}\exp(-g'd) -$$

$$U\ J_{po}\exp(g'd) = \rho_i\left\{A(1-\beta_o)\exp(\sigma_o d) + B(1+\beta_o)\exp(-\sigma_o d)\right.$$

$$\left. - U\ I_{po}\exp(-g'd) - V\ J_{po}\exp(g'd)\right\} \tag{14}$$

or

$$A\left[(1-\rho_i)-(1+\rho_i)\beta_o\right]+B\left[(1-\rho_i)+(1+\rho_i)\beta_o\right]=$$

$$I_{po}(U-\rho_i V)+J_{po}(V-\rho_i U) \tag{15a}$$

$$A\exp(\sigma_o d)\left[(1-\rho_i)+(1+\rho_i)\beta_o\right]+B\exp(-\sigma_o d)\left[(1-\rho_i)+(1+\rho_i)\beta_o\right]=$$

$$_{po}\exp(-g'd)\ (V-\rho_i U)+J_{po}\exp(g'd)\,(U-\rho_i V) \tag{15b}$$

and, solving by determinants, the denominator

$$\Delta=2\left[(1-\rho_i)^2+(1+\rho_i)^2\beta_o^2\right]\sinh\sigma_o d+4(1-\rho_i^2)\beta_o\cosh\sigma_o d \tag{16}$$

$$A=\frac{1}{\Delta}\left\{\left[J_{po}(V-\rho_i U)+I_{po}(U-\rho_i V)\right]\cdot\left[(1-\rho_i)-(1+\rho_o)\beta_o\right]\right.$$

$$\exp(-\sigma_o d)-\left[J_{po}(U-\rho_i V)\exp(g'd)+I_{po}(V-\rho_i U)\exp(-g'd)\right]\cdot$$

$$\left.\left[(1-\rho_i)+(1+\rho_i)\beta_o\right]\right\} \tag{17}$$

$$B=\frac{1}{\Delta}\left\{\left[J_{po}(U-\rho_i V)\exp(g'd)+I_{po}(V-\rho_i U)\exp(-g'd)\right]\cdot\right.$$

$$\left[(1-\rho_i)-(1+\rho_i)\beta_o\right]-\left[J_{po}(V-\rho_i U)+I_{po}(U-\rho_i V)\right]\cdot$$

$$\left.\left[(1-\rho_i)+(1+\rho_i)\beta_o\right]\exp(\sigma_o d)\right\} \tag{18}$$

Substituting for A and B in equation (7)

$$I_{(x=d)} = \frac{1}{\Delta}\left\{\left[J_{po}(V - \rho_i U) + I_{po}(U - \rho_i V)\right](4\beta_o) + \right.$$

$$\left[J_{po}(U - \rho_i V)\exp(g'd) + I_{po}(V - \rho_i U)\exp(-g'd)\right] \cdot$$

$$\left.\left[\{(1 - \beta_o^2) - \rho_i(1 + \beta_o^2)\}\ 2 \sinh \sigma_o d + 4\ \rho_i \beta_o \cosh \sigma_o d\right]\right\}$$

$$- U\ I_{po}\exp(-g'd) - V\ J_{po}\exp(g'd) \qquad (19)$$

The transmitted energies are:

for parallel radiation

$$I_p^* = (1 - \rho_{ni}) I_{p(x = d)} \qquad (20)$$

and for diffuse $I_d^* = (1 - \rho_o) I_{(x = d)}$ (21)

Since we have considered the incident radiation to be of unit intensity, the transmissivities for parallel and diffuse radiation are

$$\tau_p = I_p^* \qquad (22)$$

and

$$\tau_d = I^* \qquad (23)$$

APPENDIX IV: Description of the Three Black-Body Radiation Laws

The three black-body radiation laws and their differences are as follows:

1) The Stefan-Boltzmann Law is for the total emissive power of a black body:

$$W = \sigma T^4 \qquad (1)$$

2) Wien's Law is for the monochromatic emissive power, at wavelength λ, of a black-body:

$$W_\lambda = C_1 \lambda^{-5} \exp(-C_2/\lambda T) \qquad (2)$$

This law was found to be incorrect; and errors at long wave lengths are considerable.

3) Planck then came along, and corrected the expression derived by Wien to its correct form for the monochromatic emissive power of a black-body:

$$W_\lambda = \frac{C_1 \lambda^{-5}}{\exp(C_2/\lambda T) - 1} \qquad (3)$$

UNCLASSIFIED

Security Classification

DOCUMENT CONTROL DATA - R&D

(Security classification of title, body of abstract and indexing annotation must be entered when the overall report is classified)

1. ORIGINATING ACTIVITY (Corporate author)
Lexington Laboratories, Inc.
84 Sherman Street
Cambridge, Massachusetts

2a. REPORT SECURITY CLASSIFICATION
Unclassified

2b GROUP

3 REPORT TITLE
THERMAL RADIATION CHARACTERISTICS OF TRANSPARENT, SEMI-TRANSPARENT AND TRANSLUCENT MATERIALS UNDER NON-ISOTHERMAL CONDITIONS

4. DESCRIPTIVE NOTES (Type of report and inclusive dates)
Final Report

5. AUTHOR(S) (Last name, first name, initial)
Hobbs, Henry A.
Folweiler, Robert C.

6. REPORT DATE	7a. TOTAL NO. OF PAGES	7b. NO. OF REFS
March, 1966	112	9

8a. CONTRACT OR GRANT NO.	9a. ORIGINATOR'S REPORT NUMBER(S)
AF33(657)-11280	ASD-TDR-62-719, Part III
b. PROJECT NO. 7360	
c. Task No. 736001	9b. OTHER REPORT NO(S) (Any other numbers that may be assigned this report)
d.	

10. AVAILABILITY/LIMITATION NOTICES
Distribution of this document is unlimited.

11. SUPPLEMENTARY NOTES	12. SPONSORING MILITARY ACTIVITY
	Air Force Materials Laboratory Research and Technology Division Air Force Systems Command Wright-Patterson Air Force Base, Ohio

13. ABSTRACT

Over the range of wavelengths from one to six microns where oxide ceramics are partially transparent, radiant energy emission must be treated as a volume rather than a surface phenomena. As a result the absorption coefficient (mainly determined by composition) and the scattering coefficient (mainly determined by microstructure) are important variables. In addition, temperature gradients affect radiant energy emission so that the effective "emissivity" under non-isothermal conditions is neither a material constant nor a sample constant.

Analytical relationships have been derived for spectral radiant energy emission as a function of absorption coefficient, scattering coefficient, surface temperature and temperature gradient. Experimental measurements of non-isothermal radiant energy emission of Al_2O_3 and $SrTiO_3$ samples are in agreement with these calculations. Analytical relations and experimental measurements for diffuse and parallel light transmission are reported. Comparison of the Hamaker approximation with an exact solution show that the approximation is suitable for these materials and conditions.

DD FORM 1 JAN 64 1473

UNCLASSIFIED

Security Classification

KEY WORDS	LINK A		LINK B		LINK C	
	ROLE	WT	ROLE	WT	ROLE	WT
Refractory materials, thermal radiation transparent panels, heat transfer, aluminum compounds, oxide, absorption, thermal conductivity, solids, emissivity, single crystals, high temperature research, microstructure, diffusion, wave-transmission, crystal lattices, scattering, perturbation theory, numerical analysis, equations, integration.						

INSTRUCTIONS

1. ORIGINATING ACTIVITY: Enter the name and address of the contractor, subcontractor, grantee, Department of Defense activity or other organization *(corporate author)* issuing the report.

2a. REPORT SECURITY CLASSIFICATION: Enter the overall security classification of the report. Indicate whether "Restricted Data" is included. Marking is to be in accordance with appropriate security regulations.

2b. GROUP: Automatic downgrading is specified in DoD Directive 5200.10 and Armed Forces Industrial Manual. Enter the group number. Also, when applicable, show that optional markings have been used for Group 3 and Group 4 as authorized.

3. REPORT TITLE: Enter the complete report title in all capital letters. Titles in all cases should be unclassified. If a meaningful title cannot be selected without classification, show title classification in all capitals in parenthesis immediately following the title.

4. DESCRIPTIVE NOTES: If appropriate, enter the type of report, e.g., interim, progress, summary, annual, or final. Give the inclusive dates when a specific reporting period is covered.

5. AUTHOR(S): Enter the name(s) of author(s) as shown on or in the report. Enter last name, first name, middle initial. If military, show rank and branch of service. The name of the principal author is an absolute minimum requirement.

6. REPORT DATE: Enter the date of the report as day, month, year; or month, year. If more than one date appears on the report, use date of publication.

7a. TOTAL NUMBER OF PAGES: The total page count should follow normal pagination procedures, i.e., enter the number of pages containing information.

7b. NUMBER OF REFERENCES: Enter the total number of references cited in the report.

8a. CONTRACT OR GRANT NUMBER: If appropriate, enter the applicable number of the contract or grant under which the report was written.

8b, 8c, & 8d. PROJECT NUMBER: Enter the appropriate military department identification, such as project number, subproject number, system numbers, task number, etc.

9a. ORIGINATOR'S REPORT NUMBER(S): Enter the official report number by which the document will be identified and controlled by the originating activity. This number must be unique to this report.

9b. OTHER REPORT NUMBER(S): If the report has been assigned any other report numbers *(either by the originator or by the sponsor)*, also enter this number(s).

10. AVAILABILITY/LIMITATION NOTICES: Enter any limitations on further dissemination of the report, other than those imposed by security classification, using standard statements such as:

(1) "Qualified requesters may obtain copies of this report from DDC."

(2) "Foreign announcement and dissemination of this report by DDC is not authorized."

(3) "U. S. Government agencies may obtain copies of this report directly from DDC. Other qualified DDC users shall request through _____."

(4) "U. S. military agencies may obtain copies of this report directly from DDC. Other qualified users shall request through _____."

(5) "All distribution of this report is controlled. Qualified DDC users shall request through _____."

If the report has been furnished to the Office of Technical Services, Department of Commerce, for sale to the public, indicate this fact and enter the price, if known.

11. SUPPLEMENTARY NOTES: Use for additional explanatory notes.

12. SPONSORING MILITARY ACTIVITY: Enter the name of the departmental project office or laboratory sponsoring *(paying for)* the research and development. Include address.

13. ABSTRACT: Enter an abstract giving a brief and factual summary of the document indicative of the report, even though it may also appear elsewhere in the body of the technical report. If additional space is required, a continuation sheet shall be attached.

It is highly desirable that the abstract of classified reports be unclassified. Each paragraph of the abstract shall end with an indication of the military security classification of the information in the paragraph, represented as *(TS)*, *(S)*, *(C)*, or *(U)*.

There is no limitation on the length of the abstract. However, the suggested length is from 150 to 225 words.

14. KEY WORDS: Key words are technically meaningful terms or short phrases that characterize a report and may be used as index entries for cataloging the report. Key words must be selected so that no security classification is required. Idenfiers, such as equipment model designation, trade name, military project code name, geographic location, may be used as key words but will be followed by an indication of technical context. The assignment of links, rules, and weights is optional.